JOINT TRANSPORTATION
RESEARCH PROGRAM
INDIANA DEPARTMENT OF TRANSPORTATION
AND PURDUE UNIVERSITY

Remaining Service Life Prediction of Indiana Pavements Using Mechanistic Methods

Seonghwan Cho, Bongsuk Park, Cheng Zhang, John E. Haddock

SPR-4443 • Report Number: FHWA/IN/JTRP-2025/10 • DOI: 10.5703/1288284317854

RECOMMENDED CITATION

Cho, S., Park, B., Zhang, C., & Haddock, J. E. (2025). *Remaining service life prediction of Indiana pavements using mechanistic methods* (Joint Transportation Research Program Publication No. FHWA/IN/JTRP-2025/10). West Lafayette, IN: Purdue University. https://doi.org/10.5703/1288284317854

AUTHORS

Seonghwan Cho, PhD
Pavement Research Engineer
Indiana Department of Transportation
Research and Development Division
(765) 463-1521 ext. 252
scho@indot.IN.gov
Corresponding Author

Bongsuk Park, PhD
Assistant Professor
Department of Civil Engineering
Montana Technological University

Cheng Zhang, PhD
Post-Doctoral Research Associate
Lyles School of Civil and Construction Engineering
Purdue University

John E. Haddock, PhD, PE
Professor of Civil Engineering
Director of the Local Technical Assistance Program
Lyles School of Civil Engineering
Purdue University

JOINT TRANSPORTATION RESEARCH PROGRAM

The Joint Transportation Research Program serves as a vehicle for INDOT collaboration with higher education institutions and industry in Indiana to facilitate innovation that results in continuous improvement in the planning, design, construction, operation, management and economic efficiency of the Indiana transportation infrastructure. https://engineering.purdue.edu/JTRP/index_html

Published reports of the Joint Transportation Research Program are available at http://docs.lib.purdue.edu/jtrp/.

NOTICE

TECHNICAL REPORT DOCUMENTATION PAGE

1. Report No. FHWA/IN/JTRP-2025/10	**2. Government Accession No.**	**3. Recipient's Catalog No.**
4. Title and Subtitle Remaining Service Life Prediction of Indiana Pavements Using Mechanistic Methods		**5. Report Date** March 2025 **6. Performing Organization Code**
7. Author(s) Seonghwan Cho, Bongsuk Park, Cheng Zhang, and John E. Haddock		**8. Performing Organization Report No.** FHWA/IN/JTRP-2025/10
9. Performing Organization Name and Address Joint Transportation Research Program Hall for Discovery and Learning Research (DLR), Suite 204 207 S. Martin Jischke Drive West Lafayette, IN 47907		**10. Work Unit No.** **11. Contract or Grant No.** SPR-4443
12. Sponsoring Agency Name and Address Indiana Department of Transportation (SPR) State Office Building 100 North Senate Avenue Indianapolis, IN 46204		**13. Type of Report and Period Covered** Final Report **14. Sponsoring Agency Code**

15. Supplementary Notes

Conducted in cooperation with the U.S. Department of Transportation, Federal Highway Administration.

16. Abstract

Accurate remaining service life (RSL) prediction facilitates effective pavement maintenance strategies, extends service quality, and reduces costs. This study developed RSL prediction models for major distresses in INDOT pavement—including full-depth asphalt flexible, rigid, and composite pavement—using Falling Weight Deflectometer (FWD) and International Roughness Index (IRI) data. The structural and functional prediction models were developed based on the analysis of field data and finite element simulation results. All indicators of the structural prediction models could easily be obtained by processing raw FWD data. The IRI prediction models were developed for INDOT pavements using an enhanced approach for analyzing historical IRI databases. Consequently, the frameworks of maintenance strategy determination were developed using the RSL prediction models and the pavement condition estimation models were developed based on the FWD and IRI data for pavement assessment.

17. Key Words remaining service life, pavement structural condition, pavement functional condition, maintenance strategy determination, Falling Weight Deflectometer (FWD), finite element method	**18. Distribution Statement** No restrictions. This document is available through the National Technical Information Service, Springfield, VA 22161.

19. Security Classif. (of this report) Unclassified	**20. Security Classif. (of this page)** Unclassified	**21. No. of Pages** 102, including appendices	**22. Price**

Form DOT F 1700.7 (8-72) Reproduction of completed page authorized

EXECUTIVE SUMMARY

Introduction

The remaining service life (RSL) of pavements represents the time during which pavements can provide acceptable structural and functional conditions without major rehabilitation. Accurate RSL prediction supports effective pavement maintenance strategies, extending service quality and reducing costs. In Indiana, many pavements nearing the end of their design life exhibit distress such as fatigue cracking, rutting, corner cracks, faulting, and reflective cracking. In order to limit uncertainty in making decisions to repair, rehabilitate, or reconstruct pavements, the determination of remaining pavement service life is an important aspect of pavement management planning.

The Indiana Department of Transportation (INDOT) adopted the American Association of State Highway and Transportation Officials (AASHTO) Pavement ME pavement design software and analysis method in January 2009. Considering pavement structure, climate condition, and traffic data, Pavement ME can evaluate the performance of pavement by simulating expected accumulated damage over the pavement service life and convert the damage to pavement distress and roughness levels. However, the prediction models in the Pavement ME were globally calibrated based on data collected from wide temperature and climate regions.

The study objectives were to predict the RSL of INDOT pavements—including full-depth asphalt, rigid asphalt, and composite pavements—in terms of major distresses using Falling Weight Deflectometer (FWD) and International Roughness Index (IRI) data. The FWD is a widely used non-destructive test, assessing pavement capacity and layer properties through deflection data. Functional performance is analyzed using the IRI. Historical FWD and IRI data were collected to develop the structural and functional condition estimation models and RSL prediction models for full-depth asphalt, rigid asphalt, and composite pavements, respectively.

Findings

The research developed the RSL prediction models for full-depth asphalt, rigid pavement, and composite pavement based on the FWD and IRI data. Additionally, frameworks of maintenance strategy determinations for full-depth asphalt, rigid pavement, and composite pavement were provided. Structural and functional condition estimation models were developed based on the characteristics of INDOT pavements. The following were key study findings.

For full-depth asphalt flexible pavement

- Effective structural number (SN_{eff}) is an essential indicator in estimating flexible pavement structural condition. The prediction model developed in this research was able to determine the SN_{eff} approximately identical to the calibrated Rohde model, while using only two input parameters (area under pavement profile (AUPP) and pavement thickness), which is a more practical approach.
- Critical strains at the top of the subgrade and the bottom of the asphalt layer can be used to estimate subgrade and asphalt base layer properties. Critical strain prediction models have been successfully validated using field-measured strains and can therefore be used to conduct structural evaluations for in-service full-depth asphalt flexible pavements.
- Regardless of the pavement structure, the AUPP and base damage index (BDI) can be used to predict transverse tensile strain at the bottom of the asphalt base layer and vertical compressive strain at the top of the subgrade, respectively. The equations based on the AUPP and BDI provided acceptable accuracy ($R^2 = 0.98$) in terms of the critical strain prediction for full-depth asphalt flexible pavements.

For rigid pavement

- The developed stress-strength ratio (SSR) prediction model can be used to estimate the structural capacity of in-service rigid pavements using FWD deflection data. The SSR is primarily affected by curling conditions within the acceptable range (less than 0.45), while the curling effect was insignificant for weaker Portland cement concrete (PCC) slabs with higher SSR.
- The effect of curling on FWD deflection basin curves is larger when the PCC slab is stiffer. However, for any PCC slab stiffness level, the shapes of FWD deflection basin curve near the loading center are similar, regardless of the curling conditions.
- The surface curvature index (SCI) exhibited the strongest correlation with SSR and is selected as an input for the SSR prediction model. The accuracy of the SSR prediction model is high ($R^2 = 0.98$), with the low RMSE of 0.026, further confirming the potential error in SSR predictions is insignificant.

For composite pavement

- The PCC slab joints in composite pavements have a critical influence on the mechanical responses in FWD testing. Due to the effects of the PCC slab joint, the normal and shear strains in the longitudinal direction at the bottom of the asphalt layer show second fluctuations.
- The extreme value of shear strain in second fluctuations can be utilized to evaluate reflective cracking. At the same loading distance, the shear strain increased as the depth of the reflective crack increased. When the reflective crack depth reached 75% of the asphalt layer thickness, the shear strain increased sharply.
- Reflective cracking can be recognized and estimated by the composite pavement base damage index ($BDI_{composite}$) and SCI based on FWD testing. When both $BDI_{composite}$ and SCI show large values in routine surveys, reflective cracks may be propagating.

Implementation

The critical responses and indicators obtained from the FWD and IRI tests can be used to evaluate the pavement's structural and functional conditions. Based on the indicators, maintenance determination strategy frameworks were developed for the full-depth asphalt flexible, rigid, and composite pavements and integrated in a non-destructive test analysis tool that can be implemented in the INDOT pavement management system.

TABLE OF CONTENTS

LIST OF TABLES

LIST OF FIGURES

1. INTRODUCTION

1.1 Background

Remaining service life (RSL) of pavement is the anticipated time that a pavement can provide acceptable structural and functional conditions without further rehabilitation. The accurate prediction of pavement RSL is beneficial to make a reasonable and efficient maintenance strategy for pavement management system. An appropriate maintenance strategy can extend pavement service quality and reduce unnecessary maintenance costs (Peraka & Biligiri, 2020). Many flexible and rigid pavements in Indiana are approaching the end of their design lives. Common pavement distresses are fatigue cracking and rutting associated with flexible pavements, corner cracks and faulting on jointed plain cement concrete (PCC) pavements, and the reflective cracking in the composite pavement over the PCC slab joint. The effect of deicing/anti-acing chemicals on PCC pavement is also another issue causing damage in rigid pavements (Suraneni et al., 2016). In order to limit uncertainty in making decisions to repair, rehabilitate, or reconstruct pavements, the determination of remaining pavement service life is an important aspect of pavement management planning.

The Indiana Department of Transportation (INDOT) adopted the American Association of State Highway and Transportation Officials (AASHTO) Pavement ME pavement design software and analysis method (previously identified as *Mechanistic Empirical Pavement Design Guide (*MEPDG)) in January 2009. Considering pavement structure, climate condition, and traffic data, Pavement ME can evaluate the performance of pavement by simulating expected accumulated damage over the pavement service life and convert the damage to pavement distresses and roughness levels. From a structural standpoint, deflection testing is a potential method to aid in determining pavement RSL. The Falling Weight Deflectometer (FWD) is a widely used non-destructive test method to determine the structural performance of in-service pavements and assess the structural capacity of pavements. The deflection data collected by the FWD can be used to determine the characteristics of pavement layers through back-calculation. In terms of functional performance, the International Roughness Index (IRI) and Present Serviceability Index can be used for flexible and rigid pavements. These methods can provide information on how the performance of pavements changes over the service life (Noureldin et al., 2005). Performance prediction models (deterioration curves) and pavement condition index (PCI) developed from the correlation between pavement performance and service time can be used to predict the remaining service life of pavements in terms of structural and functional conditions using the FWD, IRI, and traffic information.

1.2 Objectives

The primary objective of this study is to predict the INDOT pavement RSL in terms of major pavement distresses using FWD and IRI data. The detailed objectives are as follows.

- Development of structural condition estimation models for the flexible, rigid, and composite pavements.
- Development of functional condition estimation models for asphalt and rigid pavements.
- Development of pavement RSL prediction model based on the structural and functional conditions.

1.3 Scope

The INDOT paved roads consist of flexible, rigid, and composite pavements. INDOT currently has a database of FWD and IRI data collected from different road sections in Indiana over the last 10 years. These historical data, combined with the finite element (FE) simulation and laboratory test results will be used to predict structural and functional conditions for flexible, rigid, and composite pavements across Indiana climatic zones. Such prediction results can be used to estimate the pavement RSL and provide recommendations on required rehabilitation or reconstruction.

For the flexible pavements, a total of 1,354 field FWD data and 3,927 FE-based FWD data were used to develop an enhanced effective structural number (SN_{eff}) prediction model and critical strain prediction models for as-constructed, in-service full-depth asphalt flexible pavements. This FWD database covered a broad range of full-depth asphalt flexible pavement structures, to increase the model accuracy. For the rigid pavement, a total of 432 FE models were simulated to encompass a broad range of pavement structures and environmental conditions. In addition, the FWD test was conducted on a field section to validate the developed FE model. For the composite pavements, thirty-two cases were simulated to develop the joint identification approach and the reflective cracking estimation model. Seventy-six labeled field data were used to verify the joint identification and the reflective cracking estimation model.

Historical IRI data was obtained from INDOT database to develop the IRI prediction model. As summarized in Table 1.1, the historical IRI data was collected annually from the same testing location between 2014 and 2021, and the collected IRI data

TABLE 1.1
IRI data description

Road Classifications	Collection Years	Number of IRI Data
Interstate Highways	2014 to 2021	129,248
U.S. Highways	2014 to 2021	410,512
State Roads	2014 to 2021	1,130,528

covered all road classifications, including interstate highways, U.S. highways, and state roads.

1.4 Research Approach

Remaining pavement service life can be determined based on the pavement structural and functional conditions. The structural and functional estimation models were developed for flexible, rigid, and composite pavements. Four main steps were taken to fulfill the study objective: literature review, laboratory and field tests, FE simulations, and RSL prediction models were conducted for different pavements, respectively.

1.4.1 State-of-the-Art Literature Review

The project began with a comprehensive literature review of current methods being used to predict pavement RSL. This included methods for estimating the structural and functional conditions of flexible, rigid, and composite pavements, and what indices and methods have been developed over the years.

1.4.2 Field Investigation and Laboratory Testing

IRI was used for pavement functional analysis and FWD data for pavement structural analysis. Various pavement sections, including flexible, rigid, and composite pavements, were selected to perform the IRI and FWD tests. Additionally, field samples were taken from the identified pavement sections, the layer thicknesses measured and recorded, and the materials mechanical properties tested in the laboratory. The laboratory results were then correlated with pavement performance as measured by the IRI and FWD. The pavement geometry information and material properties (i.e., asphalt mixture complex modulus and PCC strength) were used in the FE models to simulate pavement mechanical responses. The FE models were verified by FWD data and used to develop structural condition prediction models.

1.4.3 Structural and Functional Condition Prediction Models

The critical mechanical responses and deflection basin parameters (DBPs) were selected for flexible, rigid, and composite pavements. Additionally, the common distresses were investigated in the field for different pavement types to select practical parameters for estimating structural condition. The functional prediction models were developed using an enhanced approach for analyzing historical IRI database. And the pavement deterioration rates over the last few years were correlated to their current conditions. The structural and functional condition prediction models provide significant indicators for estimating the RSL.

1.4.4 Development of a Guideline to Predict the Pavement Remaining Service Life

Based on the results of the previous three steps, a set of decision matrixes based on pavement structural and functional prediction models were developed. RSL can be predicted in terms of equivalent single axle loads (ESAL), or number of traffic passes to failure. Thresholds were established to determine the required action for pavement management.

2. LITERATURE REVIEW

2.1 Evaluation of In-Service Pavement Structural Conditions

Currently, the surface deflection measured from the FWD is widely used as a non-destructive method to evaluate in-service pavement structural condition (Plati et al., 2016). Based on the FWD deflections, previous researchers have developed several structural condition indices for full-depth, rigid, composite pavements (Bryce et al., 2013; Ramirez & Morian, 2020).

The DBPs measured from FWD testing are widely used to assess pavement structural conditions (Kavussi et al., 2017). The central deflection (D_0), measured under the center of the FWD loading plate, is typically used to evaluate overall pavement condition, as D0 is affected by all the asphalt flexible pavement layers (Ruiz Martin et al., 2018). D_{60}, the deflection measured 60 inches from the center of loading plate, is thought to represent subgrade condition. In addition to the D_0 and D_{60} deflection values, curvature or area shape parameters have been introduced to provide more insight into the deflection basin profile (Gopalakrishnan et al., 2010; Horak et al., 2015). Thompson and Hoffman (1983) proposed the AUPP parameter. Defined as the normalized area under a deflection curve from 0 to 36 inches from the load center, the AUPP characterizes the pavement conditions in a pavement's upper layers using the deflection basin shape near the load. The surface curvature index (SCI) is the difference between D_0 and D_{12} deflections and also indicates upper layer pavement conditions using the deflections nearest the load. Both AUPP and SCI parameters are sensitive to the asphalt layer properties in a conventional flexible pavement containing an aggregate base course (Thompson & Garg, 1998; Xu et al., 2002). Lastly, the base damage index (BDI) and base curvature index (BCI) are used to characterize base layer and subgrade conditions, respectively. Previous researchers have reported that BDI is mainly related to the aggregate base modulus, while BCI is more associated with the subgrade modulus (Gopalakrishnan et al., 2010; Xu et al., 2002).

2.1.1 Full-Depth Asphalt Flexible Pavements

Full-depth asphalt flexible pavement is one of the most common Indiana pavement types. While conven-

tional flexible pavements consist of one or more asphalt layers over an aggregate base, and in some cases an aggregate subbase layer, full-depth flexible pavements consist of one or more layers of asphalt placed directly on the subgrade. The differences in pavement structures between full-depth and conventional flexible pavements significantly affects how each pavement type performs and behaves (Kim et al., 2018). Based on FWD deflections, previous researchers have developed several structural condition indices to consider conventional flexible pavement structural conditions (Bryce et al., 2013). However, concerns have been raised that many structural indicators are usually subjective without fundamental theory (Singh et al., 2018).

Critical strains have been widely used as mechanical responses to both design and assess the structural capacity of flexible pavements (Plati et al., 2016). According to the AASHTOWare Pavement ME Design, there are two major critical strains for full-depth asphalt flexible pavements: (1) transverse tensile strain at the bottom of the asphalt layer, associated with bottom-up cracking performance, and (2) vertical compressive strain at the top of subgrade, related to performance of subgrade rutting (AASHTO, 2020). Even though these critical strains are reliable mechanistic parameters for evaluating pavement structural conditions, it is difficult to measure them for in-service pavements unless strain gauges are deployed in the pavement structure. A more practical method is needed to predict critical strains.

The concept of a pavement structural number was originally developed by the American Association of State Highway Officials (AASHO) for use in flexible pavement design, with the effective structural number (SN_{eff}) representing the structural strength of an existing pavement (AASHTO, 1993). The structural number ratio (SNR), defined as the ratio of the SN_{eff} and the SN_{req} (Abd El-Raof et al., 2020; Rohde, 1994) is the most common index. In New Jersey, the SNR was used to calculate the structural adequacy index to prioritize the need for pavement maintenance (Zaghloul et al., 2004). In addition, Bryce et al. (2013) employed the SNR concept to develop, and successfully apply, the modified structural index to predict the structural adequacy of in-service conventional flexible pavements for the Virginia Department of Transportation (VDOT) pavement management system (PMS). As indicated by these previous studies, the SNR concept is a reliable approach to evaluate existing pavement structural conditions, the SN_{eff} being a key parameter affecting the accuracy of SNR (Kim et al., 2013). Therefore, the SN_{eff} must be accurately predicted to ensure an appropriate maintenance and rehabilitation strategy.

Currently, the INDOT employs the AASHTO (1993) method (AASHTO 1993 refers to this method in this report) to predict the SN_{eff} of pavements. However, INDOT engineers have raised doubts about the accuracy of the method for estimating the SN_{eff} of full-depth asphalt flexible pavements. VDOT identified a similar issue, that the AASHTO 1993 method could lead to error in the predicted SN_{eff}, as compared to the SN_{eff} obtained from their empirical relationship (Bryce et al., 2013). Since the AASHTO 1993 method is mainly dependent on total pavement thickness, it may not be suitable for full-depth asphalt flexible pavements, which in Indiana have a considerably thicker asphalt layer (minimum 10 inches) than conventional flexible pavements. This suggests the AASHTO 1993 method may induce even greater error in the structural condition index.

2.1.2 Rigid Pavements

Evaluating structural conditions is significant for rigid pavements in PMS. The structural condition is an essential index to predict the rigid pavement's remaining service life and determine the maintenance strategy. Additionally, the evaluation of the existing rigid pavement is a critical element for determining the rehabilitation design (AASHTO, 2020). In Pavement ME design, distresses such as distortion (faulting), cracking, and material disintegration (punchouts) are analyzed for evaluating existing rigid pavement capacity, which will be used to determine the asphalt overlay design features and thickness. Thus, various methods and indices were developed to evaluate rigid pavement structural conditions.

An accurate estimation of the structural conditions of in-service rigid pavements is important to ensure appropriate maintenance and rehabilitation design (Saleh & van der Walt, 2019; Sen & Khazanovich, 2023). However, for jointed plain concrete pavements (JPCP), one of the most common rigid pavement types, it is challenging to accurately estimate the structural conditions due to joint structures with dowel bars (Saleh & van der Walt, 2019). Furthermore, the behavior of rigid pavements is significantly affected by environmental loading conditions, such as temperature and moisture gradients through the PCC slab depth, which may not be accurately captured in field measurements (Kim et al., 2021; Pierce et al., 2017).

Currently, many state agencies use the FWD to estimate the structural conditions of in-service rigid pavements (Bayrak & Ceylan, 2008; Ramirez & Morian, 2020; Suleiman et al., 2011). The FWD deflection data can be used for JPCP to evaluate the structural capacity of the PCC slab, the load transfer efficiency (LTE) of the joint, and voids beneath the PCC slab (Pierce et al., 2017; Sok et al., 2020). In addition, the Pavement ME recommends back calculated layer moduli and LTE derived from FWD deflection data as design inputs for rehabilitation design (AASHTO, 2020; Zhang et al., 2022). The stress-to-strength ratio (SSR), defined as the ratio of stress to the flexural strength of the PCC, is one of the most common indicators used to assess the structural capacity of concrete materials (Delatte, 2018; Kim & Chun, 2015; Shi et al., 2021). Generally, rigid pavements with a greater SSR are more susceptible to

fatigue cracking. However, incorporating SSR into PMS is challenging due to limited methods to determine stress in the PCC slabs of in-service rigid pavements.

Since PCC slab responses, such as stress and deflections, are affected by curling conditions, several researchers have investigated methods to account for curling effects during FWD data interpretation (Crovetti, 2002; Muslim et al., 2022). Crovetti (2002) presented a methodology to analyze FWD deflections to quantify the uniformity of slab support, considering curling effect. Muslim et al. (2022) also recommended ambient temperature ranges for FWD testing to minimize curling effects, based on the results of LTPP database analyses. However, the interpretation of FWD data considering curling effects remains questionable, while previous studies have recommended adjusting FWD loading or test temperature ranges.

2.1.3 Composite Pavements

In Indiana, composite pavements are most commonly the result of rigid pavement rehabilitation. Resurfacing a moderately deteriorated PCC pavement with asphalt layers is considered an efficient and common practice (Zhu & Al-Qadi, 2024). The asphalt overlay can be placed directly on the existing PCC slabs, or the slabs can first be fractured using break and seat (JPCP), crack and seat (jointed reinforced concrete pavement), or rubblization. The use of composite pavements in roadway systems could potentially increase. Therefore, further research is needed to develop reliable and efficient methods for evaluating the condition of composite pavements.

Two types of distress are commonly associated with composite pavement: reflective cracking and interface debonding (Mezhoud et al., 2018; Xu et al., 2021). Reflective cracking is typically caused by temperature changes and traffic loadings (Ban et al., 2018). Fluctuations in temperature cause the PCC slab to expand or shrink, generating horizontal stresses at the bottom of the asphalt layer immediately over the pavement joints. Additionally, traffic loading introduces a complex stress condition in the asphalt layer (Das et al., 2020; Deilami & White, 2020). As vehicles approach or leave the joint area, one side of the PCC slab supports the majority of the traffic loading, causing vertical displacement relative to the other PCC slab and resulting in shear effects in the asphalt layer. When vehicles are moving on the joint, both sides of the PCC slabs support the traffic loading, resulting in bending deformation in the asphalt layer. Debonding distress is also associated with PCC slab joints (Isla et al., 2015). When the asphalt surface deflects at the joint area under traffic loading, the leverage effect can cause debonding between the asphalt surface and the PCC in the surrounding area. Therefore, identifying the PCC slab joint is essential for evaluating composite pavement conditions and predicting distresses, which is crucial for making well-informed maintenance decisions.

The FWD has been a widely utilized NDT for assessing pavement structures since the 1980s (Wang et al., 2019). At the project level, the LTE is commonly used as a parameter to estimate joint conditions by comparing the pavement deflections measured by two adjacent sensors: one on the loaded slab and the other on the unloaded slab. However, accurately locating the PCC slab joint in composite pavements to calculate the LTE is challenging. Al-Abbasi and Shalaby (2021) analyzed the LTE calculated from FWD tests in a composite pavement before and after asphalt layer milling and found statistical differences in the LTE values. Thus, identifying the PCC slab joint is critical to evaluating the structural condition of composite pavements. Additionally, more research on the mechanical responses under FWD loading is necessary to interpret deflection data and develop reliable indices for evaluating composite pavement structural conditions.

2.2 Evaluation of Functional Conditions of In-Service Pavements

The IRI is widely used in the PMS to quantify pavement smoothness for evaluating pavement functional conditions (Abdelaziz et al., 2020; Chen et al., 2019; Lee et al., 2020). Since rougher pavements can lead to reduced vehicle efficiency, safety, and ride quality, as well as accelerate the deterioration of pavement performance, the IRI has been used as an indicator to ensure desirable pavement performance (Dalla Rosa et al., 2017; Wang et al., 2021). In addition, the IRI is one of the design criteria in the AASHTO Pavement ME for both flexible and rigid pavements. Even though the IRI has been successfully employed to assess the current conditions of pavements, the accuracy of predicting future IRI is still questionable. Since forecasting IRI plays an important role in estimating pavement remaining life, constructing pavement deterioration curves, and determining appropriate maintenance strategies, the accurate prediction of IRI is needed for PMS.

Previous researchers have proposed IRI prediction models based on the long-term pavement performance data or local agency databases, but most previous models required numerous input variables, which is not practical (Abdelaziz et al., 2020; Albuquerque & Núñez, 2011; Khattak et al., 2014). Khattak et al. (2014) used the Louisiana Department of Transportation and Development (LDOTD) database to develop the IRI prediction model for flexible pavements. Overlay thickness, cumulative equivalent single-axle load, functional classification, and climate factors (cumulative precipitation index and temperature index) were employed as input parameters. However, the accuracy of this model was low as indicated by the coefficient of determination ($R^2 = 0.47$), despite incorporating multiple variables. Albuquerque and Nunez (2011) employed regional climate parameters, structural number, and traffic characteristics to develop an IRI prediction model. Even though their models provided reasonably accurate

IRI predictions, it was only validated with a limited number of local field sections in Brazil.

Other previous IRI prediction models applied simple equations using one or two input variables to be practical (Al-Suleiman & Shiyab, 2003; Lee et al., 2020). Lee et al. (2020) developed the empirical IRI model using pavement age and initial IRI based on the Illinois roadway information system database. However, this empirical IRI prediction model showed significant dependence on the initial IRI, although it exhibited a reasonable trend of IRI over pavement age. Al-Suleiman and Shiyab (2003) developed regression models using a single input variable, pavement age, to predict IRI practically for Dubai roads. However, this model was only verified with field data from Dubai and yielded relatively low accuracy.

As illustrated, practical methodologies to accurately predict IRI are questionable due to the limited IRI historical databases and the considerable number of factors affecting the IRI. However, the use of numerous input variables does not necessarily improve the accuracy of IRI predictions, and the accuracy of previous simple and empirical models was poor.

3. DEVELOPMENT OF EXPERIMENTAL PLAN

3.1 Field Sections

A total of 19 field sections, including seven full-depth asphalt flexible pavements, seven rigid pavements, and five composite pavements, were selected based on the availability of historical FWD and IRI data. Table 3.1 identifies sections, each of which has at least 3 years of historical FWD and IRI data.

An additional nine full-depth asphalt flexible pavement sections, consisting of two interstate highways, four U.S. highways, and three state roads, were selected to verify critical strain prediction model (Table 3.2). This combination accounts for all three INDOT road classifications. Total pavement thickness of the selected field sections ranged from 12 inches to 15 inches, typical of full-depth flexible pavement thickness ranges encountered in Indiana. Strain gauges were implemented in Sections A and B, at the bottom of the asphalt base layers (directly on the subgrade), where the maximum tensile strain occurs (i.e., critical location for bottom-up cracking). It should be noted that Sections A and B were newly constructed with the same pavement cross section and the same subgrade, but different subgrade treatments. Section B had a treated subgrade, while Section A did not. Thus, the two sections provide two different strain levels due to the different subgrade treatments.

3.2 Laboratory and Field Tests

FWD and dynamic modulus tests were conducted according to standard test methods (Figure 3.1), the details of which are described in Appendix B.

TABLE 3.1
Field sections

Full-Depth Asphalt Flexible Pavements			Rigid Pavements			Composite Pavements		
Route	**RP (from)**	**RP (to)**	**Route**	**RP (from)**	**RP (to)**	**Route**	**RP (from)**	**RP (to)**
SR-67	8+00	10+79	SR 61	4+00	8+00	SR 63	54+95	66+76
SR-69	27+00	29+00	SR 51	9+05	9+50	US 20	7+19	9+77
SR-32	58+58	60+10	US6	15+31	15+70	US 20	143+44	143+95
SR-42	39+00	42+00	US 30	0+00	2+85	US 40	97+53	100+70
SR-545	4+00	8+00	US 24	153+00	154+00	US 41	12+00	22+23
US 24	155+40	157+60	US 421	90+88	91+93	–	–	–
US 27	85+00	86+00	I-69	15+00	19+00	–	–	–

TABLE 3.2
Field sections for critical strain prediction

Section ID	Road Type	Total Pavement Thickness (in)	Strain Gauge
A	Interstate Highway	14	Yes
B	Interstate Highway	14	Yes
C	U.S. Highway	14	No
D	U.S. Highway	14	No
E	U.S. Highway	15	No
F	U.S. Highway	12	No
G	State Road	15	No
H	State Road	12	No
I	State Road	13	No

(a)

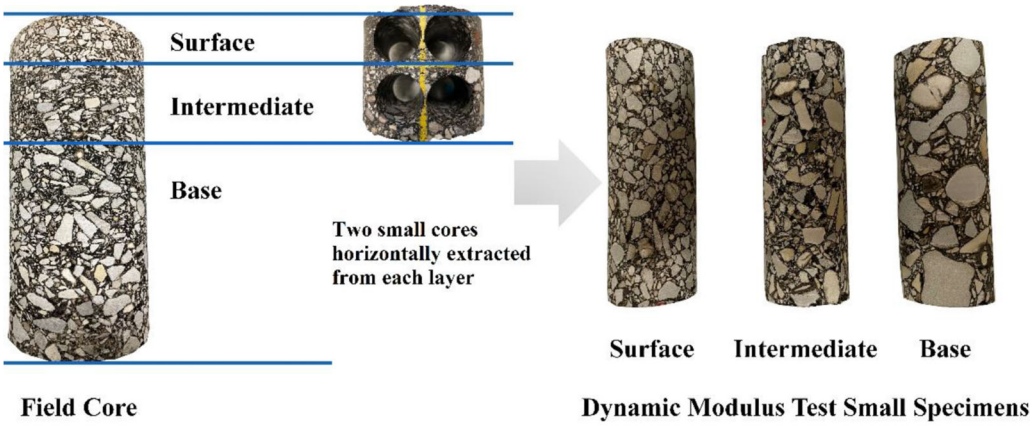

(b)

Figure 3.1 Continued.

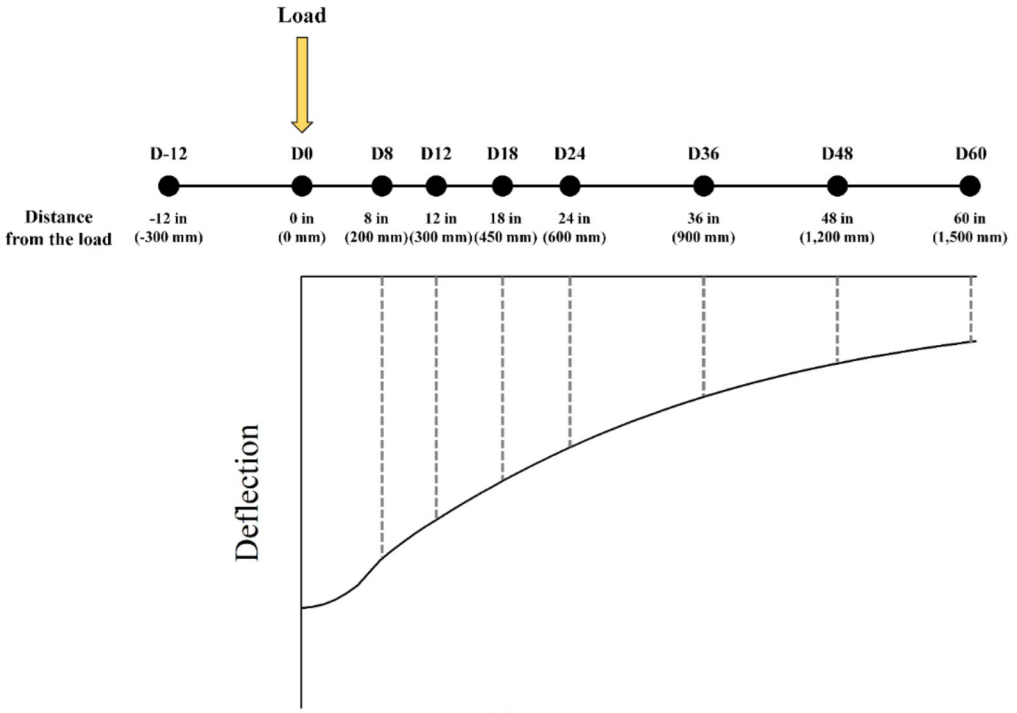

(c)

Figure 3.1 Field and laboratory tests: (a) FWD testing equipment, (b) preparation of small dynamic modulus test specimens from field cores, and (c) location of geophones for FWD tests.

4. FULL-DEPTH ASPHALT FLEXIBLE PAVEMENT MODELS FOR STRUCTURAL CONDITIONS

4.1 Introduction

The SN_{eff} has been widely used to evaluate in-service pavement structural conditions, which can represent the overall structural conditions of in-service flexible pavements. While critical strains are essential mechanistic responses for flexible pavement design and structural capacity assessment. The transverse tensile strain at the bottom of the asphalt layer can be used to predict cracking, and vertical compressive strain at the top of subgrade for rutting in the Pavement ME. In this research, the prediction models of the SN_{eff} and critical strains were developed to estimate the structural conditions of the full-depth flexible pavements. The FE models were developed to simulate mechanical responses based on the characteristics of the INDOT pavements. The prediction models were developed by analyzing the FE simulation results and the field data.

4.2 Finite Element Model Development

4.2.1 Pavement Structure and Layer Properties

A FE model was developed based on the representative INDOT full-depth asphalt flexible pavement structure type. According to INDOT specification, full-depth asphalt flexible pavement consists of three asphalt layers: surface, intermediate, and base, placed directly on a prepared subgrade (INDOT, 2024). The representative pavement structure for this project was selected from INDOT's Accelerated Pavement Test (APT) facility test section used in a concurrent INDOT study. Table 4.1 summarizes layer thicknesses and elastic material properties for the representative pavement cross section.

4.2.2 Finite Element Model Description

Figure 4.1 shows the FE model for the representative full-depth asphalt flexible pavement system. The axisymmetric model was selected, which is beneficial for simulating the circular load and requires less computational time and effort than a 3-dimensional model, without significant accuracy loss (Li et al., 2017). The details of the FE models are described in Appendix C.

4.3 Development of Critical Strain Prediction Models

4.3.1 Collection of Finite Element Model-Based FWD Data

The effect of structural properties on the critical strains was preliminarily investigated to determine appropriate structural variables for the strain prediction model. Asphalt surface and intermediate layers were combined into one layer and given the name

TABLE 4.1
Layer thicknesses and elastic properties for representative pavement structure

Layer Type	Thickness (in.)	Elastic Modulus (ksi)	Poisson's Ratio
Asphalt Surface	1.5	1,885	0.35
Asphalt Intermediate	2.5	1,740	0.35
Asphalt Base	6	1,160	0.40
Subgrade	1,000	50	0.45

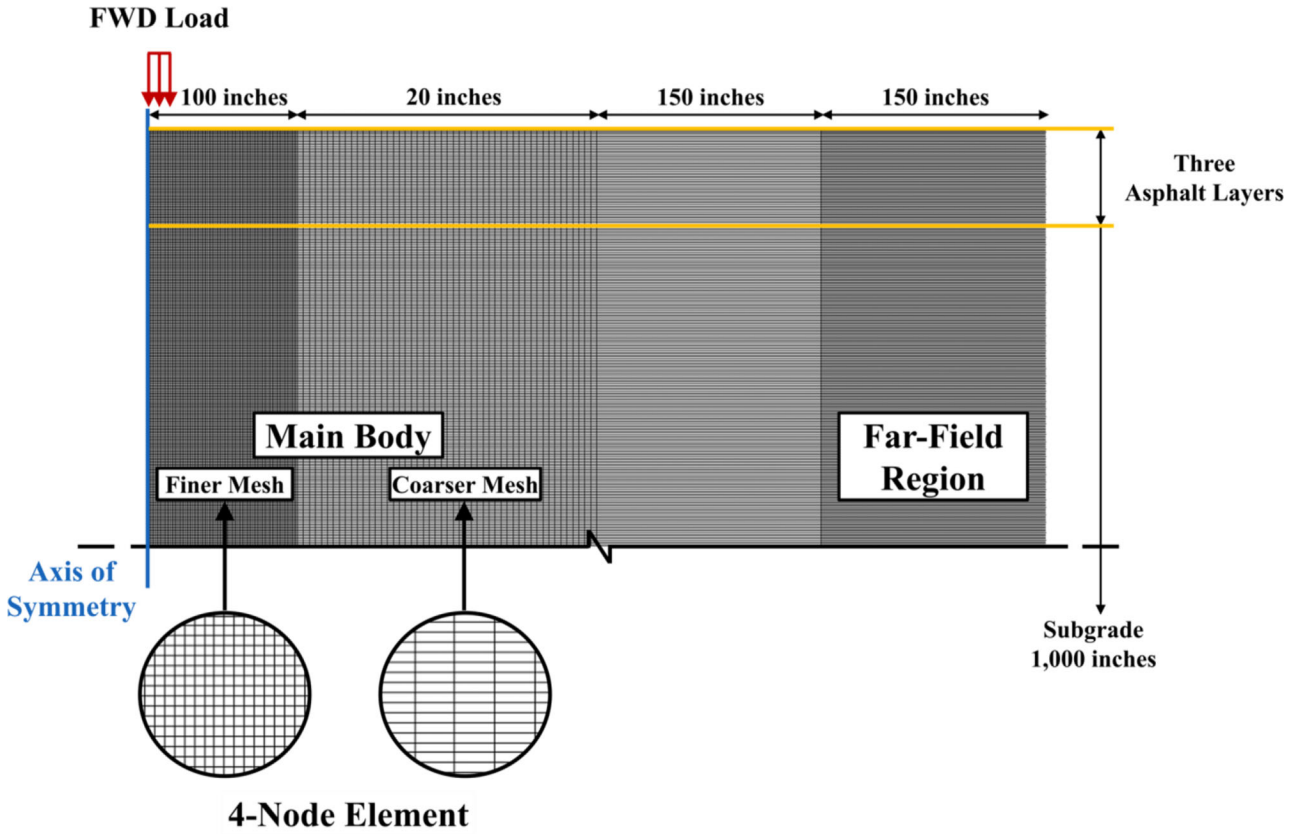

Figure 4.1 Finite element model mesh description.

"ASI," due to their similar elastic modulus values. As shown in Figure 4.2, strains were normalized to compare parameters on the same scale. Overall, strain values decreased with increasing layer modulus or thickness, but ASI properties had less influence compared to the asphalt base and subgrade. Specifically, a greater ASI modulus reduced both transverse and vertical strains approximately 10%, while increased asphalt base and subgrade moduli reduced strains by 30% to 35%. Furthermore, thicker ASI layers reduced both strains up to 15%, while thicker asphalt base layers reduced strains approximately 50%. Due to the smaller contribution of ASI in the full-depth asphalt flexible pavement, its effects are relatively insignificant compared to asphalt base and subgrade layers.

The range of structural parameters representing INDOT full-depth asphalt flexible pavements was selected based on the INDOT standard specification (INDOT, 2024). Eight moduli were selected to represent the new pavement cases. In addition, two types of damaged pavement were included: (1) 60% damaged asphalt surface layer, and (2) damaged asphalt base layer and subgrade. Consequently, a total of 3,927 structural combinations were numerically simulated to identify a relationship between FWD parameters and critical pavement responses. Additional details are described in Appendix C, Section 3.1.5.

The six DBPs presented in Table 3.3 were evaluated to determine the appropriate input parameters for critical strain prediction models. Therefore, 3,927 data sets of DBPs and critical strains were produced. A simple linear regression was conducted to evaluate the relationship between each DBP and critical strains, and the R^2 was used as an indicator of the strength of correlation. Figure 4.3 shows relationships between each DBP and transverse tensile strain. Overall, the

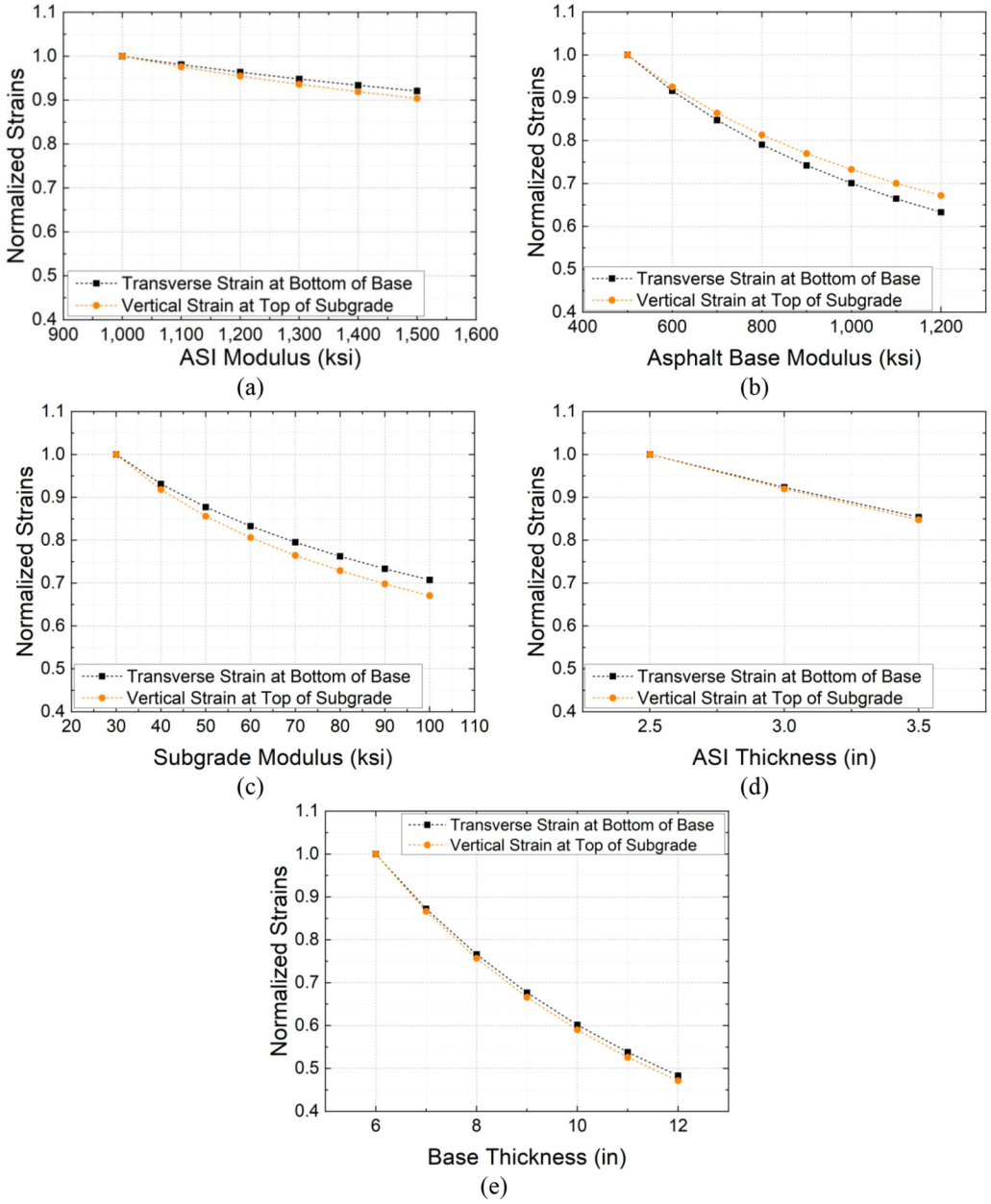

Figure 4.2 Structural property effects on critical strains: (a) ASI modulus, (b) asphalt base modulus, (c) subgrade modulus, (d) ASI thickness, and (e) asphalt base thickness.

transverse tensile strain increased as DBPs increased except for the D60 parameter. As shown in Figure 4.3(b), the D60 was mainly affected by the subgrade modulus; greater values of D60 were captured at the lower subgrade modulus. Interestingly, deflection basin shape parameters (i.e., SCI, BDI, BCI, and AUPP) generally exhibited better correlation with the transverse strain compared to the sole deflection value (i.e., D0 and D60), as shown in Figure 4.3(a) and Figure 4.3(c–f). A similar trend was identified for the relationships between each DBP and the vertical compressive strain. The D0 parameter exhibited the smallest R^2 and the R^2 of SCI, BDI, BCI, and AUPP were greater than 0.89, as shown in Figure 4.4. Specifically, the AUPP and the BDI exhibited the best correlation with transverse strain and vertical strain. Therefore, the AUPP and the BDI were selected as input parameters for the prediction of transverse tensile strain and vertical compressive strain, respectively.

4.3.2 Critical Strain Prediction Equations

The strain prediction equations were developed using a linear regression method based on the relationships identified in the previous section. Equation 4.1 expresses the predictive equation for the transverse tensile strain at the bottom of the asphalt base layer. The R^2 for Equation 4.1 was 0.98, indicating the equation can

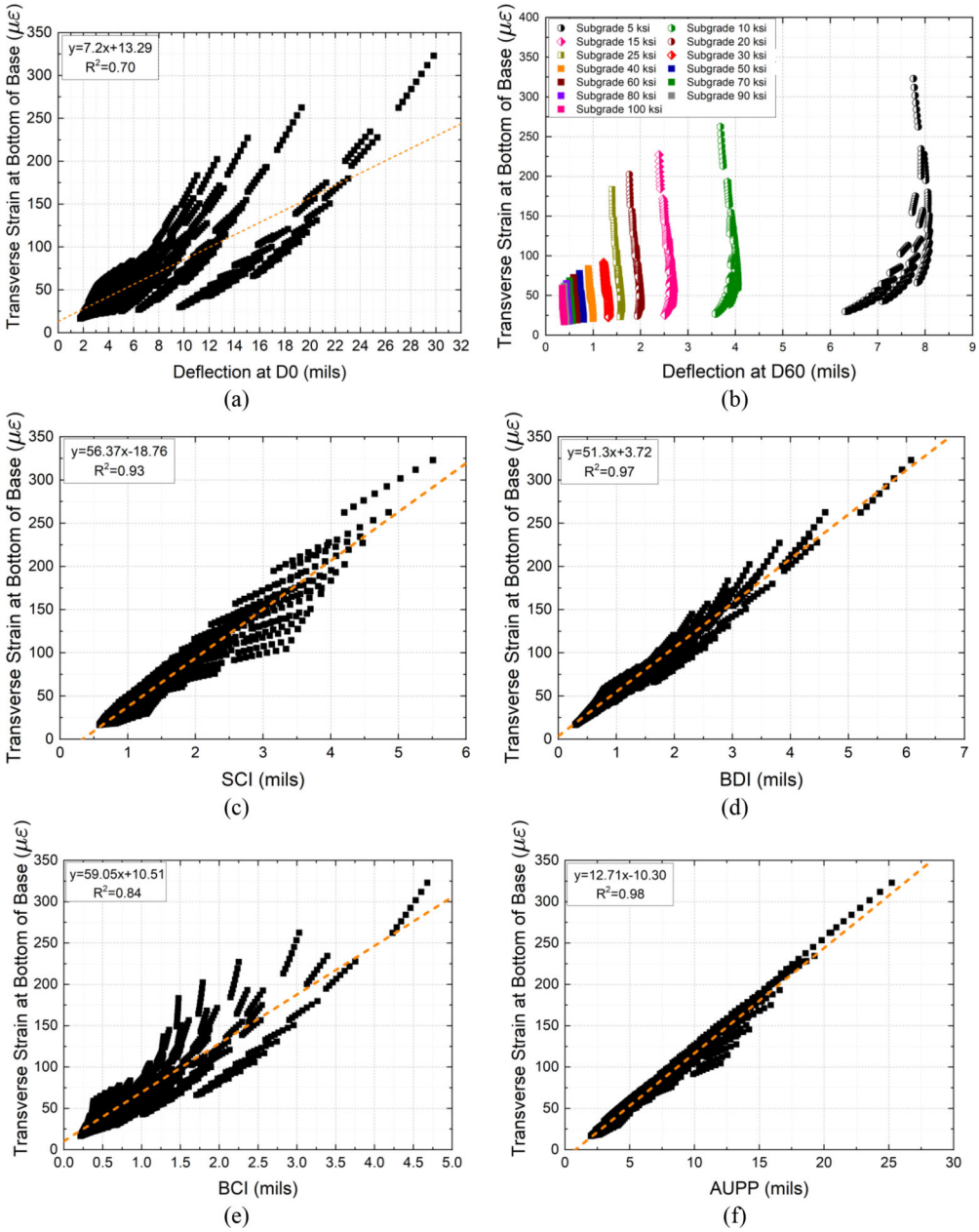

Figure 4.3 Relationships between transverse tensile strain and deflection basin parameters: (a) D_0, (b) D_{60}, (c) SCI, (d) BDI, (e) BCI, and (f) AUPP.

provide relatively accurate strain predictions. For the prediction of vertical compressive strain at the top of subgrade, Equation 4.2 was developed using BDI, and also has an R^2 value of 0.98. Equations 4.1 and 4.2 only require the AUPP or BDI, both of which can be easily determined from FWD measurements.

$$\varepsilon_t = 12.71 \times AUPP - 10.3 \qquad \text{(Eq. 4.1)}$$

where, ε_t = transverse tensile strain at the bottom of asphalt base layer (με).

$$\varepsilon_c = -124.4 \times BDI - 8.83 \qquad \text{(Eq. 4.2)}$$

where, ε_c = vertical compressive strain at the top of subgrade (με).

Further analyses were conducted to enhance Equations 4.1 and 4.2, to improve accuracy. Since several structural properties exhibited significant effects on the critical strains (see Figure 4.4), asphalt base thickness and four elastic layer moduli were added as input parameters into the prediction equations, as shown in Equation 4.3. The enhanced prediction equation includes structural coefficients (SC_1 and SC_2). The multiple linear regression method was used to develop enhanced equations, and the constant coefficients determined for critical strains are presented

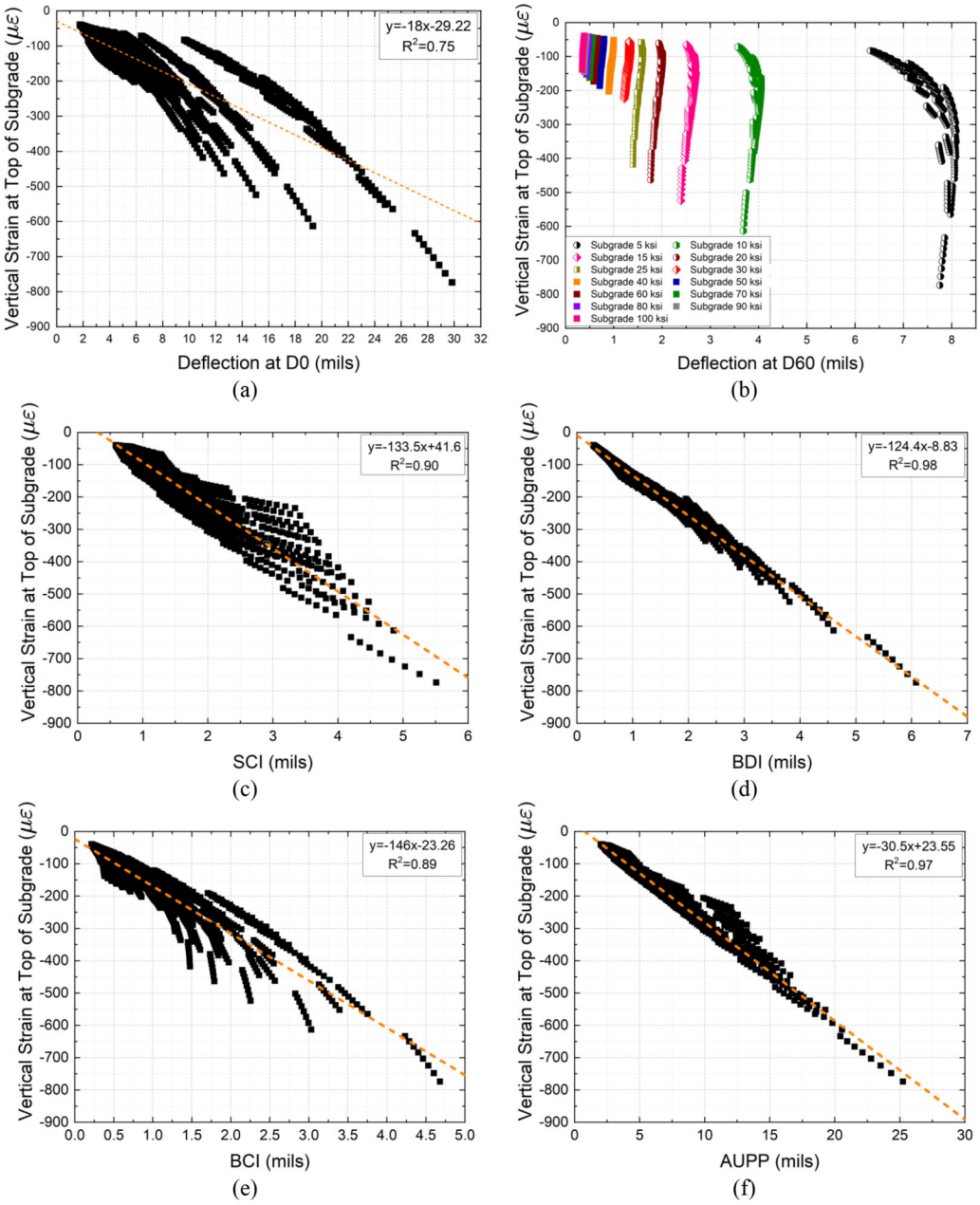

Figure 4.4 Relationships between vertical compressive strain and deflection basin parameters: (a) D_0, (b) D_{60}, (c) SCI, (d) BDI, (e) BCI, and (f) AUPP.

in Table 4.2. The inputs of Equation 4.3 require Customary units, because the coefficients were regressed using customary units.

$$\varepsilon_{critical} = C_0 + SC_1 \times BDI + SC_2 \quad \text{(Eq. 4.3)}$$

$$SC_1 = C_1 + C_2 \cdot M_R + C_3 \cdot T_{Base} + C_4 \cdot E_{Base} + C_5 \cdot E_{Surf} + C_6 \cdot E_{Int}$$

$$SC_2 = a + b \cdot M_R + c \cdot T_{Base} + d \cdot E_{Base} + C_7 \cdot E_{Surf} \cdot E_{Int}$$

$$a = C_8 \cdot M_R + C_9 \cdot T_{Base} + C_{10} \cdot E_{Base} + C_{11} \cdot E_{Surf} + C_{12} \cdot E_{Int}$$

$$b = C_{13} \cdot T_{Base} + C_{14} \cdot E_{Base} + C_{15} \cdot E_{Surf} + C_{16} \cdot E_{Int}$$

$$c = C_{17} \cdot E_{Base} + C_{18} \cdot E_{Surf} + C_{19} \cdot E_{Int}$$

$$d = C_{20} \cdot E_{Surf} + C_{21} \cdot E_{Int}$$

where, DBP = AUPP for transverse strain or BDI for vertical strain, M_R = subgrade modulus (ksi), T_{Base} = asphalt base thickness (in), E_{Base} = asphalt base modulus (ksi), E_{Surf} = asphalt surface modulus (ksi), E_{Int} = asphalt intermediate modulus (ksi), C_i constant coefficients are presented in Table 4.2.

Figure 4.5 shows the distributions of critical strains predicted by Equation 4.3. The predictions were closer to the line of equality than those of Equations 4.1 and 4.2.

TABLE 4.2
Coefficients for strain prediction equations

For Transverse Strain Equation				For Vertical Strain Equation			
C_0	21.816	C_{11}	5.671E-02	C_0	-90.8912	C_{11}	-7.269E-02
C_1	1.491E+01	C_{12}	-4.850E-02	C_1	-1.368E+02	C_{12}	7.989E-02
C_2	-7.927E-02	C_{13}	-1.612E-02	C_2	1.649E-01	C_{13}	3.449E-02
C_3	-3.139E-01	C_{14}	-8.562E-05	C_3	1.352	C_{14}	-4.050E-05
C_4	-5.528E-03	C_{15}	-1.216E-04	C_4	2.257E-02	C_{15}	2.714E-04
C_5	-6.029E-03	C_{16}	4.748E-05	C_5	4.179E-02	C_{16}	-1.480E-04
C_6	5.978E-03	C_{17}	1.078E-04	C_6	-3.275E-02	C_{17}	-2.692E-03
C_7	-2.765E-06	C_{18}	-1.374E-03	C_7	-1.854E-06	C_{18}	2.433E-03
C_8	4.501E-01	C_{19}	1.649E-03	C_8	-0.3955E-01	C_{19}	-2.588E-03
C_9	-1.902	C_{20}	-1.413E-05	C_9	4.305	C_{20}	1.338E-05
C_{10}	6.220E-03	C_{21}	1.282E-05	C_{10}	5.322E-02	C_{21}	-2.556E-05

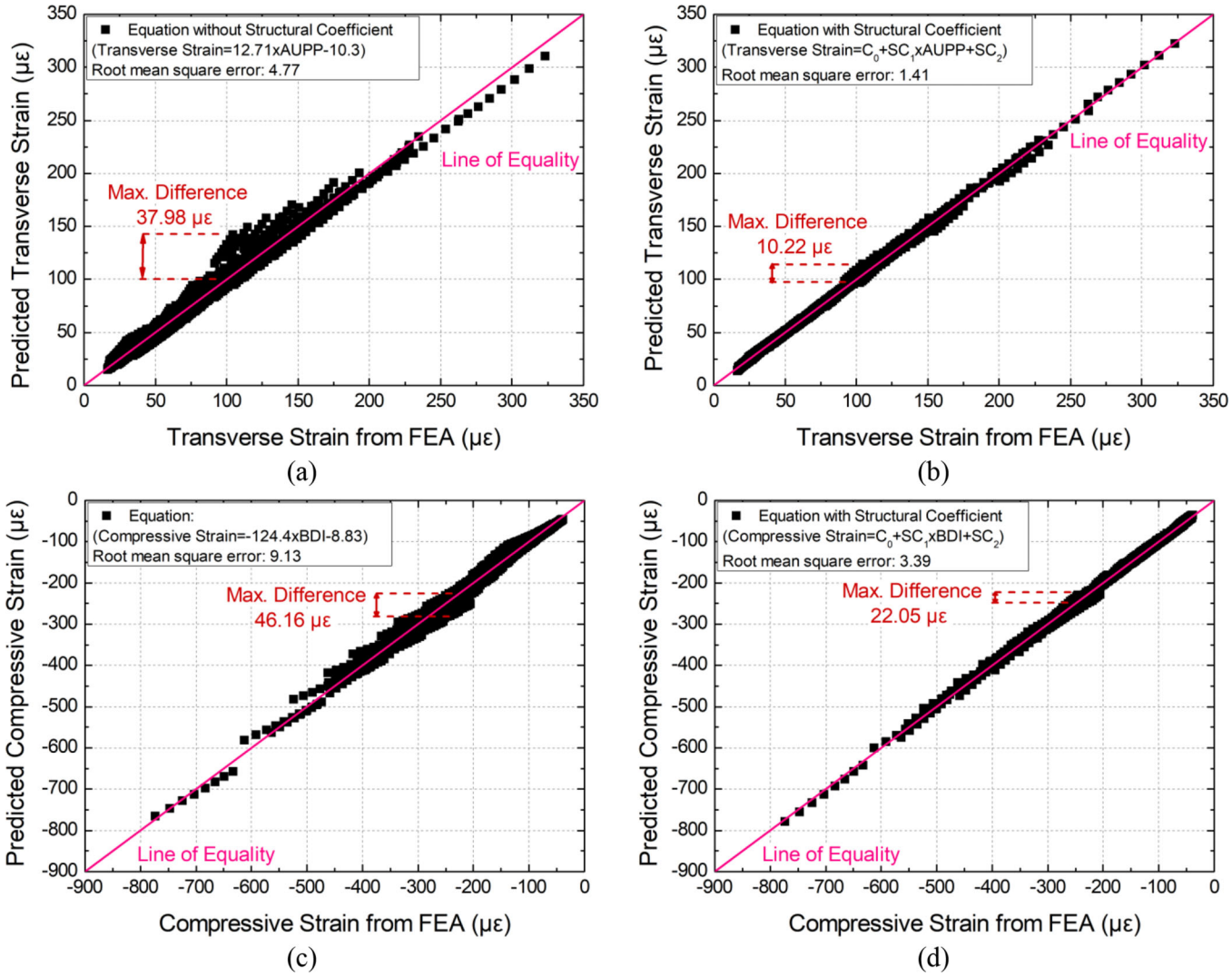

Figure 4.5 Predictive equation accuracy evaluation: (a) transverse strain equation without structural coefficients, (b) transverse strain equation with structural coefficients, (c) vertical strain equation without structural coefficients, and (d) vertical strain equation with structural coefficients.

This indicates the inclusion of structural coefficients improved the strain prediction accuracy. As shown in Figure 4.5, the root-mean-square error (RMSE) and the maximum error in the transverse tensile strain and vertical compressive strain were significantly reduced. Therefore, when structural properties are available, the enhanced equations with structural coefficients can provide more accurate prediction results.

4.3.3 Validation of Critical Strain Prediction Models

Figure 4.6 shows that the transverse tensile strains predicted by the new models are comparable to the strains measured at the bottom of asphalt layer. For Section A, the transverse tensile strain predicted by the model without structural coefficients was 4.8 με greater than the field measured transverse tensile strain, while the transverse tensile strain from the model with structural coefficients was 4.8 με less than the field measured strain. Though the models exhibit opposite trends, their error in strain prediction is similar and acceptable. However, for Section B, the model with structural coefficients exhibited a better transverse tensile strain prediction than did the model without structural coefficients. In total, the model with structural coefficients provides reasonably accurate transverse tensile strain predictions for both Sections A and B.

The strain prediction models were further validated with two field-measured strains and seven strains obtained from calibrated FE models, as strain gauges were embedded in only two sections. Figures 4.7 and 4.8 show comparisons of the predicted and measured transverse tensile and vertical compressive strains, respectively. Figure 4.7(a) shows the model without structural coefficients slightly overestimated the transverse tensile strain as compared to the measured strain at the bottom of the asphalt layer, but the strain predictions are reasonably accurate of the measured.

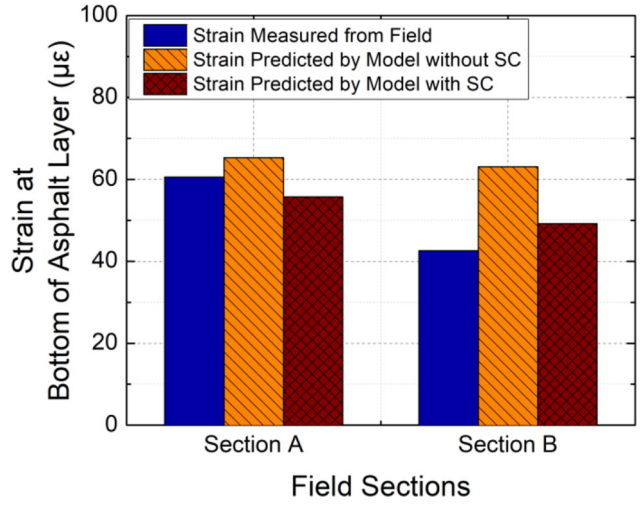

Figure 4.6 Comparison of field measured and predicted strains.

As shown in Figure 4.7(b), the model with structural coefficients exhibits a better transvers tensile strain prediction than the model without the structural coefficients. This confirms the use of additional structural information provides a more accurate strain estimation.

For the vertical compressive strain at the top of subgrade, both prediction models exhibit a similar accuracy, as shown in Figure 4.8. The same R^2 value (0.93) and a very similar RMSE (model without structural coefficients: 23.4 με, model with structural coefficients: 23.3 με) were observed from both models. Results show the model without structural coefficients can be practically applied to estimate an approximate strain level of in-service, full-depth asphalt flexible pavements for both transverse tensile strain and vertical compressive strain. In addition, the model with structural coefficients can be used to obtain a more accurate strains, if the additional structural information is available.

4.4 Development of Effective Structural Number (SN_{eff}) Prediction Models

4.4.1 Current SN_{eff} Prediction Methods

According to the literature, there are two common methods to predict the SN_{eff} using FWD data and the total pavement thickness: (1) the AASHTO 1993 NDT method currently used by the INDOT, and (2) the Rohde model (Rohde, 1994). These two methods were selected for further evaluation because both consider the pavement thickness, a main factor differentiating full-depth asphalt flexible pavements from conventional flexible pavements. The AASHTO 1993 method is expressed in Equations 4.4 and 4.5.

$$SN_{eff} = 0.0045 \times H_p \times \sqrt[3]{E_p} \qquad \text{(Eq. 4.4)}$$

$$D_0 = 1.5 \times p \times a \times \left(\frac{1}{M_R \times \sqrt{1 + \left(\frac{H_p}{a} \times \sqrt[3]{\frac{E_p}{M_R}} \right)^2}} + \frac{1 - \frac{1}{\sqrt{1 + \left(\frac{H_p}{a} \right)^2}}}{E_p} \right) \qquad \text{(Eq. 4.5)}$$

where, p is the contact pressure (psi), a is load radius (in.), H_p is total pavement thickness above the subgrade (in.), M_R is the subgrade modulus (psi), E_p is the effective pavement modulus above the subgrade (psi), and D_0 represents the measured deflection at the center of FWD loading plate (in.). The E_p can be determined by an iterative process using Equation 4.5. However, the Rohde model can estimate the SN_{eff} without an iterative process. One major drawback of the Rohde model is that $D_{1.5Hp}$ is not directly measured from the

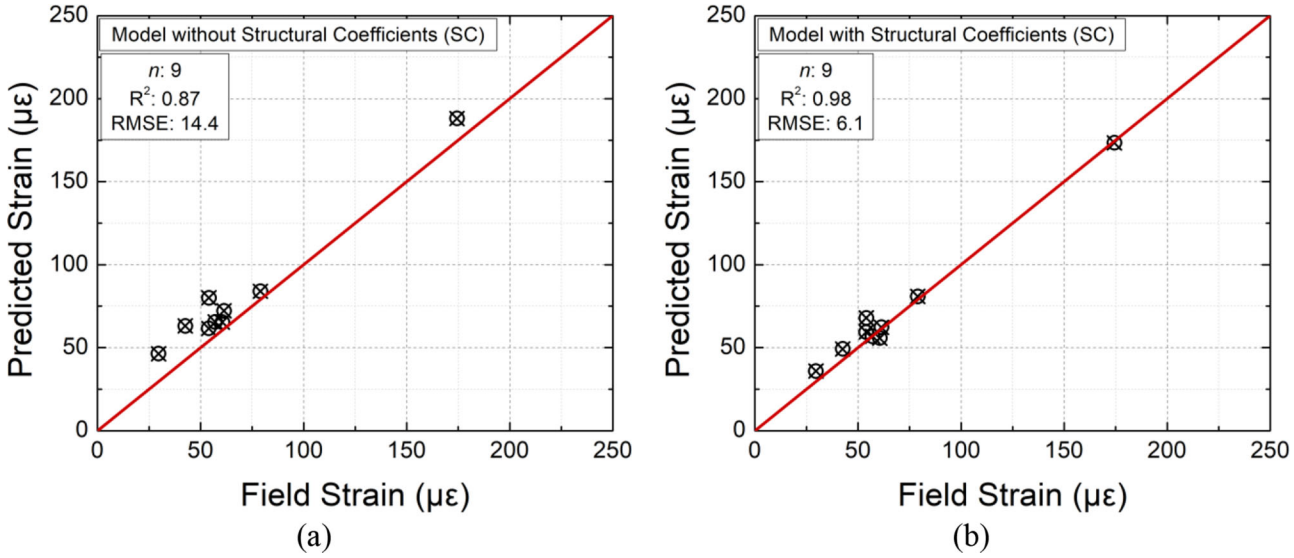

Figure 4.7 Transverse tensile strain prediction validation: (a) model without structural coefficients, and (b) model with structural coefficients.

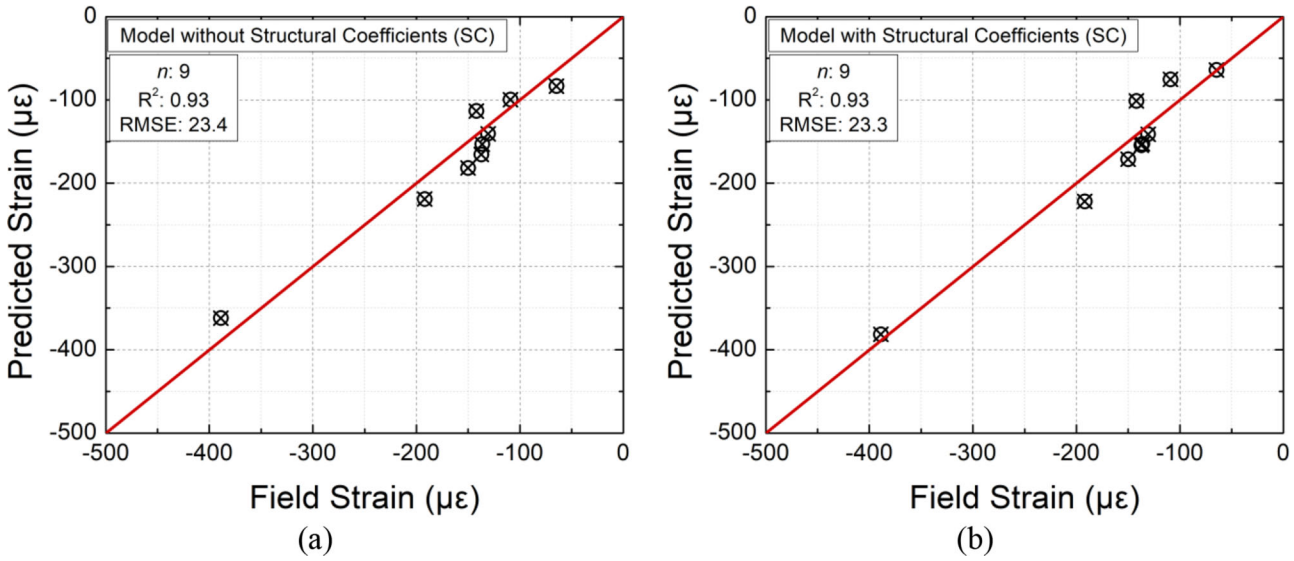

Figure 4.8 Vertical compressive strain prediction validation: (a) model without structural coefficients, and (b) model with structural coefficients.

FWD testing, but is dependent on the H_p. Therefore, caution must be exercised when using it.

Figure 4.9 shows a comparison between AASHTO 1993 and Rohde methods. Overall, the Rohde model provides slightly larger SN_{eff} as compared to the AASHTO 1993 method for both model-based and field-sourced FWD data. It should be noted that full-depth asphalt flexible pavement was not considered during Rohde model development. This indicates that the Rohde model may further overestimate structural conditions of full-depth asphalt flexible pavements, as compared to the AASHTO 1993 method. Since there is a concern about overestimating SN_{eff} from the AASHTO 1993 method, both the Rohde model and the AASHTO 1993 method may need calibration prior to use with full-depth asphalt flexible pavements.

4.4.2 New SN_{eff} Prediction Model for Full-Depth Asphalt Flexible Pavements

A new model was developed based on the SN_{eff} from the calibrated Rohde model. Ten parameters, including five FWD deflection locations (D_0, D_{12}, D_{24}, D_{36}, and D_{60}), four DBPs (AUPP, SCI, BDI, and BCI), and H_p, were examined to determine appropriate input parameters for the SN_{eff} prediction model. The Pearson correlation coefficient (Pearson's r) and Spearman's rank correlation coefficient (Spearman's ρ) were used to

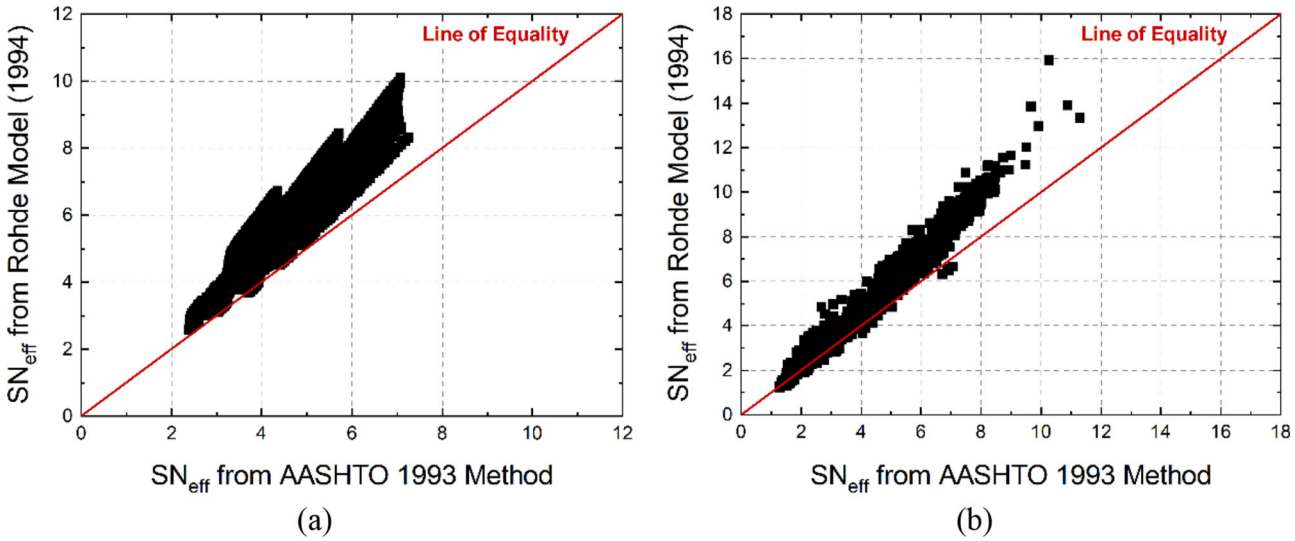

Figure 4.9 AASHTO 1993 and Rohde methods comparison: (a) model-based FWD data, and (b) field FWD data.

identify the most relevant parameters for SN_{eff} prediction. As indicated in Table 4.3, all FWD parameters are negatively correlated with the SN_{eff}, while H_p is positively correlated, based on Pearson's r and Spearman's ρ results. The AUPP and H_p were selected as input parameters for the SN_{eff} prediction model both are considered key factors for estimating full-depth asphalt flexible pavement SN_{eff}, and both exhibit fairly high correlation coefficients.

The new SN_{eff} prediction model was developed using nonlinear regression analysis of the model-based FWD data, as expressed in Equation 4.6.

$$SN_{eff} = 3.097 \times H_p^{0.2746} \times AUPP^{-0.3247} \qquad \text{(Eq. 4.6)}$$

where AUPP is the area under pavement profile (mils). The accuracy of the new SN_{eff} prediction model was investigated based on the goodness-of-fit tests shown in Equation 4.7 through 4.10 (Abd El-Raof et al., 2020; Khattab et al., 2014).

$$S_y = \sqrt{\frac{1}{n-1}\sum_{i=1}^{n}(SN_{eff,Rohde} - \overline{SN_{eff,Rohde}})^2} \qquad \text{(Eq. 4.7)}$$

$$S_e = \sqrt{\frac{\sum_{i=1}^{n}(SN_{eff,New\ Model} - SN_{eff,Rohde})^2}{n-p}} \qquad \text{(Eq. 4.8)}$$

$$R^2 = 1 - \frac{n-p}{n-1}\left(\frac{S_e}{S_y}\right)^2 \qquad \text{(Eq. 4.9)}$$

$$RMSE = \sqrt{\frac{1}{n}\sum_{i=1}^{n}(SN_{eff,New\ Model} - SN_{eff,Rohde})^2} \qquad \text{(Eq. 4.10)}$$

where, S_y is the standard deviation of the SN_{eff} from the calibrated Rohde model, and S_e is the standard deviation of the error. Higher R^2, lower S_e/S_y and RMSE values indicate higher prediction result accuracy.

Figure 4.10(a) shows a comparison of the SN_{eff} predicted by the new model with the SN_{eff} calculated using the calibrated Rohde model, using the model-based FWD data. The new model demonstrates high accuracy, with $R^2 = 0.99$, $S_e/S_y = 0.07$, and RMSE = 0.034. The same analyses for BDI and SCI exhibited lower correlations ($R^2 = 0.96$ and 0.98, respectively), confirming AUPP as the best DBP input to predict SN_{eff}.

Additionally, both the calibrated Rohde and new models were also applied to field-sourced FWD data for validation. It is important to note that the field FWD data was not used for the new prediction model development but only used for the model validation. As shown in Figure 4.10(b), the new model again exhibited high accuracy in terms of SN_{eff} prediction. The new model shows $R^2 = 0.99$ and Se/Sy = 0.06, while the RMSE slightly increased from 0.034 to 0.070. These results indicate the new model predicts SN_{eff} as accurately as the calibrated Rohde model for full-depth asphalt flexible pavements. In addition, the new model is more practical, as it eliminates the need for $D_{1.5Hp}$.

4.5 Summary

Finite element analyses were conducted to explore the relationship between DBPs and critical strains in full-depth asphalt flexible pavements. These relationships led to the development of critical strain prediction models based on FWD data. A new SN_{eff} prediction model was developed using both field- and model-based FWD data. The models were validated using field data, including FWD test results, strain measurements, and material properties of field cores. These models can estimate the structural capacity of full-depth flexible pavements. Key findings are as follows.

TABLE 4.3
Correlation coefficients between effective structural number and deflection parameters

FWD Parameters	Correlation to SN_{eff}	
	Pearson's *r*	Spearman's *ρ*
H_p	0.704	0.731
D_0	-0.672	-0.727
D_{12}	-0.617	-0.654
D_{24}	-0.545	-0.553
D_{36}	-0.489	-0.482
D_{60}	-0.416	-0.381
AUPP	-0.839	-0.954
SCI	-0.828	-0.927
BDI	-0.831	-0.944
BCI	-0.751	-0.801

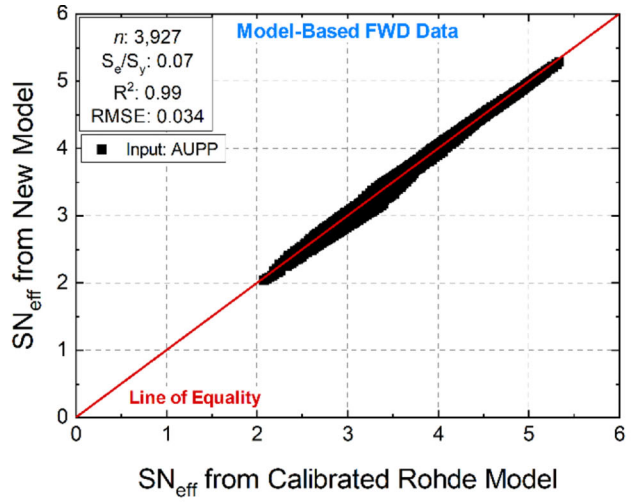

(a)

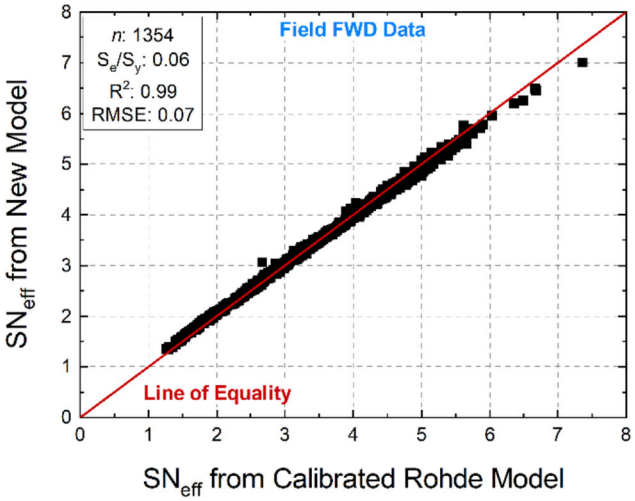

(b)

Figure 4.10 Comparison of the effective structural numbers predicted from the new model and the calibrated Rohde model: (a) model-based FWD data, and (b) field-sourced FWD data.

- The finite element (FE) model developed using field cores accurately simulated pavement behavior, closely matching measured strains at the asphalt layer bottom.
- Subgrade and asphalt base properties have a more significant influence on pavement responses than asphalt surface and intermediate layers due to the relatively smaller thicknesses of the latter two.
- Deflection basin shape parameters correlate better with critical strains than individual deflection values, underscoring their importance in structural condition assessments.
- AUPP and BDI were effective predictors of transverse tensile strain at the bottom of the asphalt base layer and vertical compressive strain at the subgrade top, respectively. The models achieved an R^2 of 0.98, confirming their reliability. Incorporating structural properties improved prediction accuracy.
- Transverse tensile strains predicted by the models aligned well with strains from two field sections. Including structural parameters improved accuracy in predicting transverse tensile strains, while vertical compressive strain predictions showed consistent accuracy across models.
- AUPP exhibited the strongest correlation with SN_{eff}, while pavement thickness (H_p) also significantly influenced SN_{eff} predictions.
- The new SN_{eff} model predicts nearly identical results to the calibrated Rohde model using only AUPP and Hp, simplifying the process.

Further work is recommended to extend the new SN_{eff} prediction model to other full-depth asphalt flexible pavement structures (i.e., additional layer thicknesses and layer moduli combinations), following the approach presented herein.

5. RIGID PAVEMENT MODELS FOR STRUCTURAL CONDITIONS

5.1 Introduction

The SSR, defined as the ratio of applied stress to flexural strength, has been widely used to assess the fatigue of concrete materials. Delatte (2018) reported that damage to PCC slab due to stress may be insignificant when the SSR is less than 0.45. For rigid pavements, Equation 5.1 can be used to calculate the SSR of a PCC slab.

$$SSR = \frac{\sigma_{max}}{f_r} \qquad \text{(Eq. 5.1)}$$

where, σ_{max} is the maximum stress in the PCC slab, and f_r is the PCC modulus of rupture (or flexural strength). Equation 5.2, dictated in ACI 318-19, can be used to estimate PCC flexural strength from the compressive strength (ACI, 2022).

$$f_r = 7.5 \times \sqrt{f'_c} \qquad \text{(Eq. 5.2)}$$

where, f_r is the PCC modulus of rupture (or flexural strength) (psi), f'_c is a compressive strength (psi).

When a collection of field cores is not available, the PCC slab elastic modulus, back calculated from FWD deflections, can be used to estimate the flexural strength

of the PCC slab. According to ACI 318-19, the elastic modulus of PCC can be estimated from the compressive strength using Equation 5.3 (ACI, 2022). Solving Equation 5.2 and Equation 5.3, the flexural strength can be determined from the back calculated elastic modulus using Equation 5.4.

$$E = w^{1.5} \times 33 \times \sqrt{f_c'} \qquad \text{(Eq. 5.3)}$$

$$f_r = \frac{0.227 \times E}{w^{1.5}} \qquad \text{(Eq. 5.4)}$$

where, w is the PCC unit weight (pcf), and E is the modulus of elasticity (psi). Even though the PCC slab flexural strength can be estimated, it is challenging to measure the maximum stress of in-service pavements. Thus, this study focuses on identifying the relationships between FWD deflections and the maximum stress in a PCC slab to develop an SSR prediction model.

5.2 Finite Element Model Development

An FE model was developed to generate a synthetic database, covering a broad range of pavement structures and environmental conditions. The synthetic database consists of FWD deflections and corresponding SSR and was used to develop an SSR prediction model. A total of 432 FE models were developed to simulate various rigid pavement structures and environmental loading conditions. The FE model details are described in Appendix C.

5.2.1 Pavement Structure and Material Properties

A typical INDOT JPCP structure was simulated using the commercial FE software Abaqus. The simulated pavement cross section consists of two layers on top of the subgrade, a PCC slab and an underlying aggregate base layer. As presented in Table 5.1, all layers were modeled as linear elastic materials. In addition, the coefficient of thermal expansion was used for PCC slabs to simulate PCC slab curling behavior under various temperature conditions.

The parameters considered for the compilation of the synthetic database are summarized in Table 5.2 and were selected based on the typical INDOT JPCP structures. Three levels of temperature gradient were applied to consider a wide range of environmental conditions: no curling (32°F), upward curling (10.4°F), and downward curling (53.6°F). Given the parameter ranges in Table 5.2, data was collected from a total of 432 combinations, covering most JPCP structures and environmental conditions in Indiana.

TABLE 5.1
Finite element JPCP structure model

Layer	Material Type	Poisson's Ratio	Thermal Expansion
PCC Surface	Linear elastic	0.20	Yes
Aggregate Base	Linear elastic	0.40	No
Subgrade	Linear elastic	0.45	No

5.3 Development of Stress-to-Strength Ratio Prediction Model

5.3.1 Relationships Between Deflection Basin Parameters and Stress-to-Strength Ratio

The synthetic database was used to investigate the correlations between FWD deflection parameters and SSR. The maximum stress was obtained from the FE analysis to calculate the SSR. The flexural strength was estimated based on the Equation 5.4. The unit weight of PCC was assumed to be 140 lbs/ft^3.

Figure 5.1 shows a comparison of SSR with six FWD deflection parameters. Overall, SSR increased as deflection parameters increased except for the D60. Otherwise, as shown in Figure 5.1(b), D60 values were mainly affected by the subgrade modulus; a greater subgrade modulus resulted in a smaller D60 deflection.

As shown in Figure 5.1, both AUPP and SCI exhibit strong linear correlations with SSR, as they represent the structural conditions in the upper pavement layer PCC slab. The curling effect was insignificant for AUPP and SCI, improving their correlations with SSR. Figure 5.2 compares FWD deflection basin curves for less stiff and higher stiffness PCC slabs with elastic moduli of 800 ksi and 5,000 ksi, respectively. Curling significantly affected the deflection basin curve for the stiffer slab, while the less stiff slab showed negligible differences under varying curling conditions. However, the shape of the deflection basin curves near the loading center remained consistent for all stiffness levels, regardless of curling effects. As AUPP and SCI are derived from interpreting the shape of deflection basin curve near the loading center, they were unaffected by curling, ensuring reliable correlations with SSR.

Additionally, a statistical analysis was conducted to identify the best deflection parameter for use as an input for SSR prediction. Pearson's r and Spearman's ρ were used to evaluate the strength of correlation between DBPs and SSR. As presented in Table 5.4, all FWD parameters exhibited positive correlations with SSR. Furthermore, SCI exhibited the highest values for both Pearson's r and Spearman's ρ which is a consistent trend observed in Figure 5.1. Thus, SCI was selected as the input parameter for predicting SSR.

5.3.2 Stress-to-Strength Ratio Prediction Model

A linear regression method was used to develop the SSR prediction model based on the synthetic database. Equation 5.5 expresses the developed predictive equation for SSR using SCI as the input.

$$SSR = 0.3471 \times SCI + 0.005656 \qquad \text{(Eq. 5.5)}$$

where, SSR is a stress-to-strength ratio, and SCI is a surface curvature index (*mils*).

TABLE 5.2
Parameters and parameter ranges for the synthetic database

Parameters	Range
PCC Slab Thickness, inch	9, 12, 14
PCC Modulus, ksi	800; 1,000; 2,000; 3,000; 4,000; 5,000
Aggregate Base Layer Thickness, inch	9
Aggregate Base Modulus, ksi	30, 40, 100
Subgrade Modulus, ksi	10, 15, 30
PCC CTE, /°F	9.72×10^{-6}
Temperature Gradient, °F	10.4, 32, 53.6

TABLE 5.3
Correlation coefficients between SSR and FWD deflection parameters

	Correlation to SSR	
FWD Parameters	Pearson's r	Spearman's ρ
D_0	0.671	0.630
D_{60}	0.146	0.158
AUPP	0.978	0.952
SCI	0.989	0.976
BDI	0.948	0.917
BCI	0.841	0.799

The accuracy of the SSR prediction model was assessed using the R^2 and the RMSE. Figure 5.3 shows a comparison of the predicted and calculated SSR from FE analysis. The R^2 of 0.98 indicates that the accuracy of the SSR prediction model is fairly high, and the low RMSE of 0.026 further confirms that the potential error in SSR prediction is insignificant.

In addition, the SSR predicted can be used to estimate the remaining service life of JPCP, following the MEPDG approach, as expressed in Equation 5.6 (AASHTO, 2020). It should be noted that the calibration constants in Equation 5.6 can be determined based on the historical database, depending on field conditions.

$$logN_f = C_1 \times \left(\frac{1}{SSR}\right)^{C_2} \qquad \text{(Eq. 5.6)}$$

where, N_f is allowable number of load applications, SSR is a stress-to-strength ratio, and C_i are calibration constants.

5.4 Effect of Curling on Stress-to-Strength Ratio Prediction

The effect of curling on SSR prediction was investigated. A dataset of SSR calculated without curling conditions was used as a reference, and Figure 5.4 shows the differences between the reference SSR (no curling) and the SSR under daytime or nighttime curling conditions. Depending on the level of SSR, the variation of SSR was altered by up to 0.07 due to curling stress. The curling effect was generally greater at lower SSR levels (less than 0.45 recommended by Delatte (2018)). This means that the curling conditions have a great influence on SSR when the PCC slab is stronger, which aligns with the trend observed in Figure 5.2. Since the primary application of SSR prediction in the PMS focuses on weaker pavements, the errors in SSR prediction due to curling conditions, may be negligible for PMS purpose. Furthermore, it is important to note that the potential error in practice may be smaller than 0.07. Therefore, the developed SSR prediction model can be used to estimate the structural capacity of JPCP without considering curling conditions during FWD tests.

5.5 Summary

In this study, the SSR prediction model was developed to evaluate the structural conditions of in-service rigid pavements using the FWD deflection data. A synthetic database was established to consider various pavement structures and environmental conditions, and it was used for SSR prediction model development. A summary of findings is presented as follows.

- The FE model was successfully developed to accurately simulate the behavior of JPCP under the FWD loading and was validated with field FWD data.
- Both AUPP and SCI exhibited stronger linear correlations with SSR compared to the other parameters, because they represent the structural conditions of the upper layer, which is typically the PCC slab in rigid pavements, and SSR is a structural indicator of the PCC slab.
- The effect of curling on FWD deflection basin curve was greater when the PCC slab was stiffer. However, for any stiffness level of the PCC slab, the shapes of FWD deflection basin curve near the loading center were similar, regardless of the curling conditions.
- The SCI exhibited the strongest correlation with SSR and was selected as an input for the SSR prediction model. The accuracy of the SSR prediction model was fairly high, with an R^2 of 0.98, and the low RMSE of 0.026 further confirms that the potential error in SSR prediction is insignificant.
- The SSR was primarily affected by curling conditions within the acceptable range (less than 0.45), while the curling effect was insignificant for weaker PCC slabs with higher SSR.

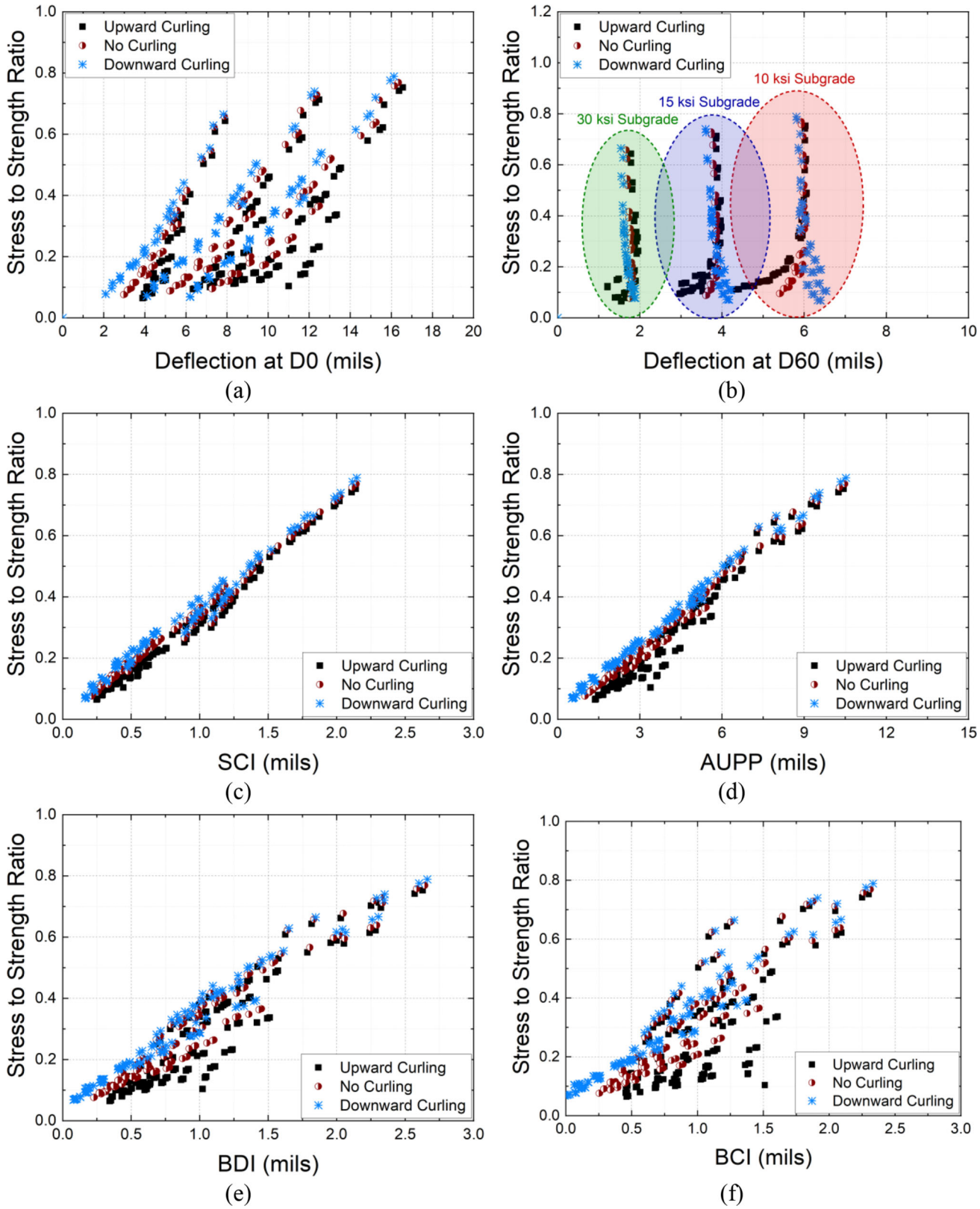

Figure 5.1 Relationships between FWD deflections and DBPs, and stress-to-strength ratio: (a) deflection at D0, (b) deflection at D60, (c) SCI, (d) AUPP, (e) BDI, and (f) BCI.

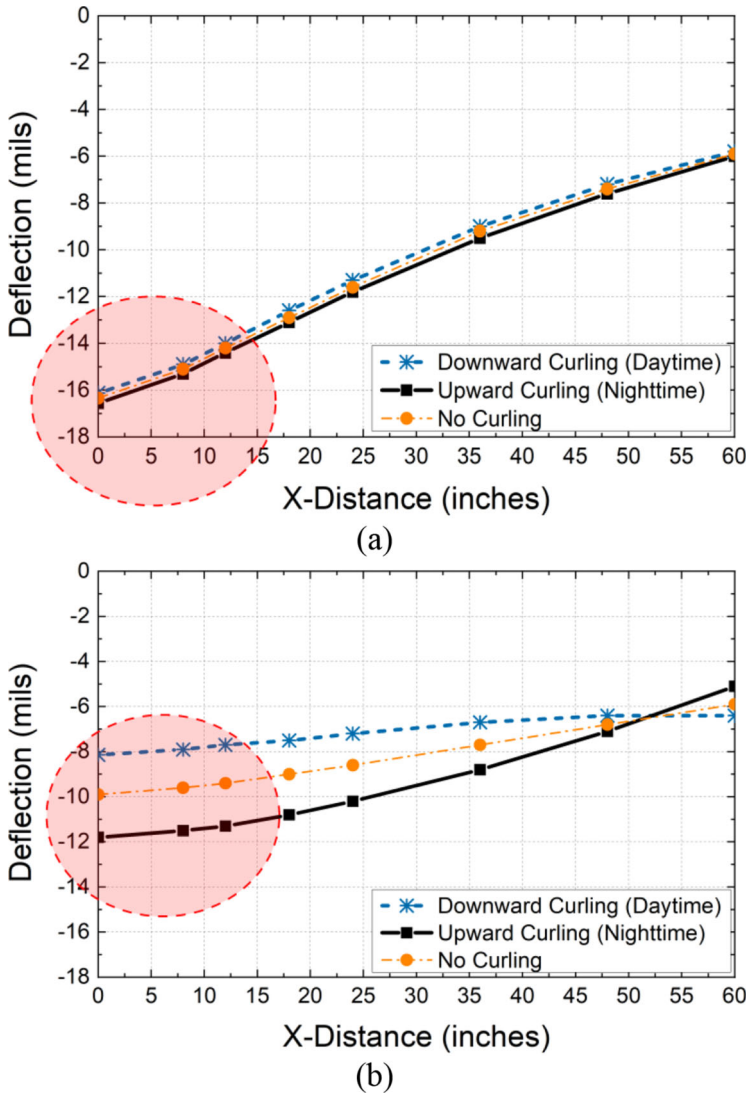

Figure 5.2 PCC slab curling effects on FWD deflection basin curves: (a) less stiff PCC slab, elastic modulus of 800 ksi, and (b) stiffer PCC slab, elastic modulus of 5,000 ksi.

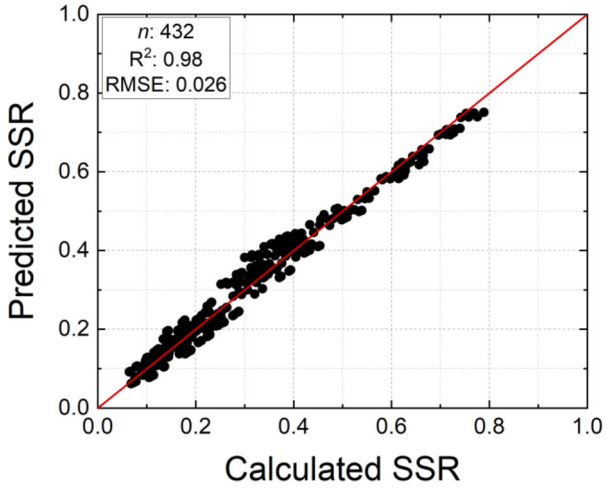

Figure 5.3 Validation of SSR prediction model.

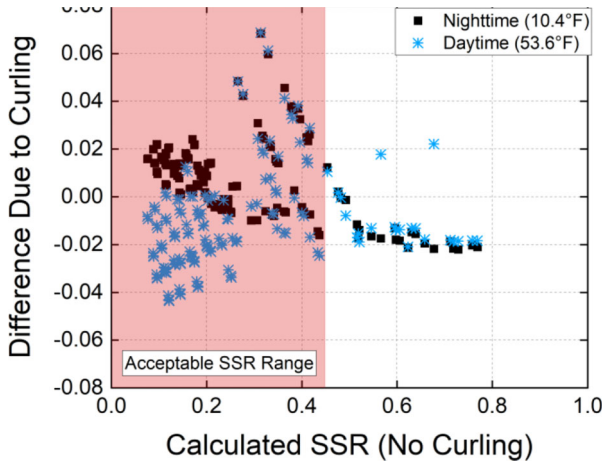

Figure 5.4 Curling effects on SSR.

Based on these findings, it is concluded that the developed SSR prediction model effectively estimates the structural capacity of in-service rigid pavements using FWD deflection data without requiring structural analysis to calculate maximum stress. The curling effect on SSR prediction was found to be insignificant, enabling the model's application without accounting for curling conditions, which is beneficial given the challenges in estimating curling in-service pavements.

Although based on a synthetic database encompassing a wide range of pavement structures, further research is recommended to improve accuracy by incorporating various aggregate base thicknesses and stiffness levels for the base and subgrade. In addition, joint FWD testing is also important to understand the LTE of in-service JPCP. It is recommended to investigate joint behavior under FWD loading using the FE model presented in this study. Such studies could offer valuable insights for assessing LTE in-service pavements and enhancing pavement management systems.

6. COMPOSITE PAVEMENT MODELS FOR STRUCTURAL CONDITIONS

6.1 Introduction

The mechanical responses of composite pavements during FWD testing are more complex than those of conventional flexible pavements. Even though the research primarily focuses on characterizing the mechanical responses of the asphalt layer, the FWD tests can present three potential scenarios: (a) loading plate over the PCC slab joint, (b) loading plate and sensors over different PCC slabs, and (c) loading plate and sensors over the same PCC slab, as shown in Figure 6.1. The study focuses on the (b) and (c) scenarios, as scenario (a) is uncommon during field tests. Considering that composite pavement is inhomogeneous in the longitudinal and transverse directions, the distribution of mechanical responses should also be analyzed from both directions.

6.2 Finite Element Model Development

Three-dimensional FE models were developed to simulate the mechanical responses of composite pavements under FWD loads. A total of 20 conditions were simulated, considering variables such as asphalt layer moduli, asphalt layer thickness, distance between the PCC slab joint and loading position, and reflective crack depth. These variations, listed in Table 6.1, were selected to cover a wide range of pavement material properties and structures most commonly found in Indiana. It is important to note that "loading distance" refers to the distance between the PCC slab joint and loading position. Additionally, different crack depths were used to simulate the mechanical responses of reflective crack propagation. Models Nos. 19 and 20 were developed based on data from US 20 and US 40, for verification purposes. The details of the FE model are described in Appendix C.

6.3 Development of the PCC Slab Joint Recognition Model

6.3.1 Analysis of Finite Element Model-Based FWD Data

The homogeneity of horizontal strain in composite pavement was analyzed based on the FE simulations. The simulation results indicate that composite pavement exhibits different mechanical responses in various directions near the joint area. Figure 6.2(a) shows the mechanical responses at the bottom of the asphalt layer in the longitudinal direction when the FWD impact occurs 6 inches away from the PCC slab joint (Case 8). Figure 6.2(b) presents mechanical responses in the transverse direction on the joint (the vertical red line in Figure 6.2(a)). As seen in Figure 6.2, the shear and normal strains in the longitudinal direction are significantly larger than those in the transverse direction. These results are consistent with expectations, as PCC slab joints can cause substantial horizontal tensile normal and shear strains in the asphalt layer. Consequently, the subsequent analysis focuses on the tensile normal and shear strains in the longitudinal direction.

FE models were developed to simulate responses at varying loading distances. Figure 6.3(a) and (b) illustrate the effect of the loading distance on normal and shear strains. Under the FWD loading plate, the mechanical responses show the most significant fluctuation at the bottom of the asphalt layer. This fluctuation, referred to as the "first fluctuation," is directly induced by the FWD loading. The normal strain exhibits a half-sine waveform, while the shear strain shows a sine waveform. The amplitudes of the normal strain are approximately twice those of the shear strain. When focusing on the PCC slab joint area, the normal and shear strains present additional fluctuation that can affect the deflection basin. This fluctuation, named the "second fluctuation," results from the combined effects of FWD loading and the PCC slab joint. Therefore, the second fluctuation could be used to identify the PCC slab joint position. The extreme values in the second fluctuation were extracted and plotted in Figure 6.3(c) to observe the trends. With the loading distance increasing, the extreme values of the normal and shear strains decrease from 32.0 to -6.2 με and from 42.8 to 1.2 με, respectively. It is worth noting that when the loading position is within 27 inches of the joint, tensile strain appears at the bottom of the asphalt layer. When the loading distance exceeds 27 inches, a low-level compressive strain is observed in the asphalt layer. This indicates that the normal strain could be a suitable mechanical response to identify the loading distance.

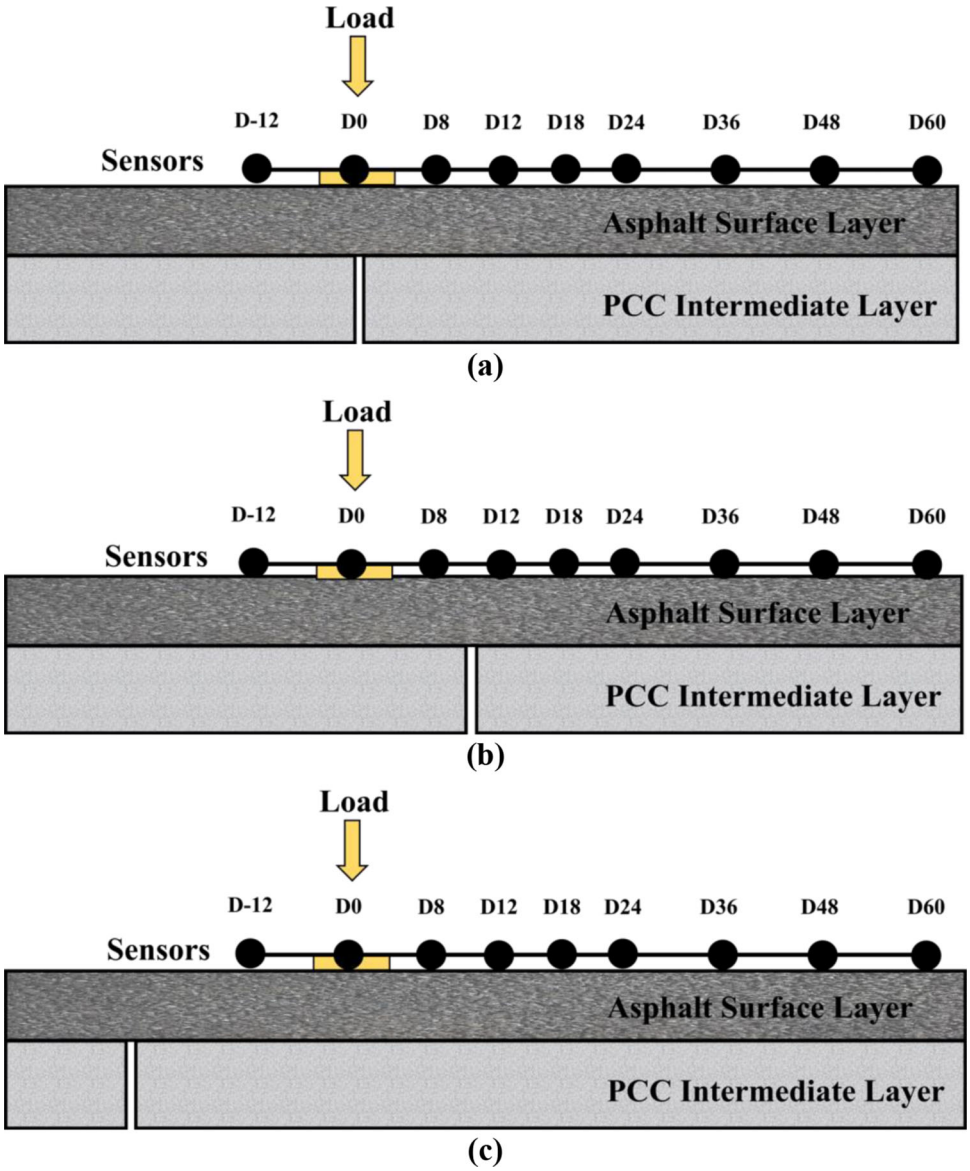

Figure 6.1 FWD testing scenarios: (a) loading plate on the joint, (b) loading plate and sensors on different slabs, and (c) loading plate and sensors on the same slab.

The stability of the normal and shear strains is verified in the following sections.

Figures 6.4 and 6.5 illustrate the influence of the asphalt layer modulus and thickness on the mechanical responses when the loading distance is 30 inches. In these simulations, the asphalt layer modulus and thickness were varied while keeping the other parameters in the FE models constant. In Figures 6.4 and 6.5, normal and shear strains present the first and second fluctuations as expected. The extreme values in the second fluctuation are illustrated in Figure 6.6. From Figure 6.6(a), the extreme values of compressive normal and shear strains decrease as the asphalt layer modulus increases. From Figure 6.6(b), the extreme values of compressive normal and shear strains decrease as the asphalt layer thickness increases.

The effects of loading distance, asphalt layer modulus and thickness on the normal and shear strains are shown in Table 6.2. The data indicate the normal and shear strains are sensitive to changes in loading distance. Thus, both the asphalt layer modulus and thickness can be considered as indices to identify PCC slab joint locations. However, the asphalt layer modulus and thickness have less influence on the normal strain than the shear strain. This suggests the normal strain in the second fluctuation has better stability than the shear strain. As aforementioned, the compressive normal strain can change to tensile normal strain when the FWD loading is close to the PCC slab joint. Therefore, it is recommended the extreme value of normal strain in second fluctuation be used to identify PCC slab joint locations.

TABLE 6.1
FE model variables

No.	Layer Thickness (inches)		Asphalt Layer Modulus (ksi)	Loading Pressure (psi)	Loading Distance (inches)	Cracking Depth (inches)
	Asphalt Mix	PCC				
1	5	9	885	62.5	0	0
2					6	
3					18	
4					30	
5					42	
6					54	
7					66	
8			885	80	6	0, 1.25, 2.5, 3.75
9					30	
10					66	0
11			285		30	
12			585			
13			1,185			
14			1,485			
15	7		885			
16	9					
17	11					
18	4				6	1, 1.25, 2, 2.5, 3, 3.5, 3.75
19	7	8.7	885		30	0
20	11.5	8.4	885		30	

Note: A crack depth of "0" indicates no reflective crack.

6.3.2 Development of the Reflective Crack Damage Estimation Model

Upon confirming the PCC slab joint location, reflective cracking propagation can be investigated. The FE models simulated reflective cracking ranging from 1 to 3.75 inches in a 4-inches asphalt layer (Case 18). Figure 6.7 shows the extreme values of mechanical responses in the second fluctuation with different reflective crack depths. It is observed that the extreme value of shear strain increases as the crack depth increases, having an exponential curve. When the crack depth reaches 75% of the asphalt layer thickness, the shear strain sharply increases, while the normal strains in longitudinal and vertical directions increase slightly. This suggests the extreme value of shear strain can be used as a critical mechanical response to evaluate reflective cracking.

To estimate reflective cracking using the field test data, the correlations between the DBPs and the shear strain were tested. Figure 6.8 presents the DBPs at various reflective crack depths. The SCI and AUPP exhibit a similar trend with the extreme value of shear strain in the second fluctuation. Pearson correlation coefficients demonstrate that SCI has a strong correlation with shear strain, as shown in Figure 6.8. Hence, SCI can be used to estimate reflective crack depths in composite pavements during FWD testing. Maintenance options may be considered when the SCI increases drastically in the PCC slab joint area.

The result from Figure 6.8 shows that an exponential trend exists between the SCI and reflective crack depth. Reflective Crack Damage (RCD), which is the ratio of the crack depth to the asphalt overlay thickness, can be used to evaluate the composite pavement. The regression model is shown in Equation 6.1.

$$RCD = a\ ln\ (b \times SCI),\ RCD > 0 \qquad \text{(Eq. 6.1)}$$

where a and b are regression parameters. Based on the FE simulation results, a = 2.044 and b = 0.596. A large RCD indicates a short remaining service life. A fatigue fracture model was utilized to estimate pavement fatigue life, as shown in Equations 6.2 and 6.3 (AASHTO, 2020).

$$\frac{dRCD}{dN} = A'(J_R)^{n'} \qquad \text{(Eq. 6.2)}$$

$$J_R = \frac{1-v^2}{E_R}(K_I^2 + K_{II}^2) + \frac{1-v}{E_R}K_{III}^2 \qquad \text{(Eq. 6.3)}$$

where A', n' are fracture properties of asphalt mixtures, J_R is a pseudo J-integral, v is the materials Poisson's ratio, E_R is a representative elastic modulus, K_I is the stress intensity factor in Mode I cracking (opening), K_{II} is the stress intensity factor in Mode II cracking

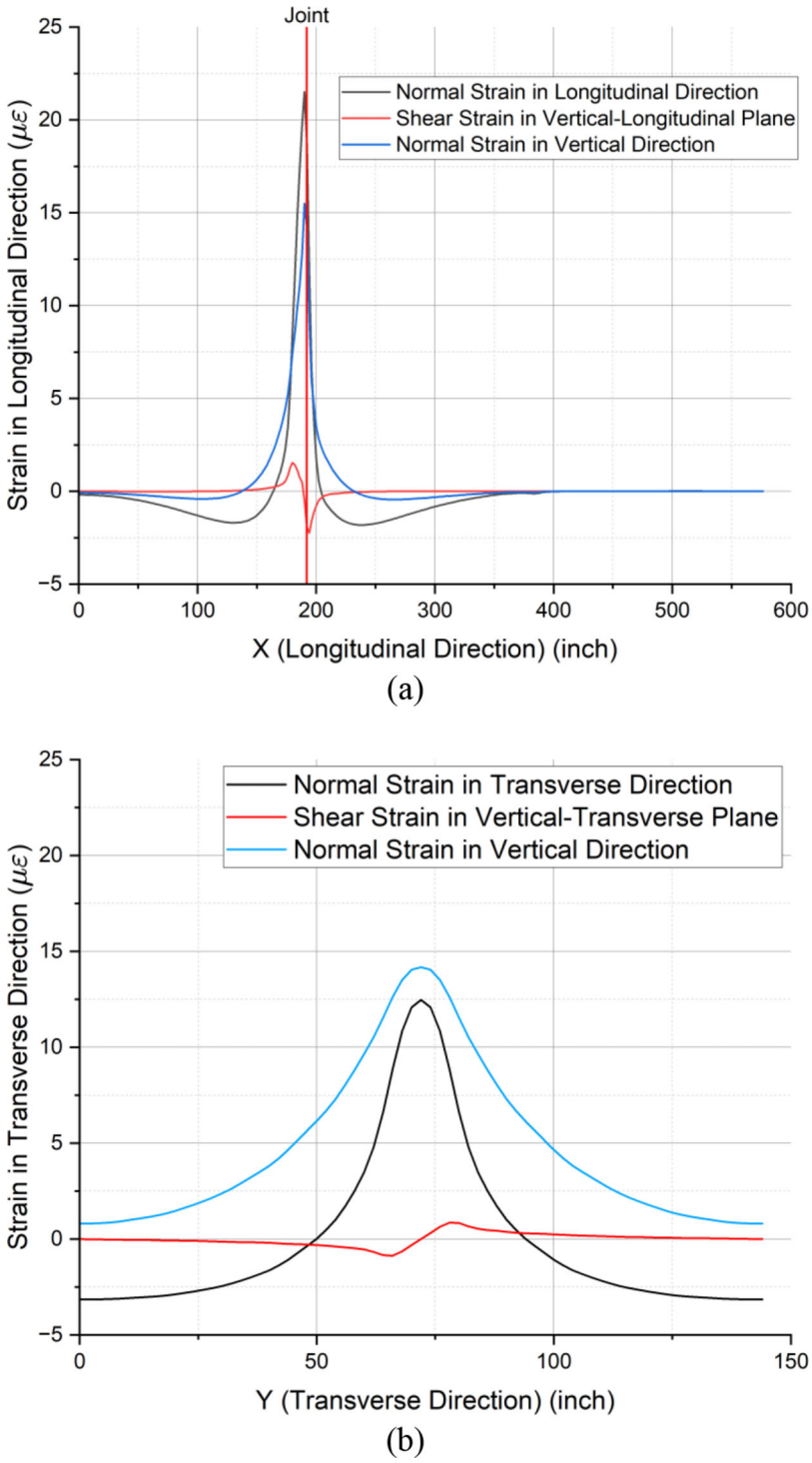

Figure 6.2 Composite pavement strain at the bottom of the asphalt layer: (a) longitudinal direction, and (b) transverse direction.

(in-plane shear), and K_{III} is stress intensity factor in Mode III cracking (out-of-plane share). Figure 6.7 indicates that in-plane shear stress mainly affects fatigue cracking. Consequently, K_I and K_{III} are assumed to be 0, while

$$K_{II} = \tau\sqrt{\pi a} \qquad \text{(Eq. 6.4)}$$

where τ is the shear stress and a is the reflective cracking depth. Combining Equations 6.2, 6.3, and 6.4, the RCD can be estimated using Equation 6.5.

$$RCD = A'\left[\pi a E_R (1-\nu^2)\tau^2\right]^{n'} N_f \qquad \text{(Eq. 6.5)}$$

where N_f is the estimated service life (the number of loading repetitions or years). Using Equations 6.1 and 6.5 and simplifying by merging regression parameters, the RSL prediction model can be expressed as Equation 6.6.

$$N_f = A\frac{RCD}{SCI^B} + N_0 = A\frac{2.044\ ln\ (0.596 \times SCI)}{SCI^B} + N_0 \quad \text{(Eq. 6.6)}$$

where N_0 is the initial service life, and A and B are regression parameters. The deflection data collected from US 20 was utilized to validate the relationship between DBPs and reflective cracking. As seen in Figure 6.9, the x-axis at the bottom of the figure presents the FWD test location, while the top x-axis illustrates the reflective crack conditions recorded by the FWD testing operator in the field. "Joint-crack" means cracking was observed at the pavement surface, while "no joint-crack" means cracking was not observed at the surface. "Nan" refers to no recorded visual inspection. In most sections, joint cracks were

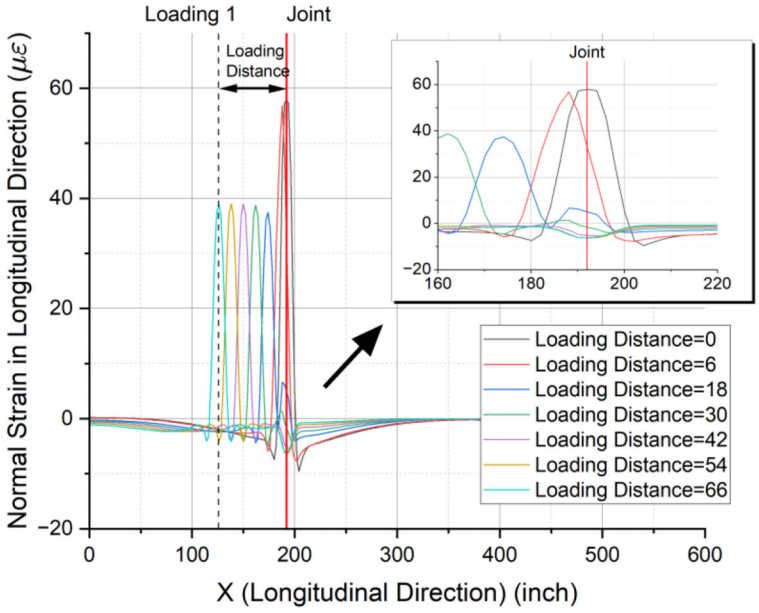

(a)

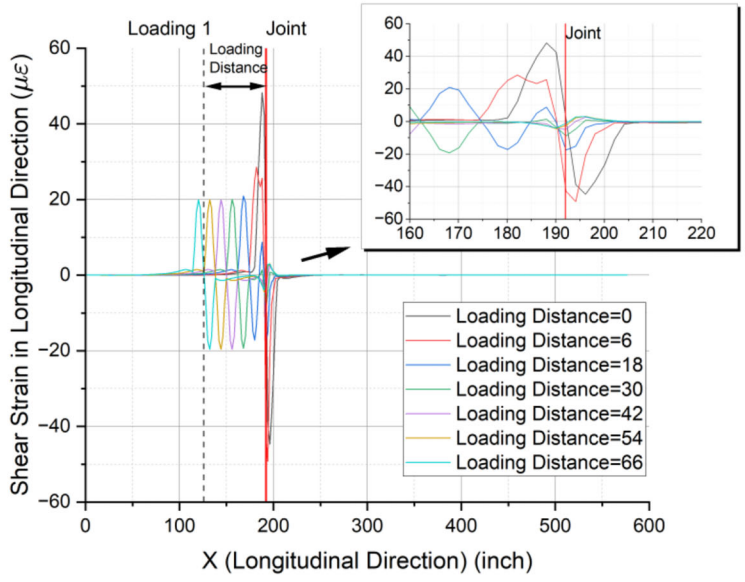

(b)

Figure 6.3 Continued.

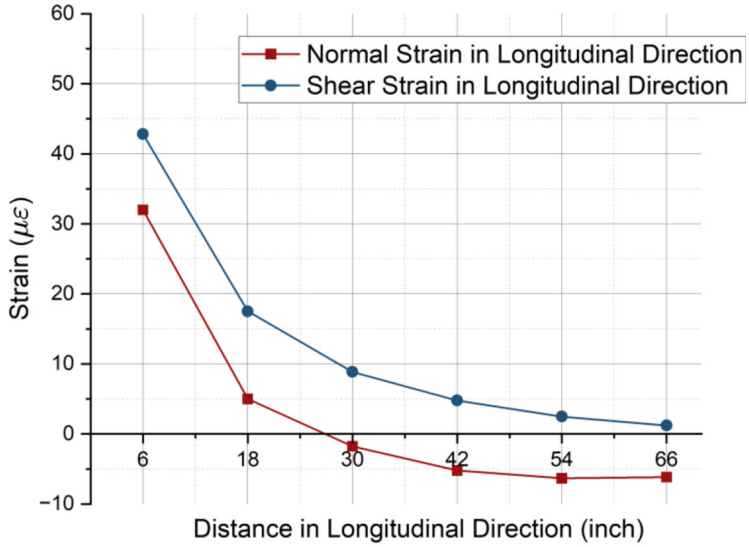

(c)

Figure 6.3 Mechanical responses for various loading distances: (a) normal strain; (b) shear strain; (c) extreme values in the second fluctuation.

recorded when both $BDI_{composite}$ and SCI exceeded 1.0, a result consistent with the analysis of FE simulations. Therefore, combining the $BDI_{composite}$ and SCI may be a good estimate of reflective cracking depth.

6.4 Summary

FE models were utilized to simulate the mechanical behaviors of composite pavement during FWD testing. The effects of different parameters, including loading distance, asphalt layer modulus and thickness, on the critical mechanical responses and DBPs were evaluated. Correlations between the DBPs and the critical mechanical responses were established. The critical mechanical responses and DBPs were selected to identify the PCC slab joint location and reflective crack depths to facilitate maintenance decisions. The results were validated using field data collected from routine FWD surveys in INDOT road, and the following were the specific findings.

- The PCC slab joints in composite pavements have a crucial influence on the mechanical response of such pavements during FWD testing, and therefore during traffic loading. Due to the effects of the PCC slab joint, the normal and shear strains in the longitudinal direction at the bottom of the asphalt layer show second fluctuations.
- The extreme value of normal strain in the second fluctuation can be used as a critical index for locating the PCC slab joint. This index is sensitive to the loading distance and has an appropriate stability for the asphalt layer modulus and thickness variations.
- The extreme value of shear strain in the second fluctuation can be utilized to evaluate reflective cracking. At a given loading distance, the shear strain increases as the reflective crack depth increases. When the reflective crack depth reaches 75% of the asphalt layer thickness, the shear strain increases sharply.
- The BDI was adjusted to the $BDI_{composite}$, designed to identify the PCC slab joint location in composite pavements. The $BDI_{composite}$ shows a strong correlation with the extreme value of normal strain in the second fluctuation, with a Pearson correlation coefficient of 97.8%.
- The SCI is highly correlated (Pearson's $r = 98.4\%$) with the extreme value of shear strain making it a reasonable indicator for assessing reflective crack progression based on FWD testing.
- Reflective cracking can be recognized and estimated by the $BDI_{composite}$ and SCI based on FWD testing. When both $BDI_{composite}$ and SCI show large values in routine surveys, reflective cracks are likely propagating.

In future studies, more simulations need to be conducted to refine the relationship between SCI and reflective crack depth to support informed maintenance decisions. Additionally, more field data (e.g., ground penetrating radar (GPR) and core samples) must be collected to verify the relationship between the $BDI_{composite}$ and the loading distance.

After verifying with additional field data, it is recommended that the SCI and $BDI_{composite}$ be incorporated into the maintenance decision matrix for composite pavements. This will facilitate accurate maintenance decisions for each test section. Additionally, selecting a maintenance strategy for reflective cracking using the proposed FE approach and analysis warrants further research. The FE analysis can be used to simulate the mechanical response of the composite pavements under various maintenance strategies to allow for predictions regarding the effectiveness of the maintenance.

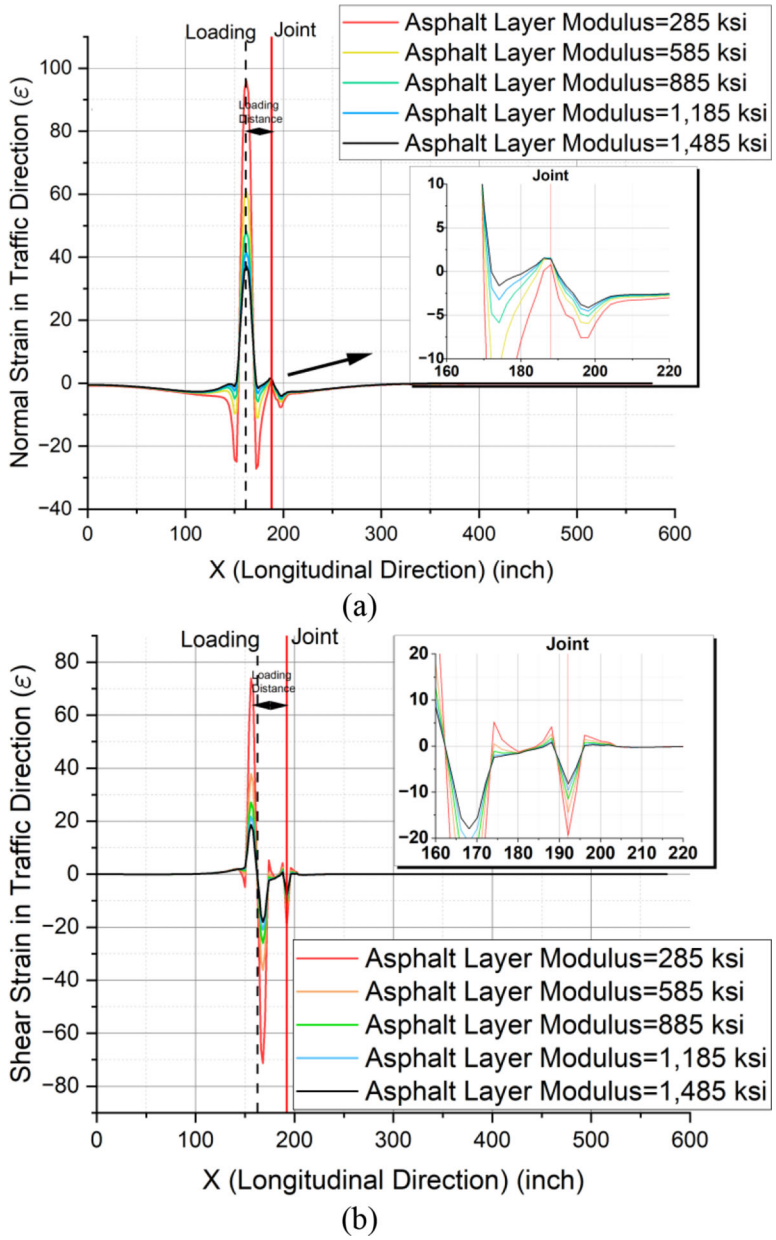

Figure 6.4 Mechanical responses for different asphalt layer moduli: (a) normal strain; (b) shear strain.

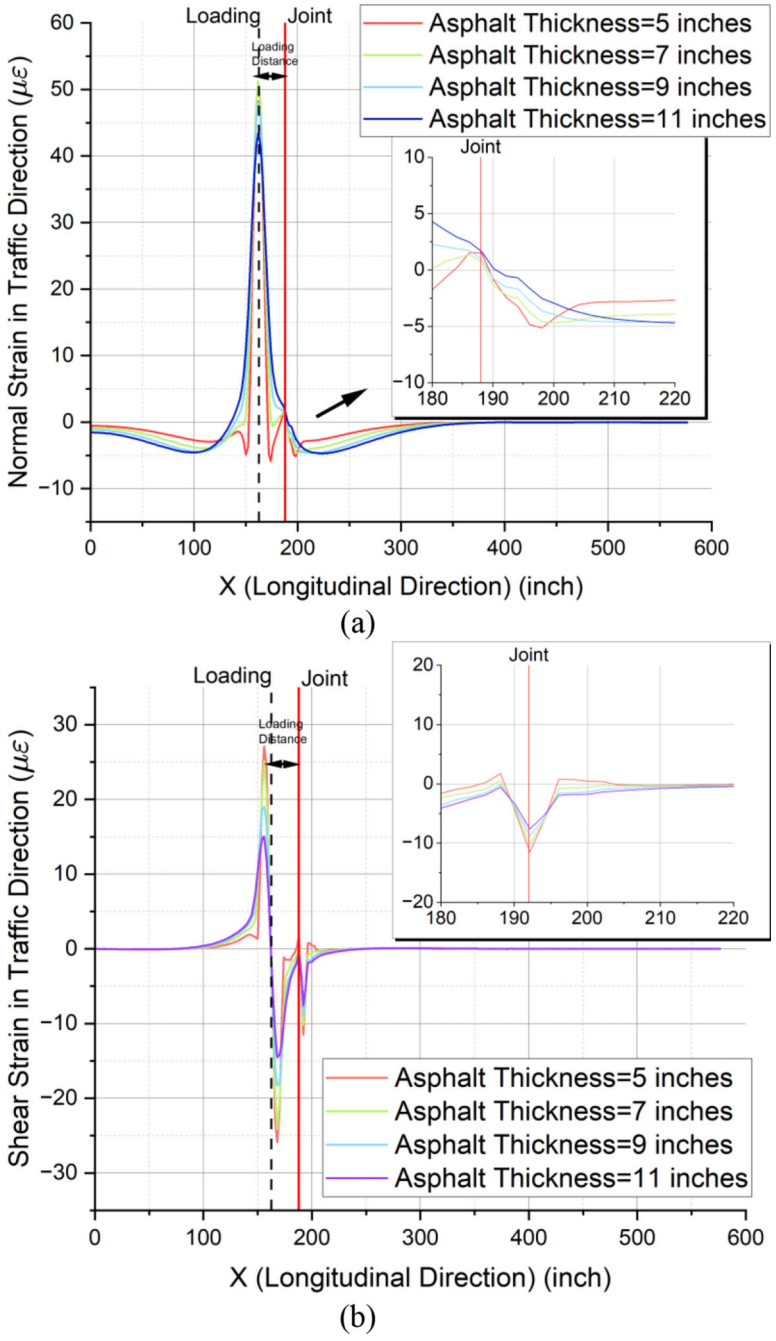

Figure 6.5 Mechanical response for different asphalt layer thicknesses: (a) normal strain; (b) shear strain.

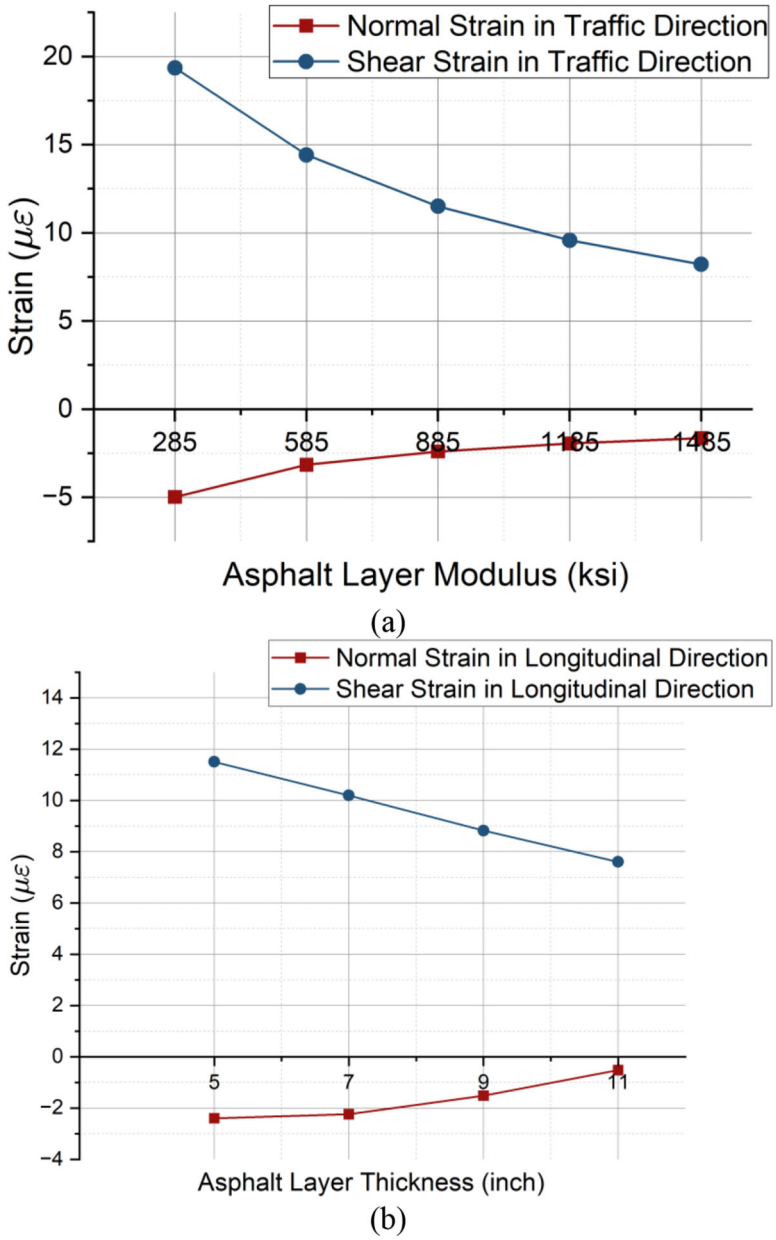

Figure 6.6 Extreme values of normal and shear strain in: (a) different asphalt layer moduli; (b) different asphalt layer thicknesses.

TABLE 6.2
Changes of normal and shear strains

Influence Factors	Ranges	Changes of Normal Strain (με)	Changes of Shear Strain (με)
Loading Distance	0–66 inches	38.2	41.6
Asphalt Layer Modulus	285–1,485 ksi	3.3	11.2
Asphalt Layer Thickness	5–11 inches	1.6	6.4

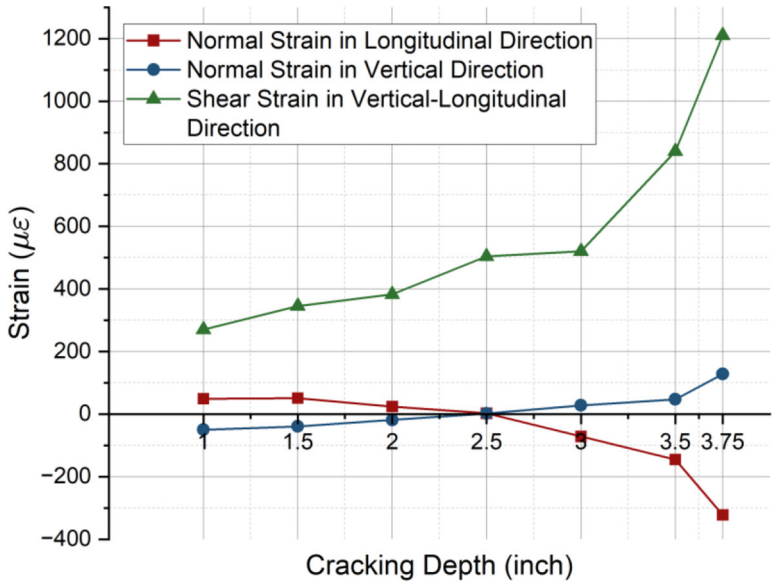

Figure 6.7 Extreme values of mechanical responses in the second fluctuation with different reflective crack depths.

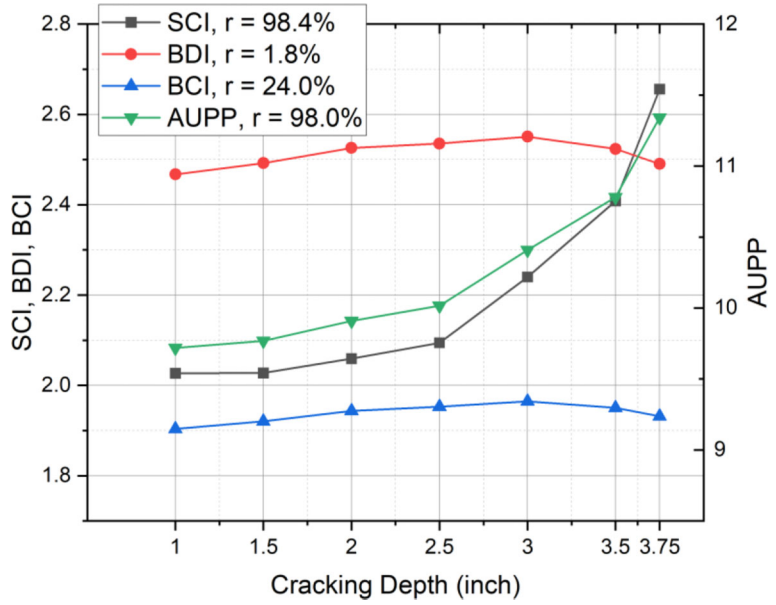

Figure 6.8 The DBPs at different reflective crack depths.

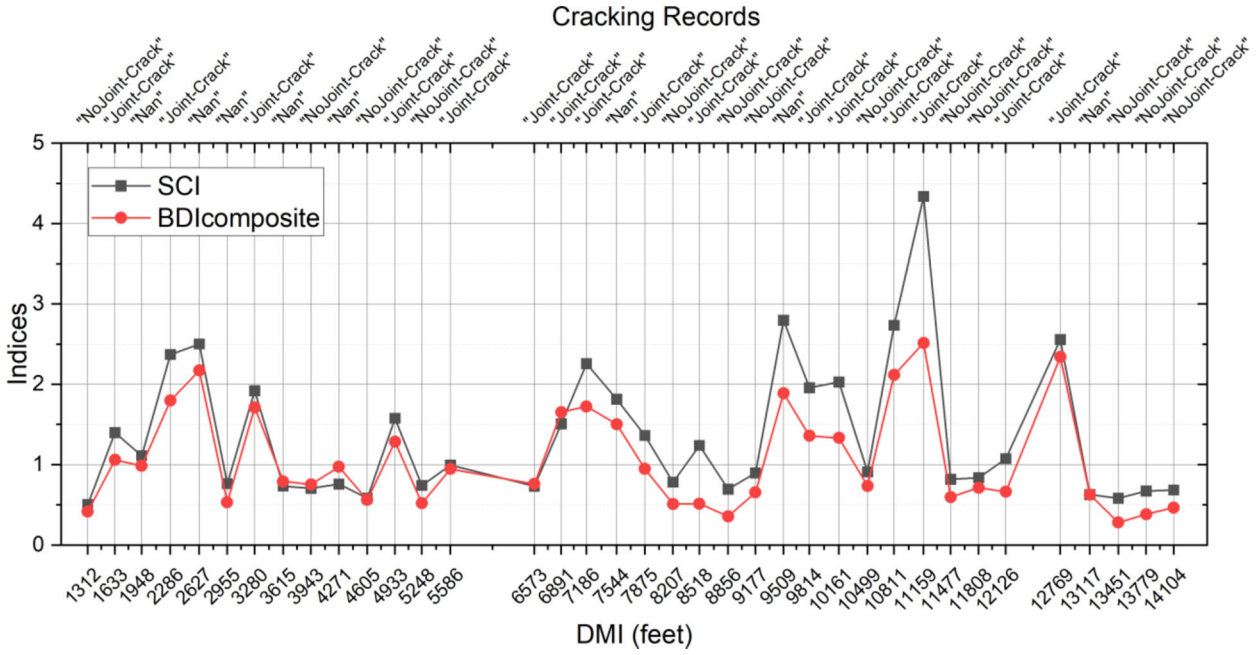

Figure 6.9 Deflection basin in different loading positions.

7. INTERNATIONAL ROUGHNESS INDEX (IRI) PREDICTION MODELS FOR FUNCTIONAL CONDITIONS

7.1 Introduction

The IRI is widely used in the INDOT PMS to quantify the smoothness of pavement for evaluating functional conditions of pavements. In this research, the IRI was measured at approximately 525-feet interval, and the resulting number of IRI data points were 128,248 for interstate highways, 410,512 for U.S. highways, and 1,130,528 for state roads. Consequently, a total of 1,670,288 IRI measurement data points were collected for the study.

7.2 Historical IRI Data Process

7.2.1 IRI Data Filtering

The historical IRI data was filtered based on the assumption the IRI of a given pavement increases over time if no pavement maintenance is performed. Therefore, any pavement IRI number that decreased from the previous collection year, was considered an outlier and eliminated from the datasets. However, as shown in Figure 7.1, no clear trend is observed between the filtered IRI data and time. Further data processing is needed to convert the time index of the data from the data collection year to the pavement age to accurately identify the IRI trends over time.

7.2.2 Time-Series IRI Data Shift

For each testing location, the pavement age of the first data point, collected in 2014, was estimated using an empirical IRI model developed by Lee et al. (2020), as expressed in Equation 7.1, to convert time index from data collection year to pavement age.

$$IRI_n = IRI_{ini} \cdot e^{a \cdot n} \qquad \text{(Eq. 7.1)}$$

where, n is pavement age (year), IRI_n is the IRI value at pavement age n (in./mile), IRI_{ini} is the initial IRI (in./mile), and a is a coefficient of 0.0242 for full-depth asphalt flexible pavements (Lee et al., 2020).

The IRI_{ini} was assumed to be 34.2 in./mile, which is the maximum allowable IRI value immediately after construction for INDOT flexible pavements (INDOT, 2024). Additionally, a new "a" coefficient was determined for INDOT flexible pavements using Equation 7.2. The average value of the "a" coefficient from all test locations of a given road classification were used as the new coefficients. These are 0.1002 for interstate highways, 0.1187 for U.S. highways, and 0.1108 for state roads.

$$a = -\ln\left(\frac{IRI_n}{IRI_{n+1}}\right) \qquad \text{(Eq. 7.2)}$$

With the known values of IRI_{ini} and the new "a" coefficients, the pavement age of the first 2014 data point is calculated using Equation 7.3, which is solved for pavement age "n" based on Equation 7.1.

$$n = \frac{1}{a} \cdot ln\left(\frac{IRI_n}{IRI_{ini}}\right) \qquad \text{(Eq. 7.3)}$$

As shown in Figure 7.2(a), for each road classification dataset (interstate, US highway, state road), pavement age was assigned to all IRI data based on the calculated pavement age of the 2014 first data point.

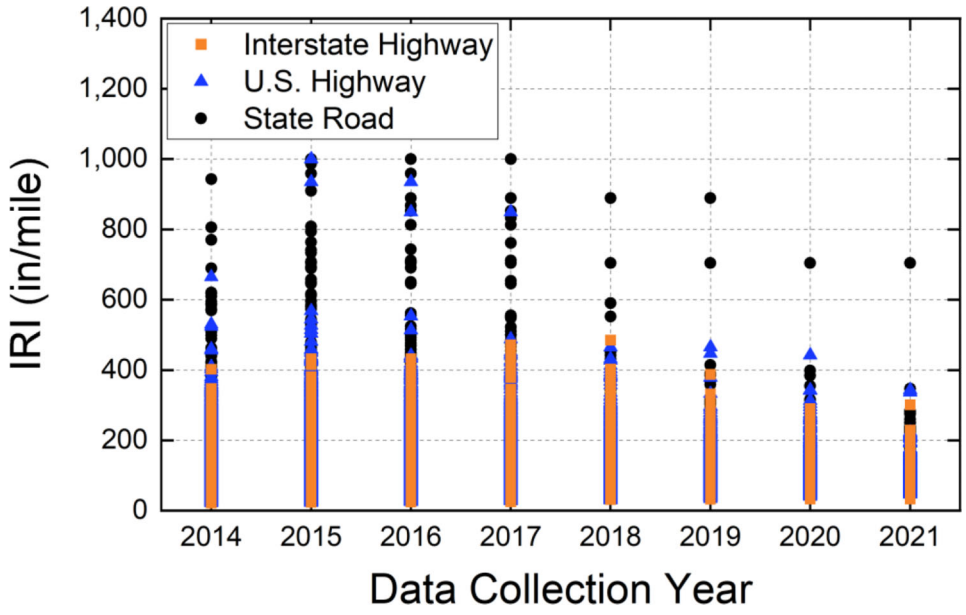

Figure 7.1 Filtered IRI data.

For example, the pavement age of IRI data collected in 2018 is the calculated pavement age of first data plus four, "n+4." Figure 7.2(a) shows the shifted IRI data exhibit a significantly clearer trend with pavement age. Figure 7.2(b) shows the shifted IRI data for all road classifications exhibit a reasonable trend in that the IRI generally increases as the pavement age increases. Furthermore, the rate of IRI increment for interstate highways was slightly less than other road classifications. This indicates that the trend of IRI over time is affected by road classifications, and that individual IRI prediction models may be needed for each road classification.

7.3 Development of IRI Prediction Model

A non-linear regression analyses were conducted on the shifted IRI data to develop the IRI prediction model for each road classification. As expressed in Equation 7.3, a simple exponential function was selected for the IRI prediction model. Furthermore, only one input, the pavement age, was used for the IRI prediction model, and it allows for estimating functional pavement age from the current IRI measurement.

$$IRI_n = a \cdot e^{b \cdot n} + c \qquad \text{(Eq. 7.4)}$$

where, n is pavement age (years), IRI_n is the IRI value at pavement age n (for SI units: m/km, for US units: in./mile), and a, b, and c are regression coefficients.

Figure 7.3 shows the IRI prediction models for all three road classifications. The IRI prediction model trends, plotted in blue dashed lines, generally represent the trend of the shifted IRI data with respect to pavement age. Furthermore, the IRI prediction models reflected the relatively slow IRI increase for interstate highways, compared to the other two road classifications. In addition, all road classifications reached the IRI limit of 170 in./mile recommended by the Federal Highway Administration (FHWA) when pavement age is between 15 and 20 years. This indicates the IRI prediction models generally follow reasonable trends.

Figure 7.4 shows the IRI prediction models' accuracies by comparing the models to measured IRI values. Even though the outliers were not completely eliminated for U.S. highways and state roads, the IRI prediction models for all three road classifications exhibit similar accuracy as indicated by the R^2 and RMSE. All road classifications exhibit high values of R^2 ($R^2 > 0.85$) and small RMSE. Therefore, the IRI prediction models can be used in the PMS to predict future IRI values and estimate remaining pavement life based on pavement functional condition.

7.4 Summary

IRI prediction models were developed for flexible pavements using an enhanced approach for analyzing historical IRI data. Since the pavement age information was unavailable from the historical IRI dataset, an enhanced approach is proposed to process historical IRI data to estimate pavement age of field sections. Once this was accomplished, three IRI prediction models were developed for the three road classifications based on the processed historical IRI data. To be practical, the models only consider pavement age as input. The models can represent typical pavement IRI behavior over time and exhibit reasonable IRI prediction accuracy. Therefore, the IRI prediction models can be used with the PMS to provide additional insights into the functional conditions of in-service flexible pavements.

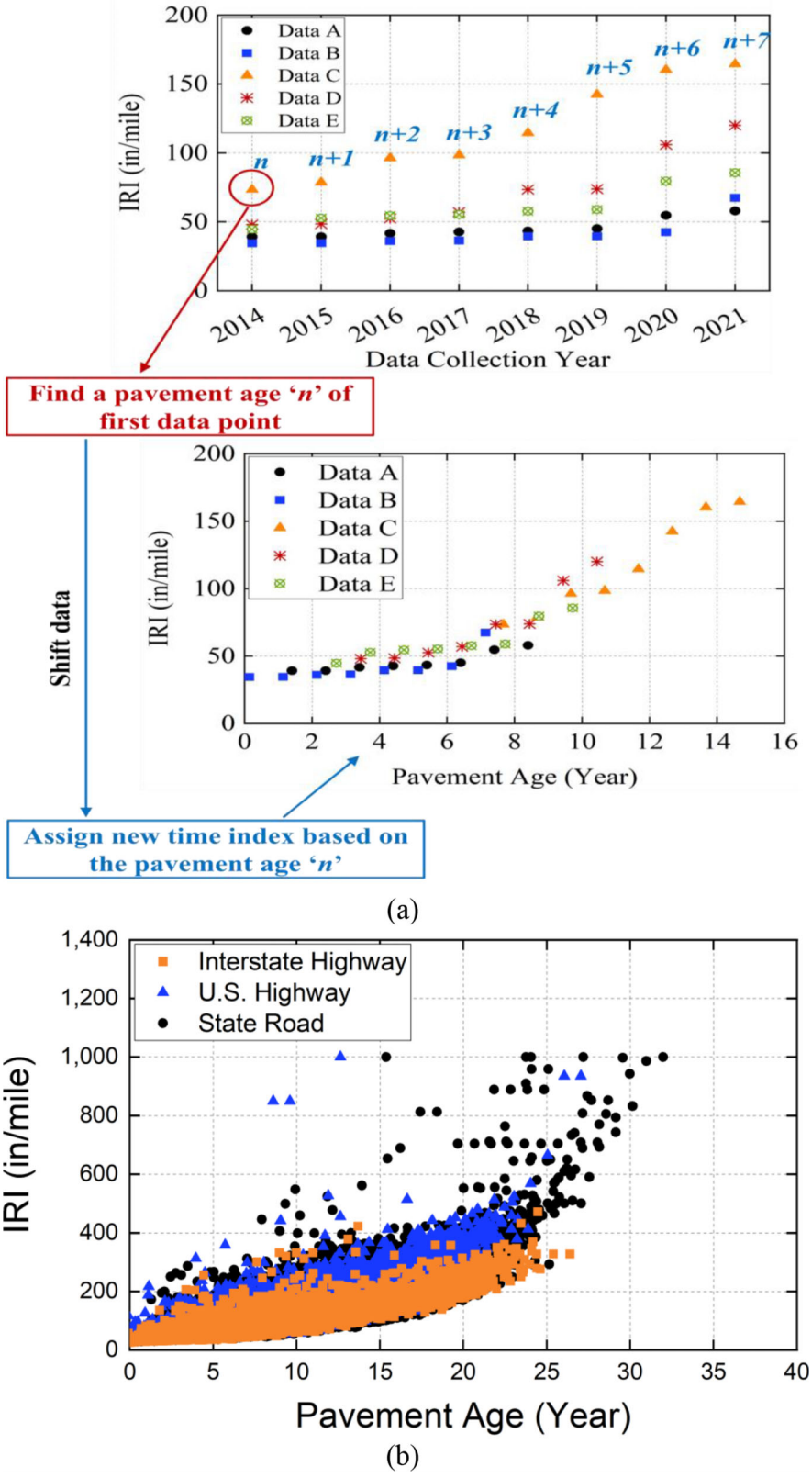

Figure 7.2 Time-series IRI data shift: (a) data shift concept; (b) shifted IRI data.

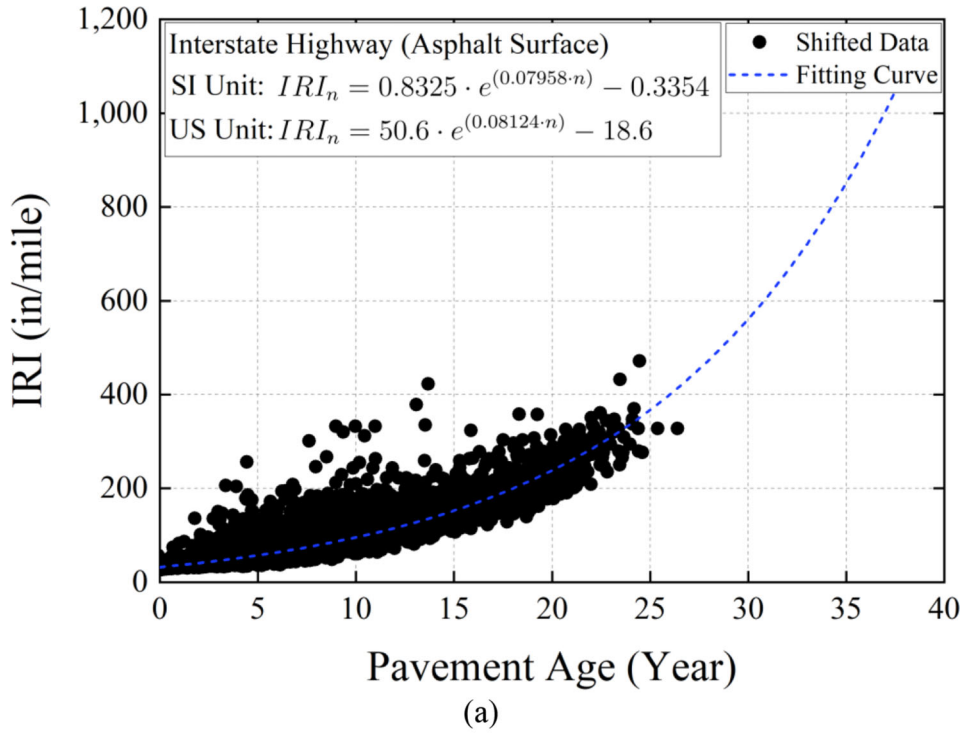

(a)

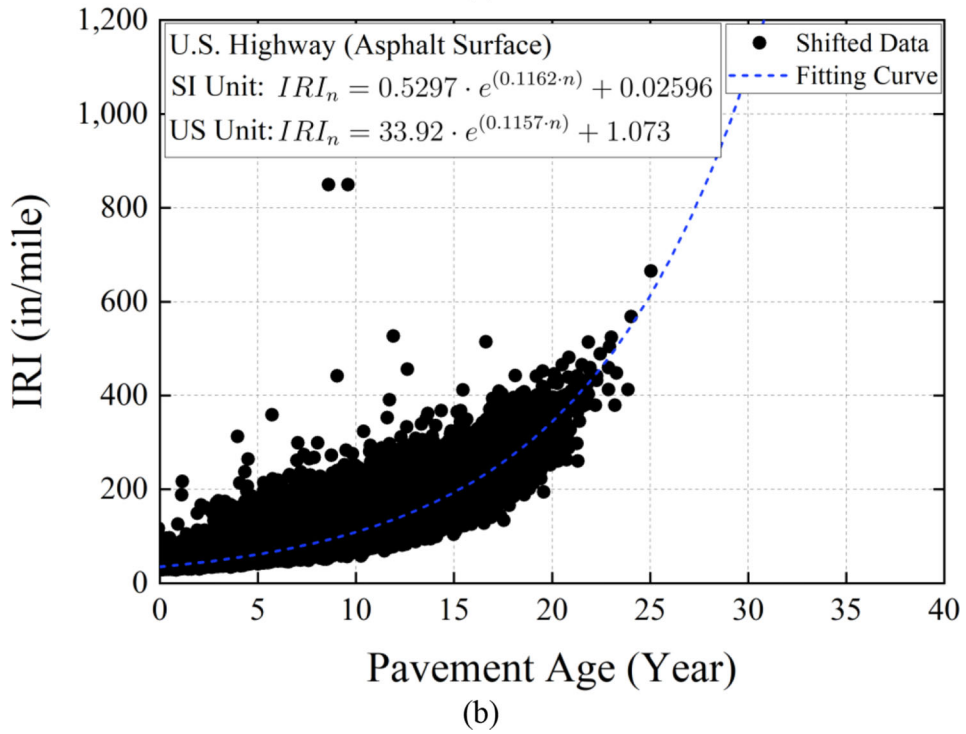

(b)

Figure 7.3 Continued.

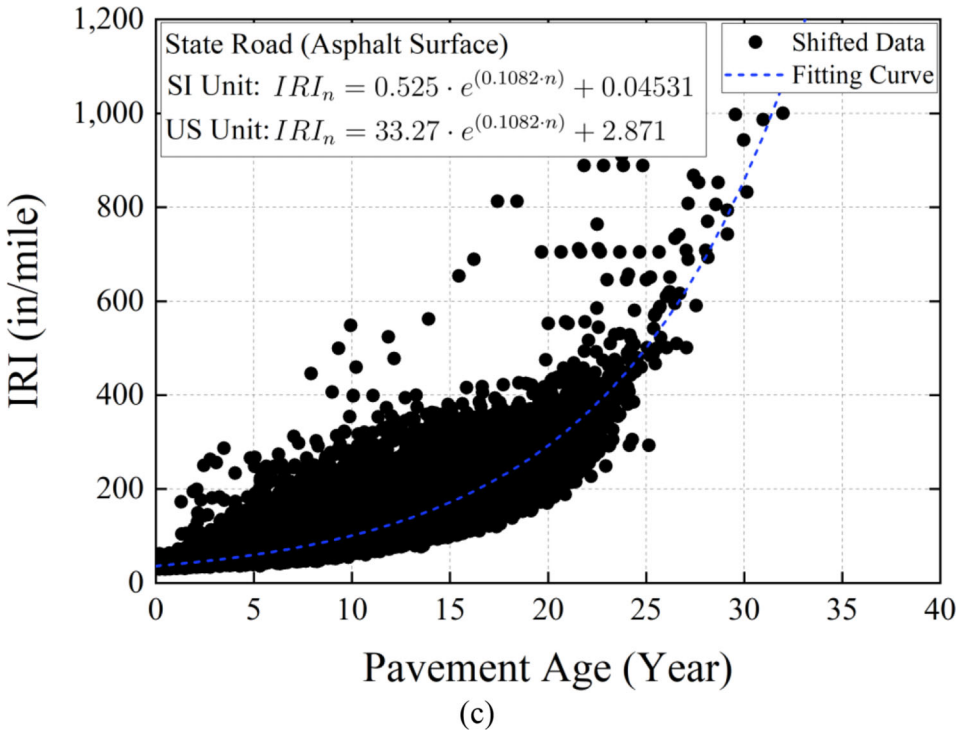

Figure 7.3 IRI prediction models: (a) interstate highways, (b) U.S. highways, and (c) state roads.

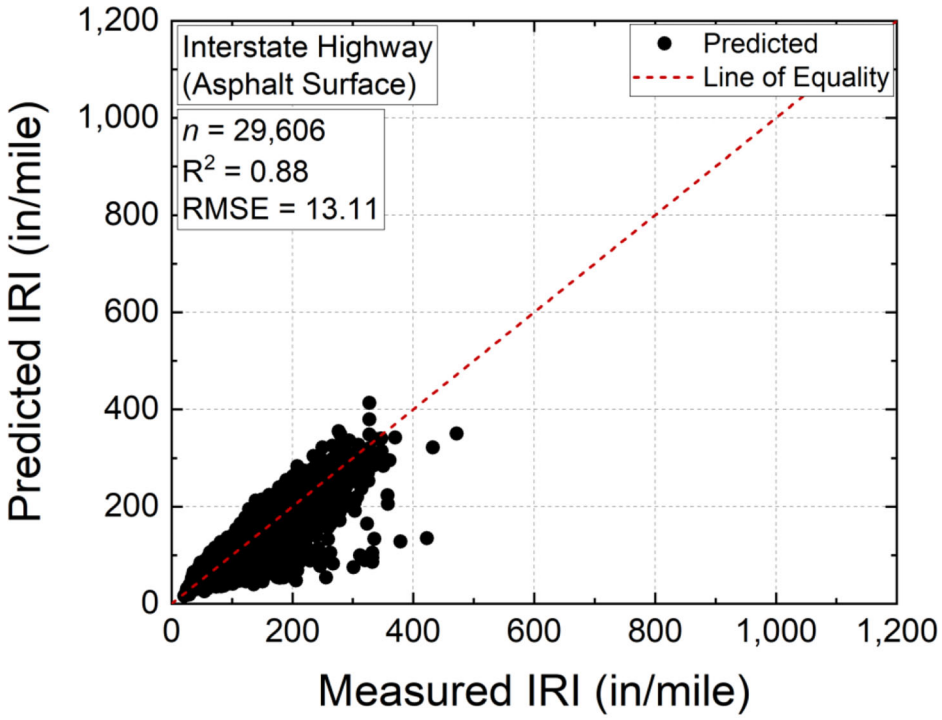

(a)

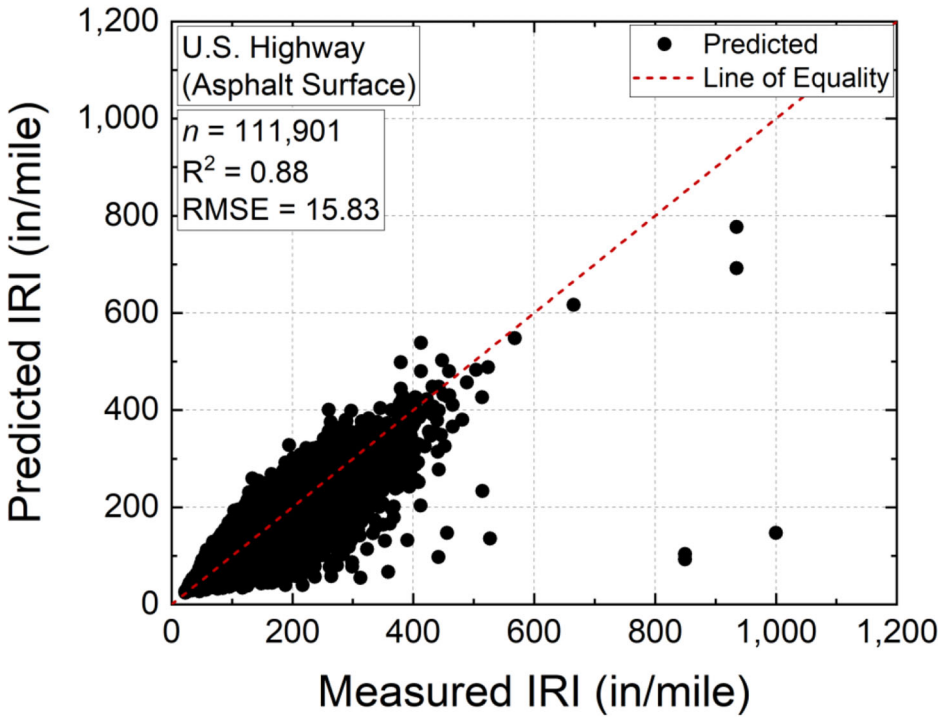

(b)

Figure 7.4 Continued.

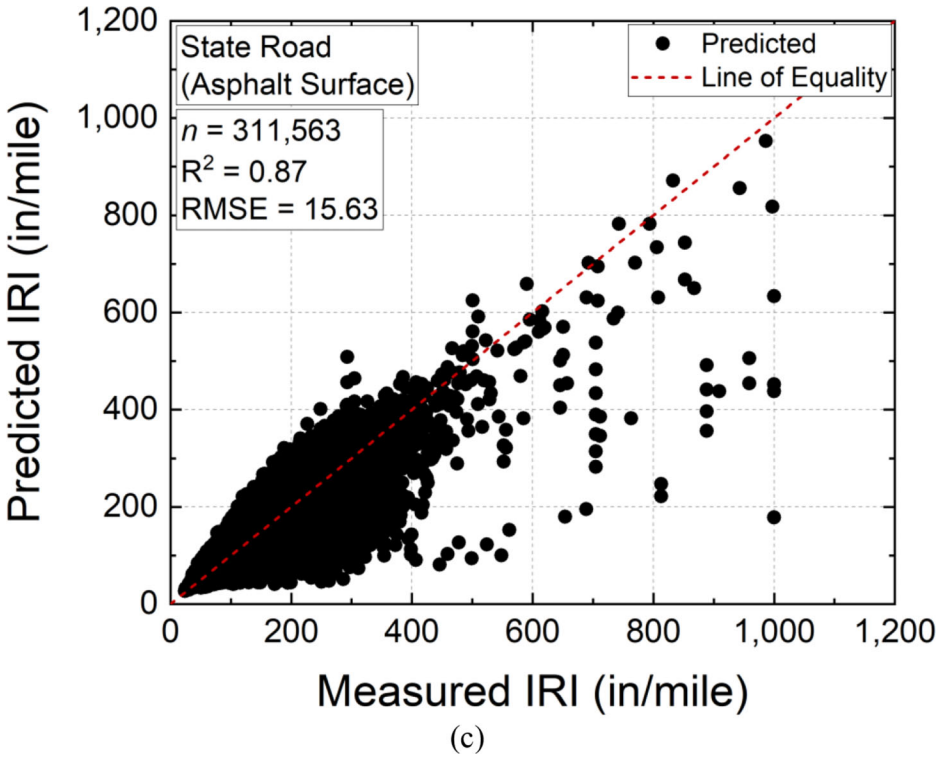

(c)

Figure 7.4 IRI prediction model validation: (a) interstate highways, (b) U.S. highways, and (c) state roads.

8. DEVELOPMENT OF A FRAMEWORK FOR MAINTENANCE STRATEGY DETERMINATION AND REMAINING SERVICE LIFE

8.1 Introduction

A decision model is one of the most important components in PMS to determine appropriate maintenance strategies, ensuring desirable conditions of in-service pavements within the given time and budget (Peraka & Biligiri, 2020). Decision frameworks were developed for determining a more appropriate maintenance strategy based on both structural and functional conditions. Several indicators with corresponding thresholds were identified to represent the structural and functional conditions, which are integrated into the decision framework. Furthermore, an approach to calibrating or determining necessary thresholds is described to allow the implementation of the proposed decision framework in different states or countries.

8.2 Maintenance Strategy Determination Framework for Full-Depth Asphalt Flexible Pavements

Figure 8.1 shows a decision framework to determine the maintenance strategy for full-depth asphalt flexible pavements, requiring FWD and IRI measurements to consider both structural and functional conditions. This decision framework is designed to provide a maintenance strategy for individual testing locations within the target section. Eight levels of maintenance strategies, reflecting INDOT maintenance methods, are considered depending on the pavement conditions: "no action required," "preventive crack sealing," "surface patching," "mill and fill," "partial-depth repair," "rehabilitation (full-depth reclamation or cold in-place recycling)," "full-depth repair," and "reconstruction." Overall, a stepwise approach is applied to the proposed decision framework to determine the most appropriate maintenance strategy. The steps are described in Appendix D.

8.3 Maintenance Strategy Determination Framework for Rigid Pavements

Figure 8.2 shows a decision framework to determine the maintenance strategy for rigid pavements, requiring SSR and IRI measurements to consider both structural and functional conditions. This decision framework is designed to provide a maintenance strategy for individual testing locations within the target section. Four levels of maintenance strategies are considered depending on pavement conditions: "no action required," "preventive repair," "partial-depth repair," and "full-depth repair." The steps of the maintenance strategy determination are described in Appendix D.

8.4 Maintenance Strategy Determination Framework for Composite Pavements

Figure 8.3 shows a decision framework to determine the maintenance strategy for composite pavements,

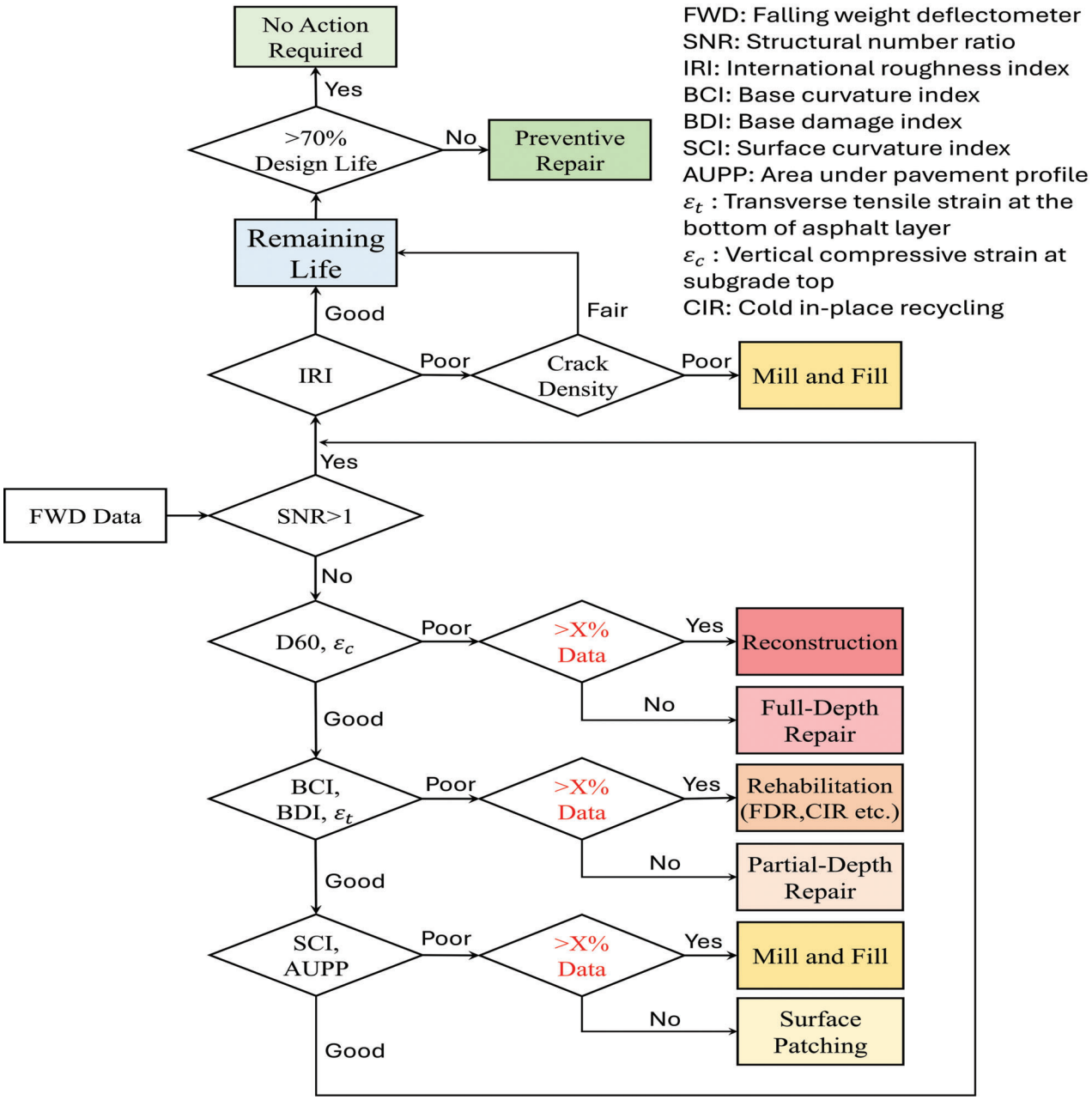

Figure 8.1 Maintenance strategy framework for full-depth asphalt flexible pavements.

requiring RCD and IRI measurements to consider both structural and functional conditions. This decision framework is designed to provide a maintenance strategy for individual testing locations within the target section, because pavement conditions may be inconsistent even within the same pavement section. Four levels of maintenance strategies are considered depending on the pavement conditions: "no action required," "preventive repair," "partial-depth repair," and "full-depth repair." A stepwise approach is applied to the proposed decision framework to determine the most appropriate maintenance strategy. In the first step, two primary categories can be defined using the RCD: (1) pavements with sufficient structural capacity, and (2) pavements with insufficient structural capacity. The remaining steps are described in Appendix D.

8.5 Application of the Proposed Framework

8.5.1 User-Friendly Software Development

The decision framework was developed to determine a specific maintenance strategy for the individual testing location, while numerous non-destructive testing

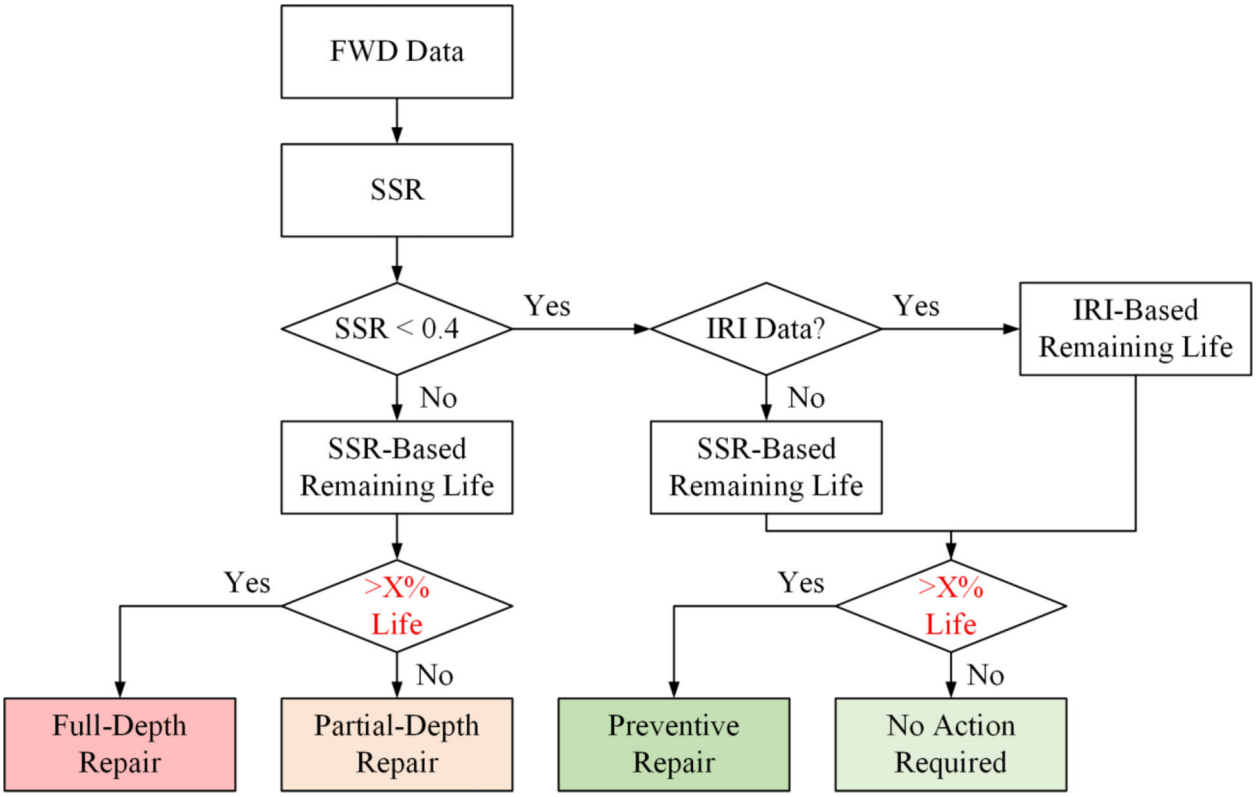

Figure 8.2 Maintenance strategy framework for rigid pavements.

data points are typically collected from one target pavement section. User-friendly software was developed to analyze all non-destructive test data and practically implement the decision framework, regardless of the number of test locations or the length of target pavement section. Figure 8.4 shows the developed software interface, which can process raw data to calculate all structural and functional indicators presented in the study. The details of the software are described in Appendix D.

8.5.2 Demonstration of Data Analysis

One full-depth asphalt rigid pavement field section, an INDOT road, was selected for demonstration of the decision framework. As shown in Figure 8.5, a total of 54 data points were collected from the 3 miles section in 2022. The collected data was analyzed using the software, after which the proposed decision framework was applied.

A data point collected from the last testing location was used to demonstrate the determination of maintenance for each testing location. It should be noted that the 70% severe damage limit was used for this demonstration. As shown in Figure 8.5(a), the SNR was less than one, but the subgrade condition was good, as the D60 shows 1.93 mils of deflection, which is within the D60 threshold, as shown in Figures 8.5(a) and (b). Thus, the condition of the base layer was evaluated using BDI and BCI. Figures 8.5(c) and (d) show that both BDI (4.79 mils of deflection) and BCI (3.49 mils of deflection) measurements exceeded the threshold values, indicating poor conditions in the pavement lower layers. In addition, both BDI and BCI indicate the damage severity (87% for BDI and 90.7% for BCI) exceeded the severe damage limit. Therefore, "rehabilitation" is selected as the maintenance strategy for the last location.

Figure 8.5(e) shows that the maintenance strategy was determined for all testing locations, following the proposed decision framework. This allows engineers to decide on specific maintenance activities for the entire section or specific segments within the target pavement section.

8.6 Summary

For the three INDOT road classifications, decision frameworks were developed to determine an appropriate and optimized maintenance strategy for in-service pavements, based on both structural and functional conditions. The structural indicators, calculated from FWD deflections, are used for evaluating pavement structural capacity, while the IRI measurement is used to assess functional conditions. The use of various structural indicators allows for the assessment of specific pavement layer conditions, such as subgrade, lower layer (base or subbase layers), and upper

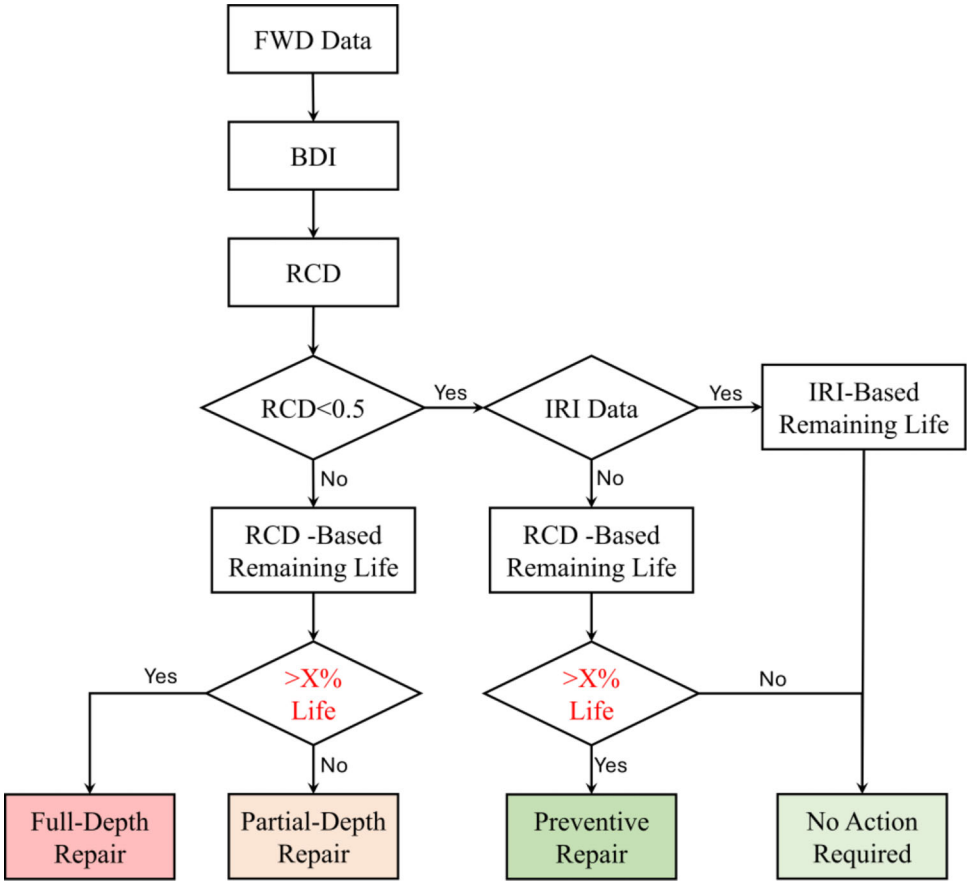

Figure 8.3 Maintenance strategy framework for composite pavements.

layers (surface or intermediate layers). This leads to the application of a stepwise approach to the decision framework, providing a more accurate maintenance strategy. In addition, the RSL estimation models are leveraged in the frameworks for an efficient maintenance strategy. All indicators used for the decision framework can be easily obtained by processing raw FWD and IRI data using the user-friendly software developed in this study. Since the decision framework employs common non-destructive test data, FWD deflections and IRI data, routinely collected by most agencies, it can be easily implemented in current PMS practices. Furthermore, the use of common non-destructive test data is beneficial for the local calibration of thresholds using a historical PMS database. Therefore, the concept of the proposed decision framework can be implemented in various states or countries.

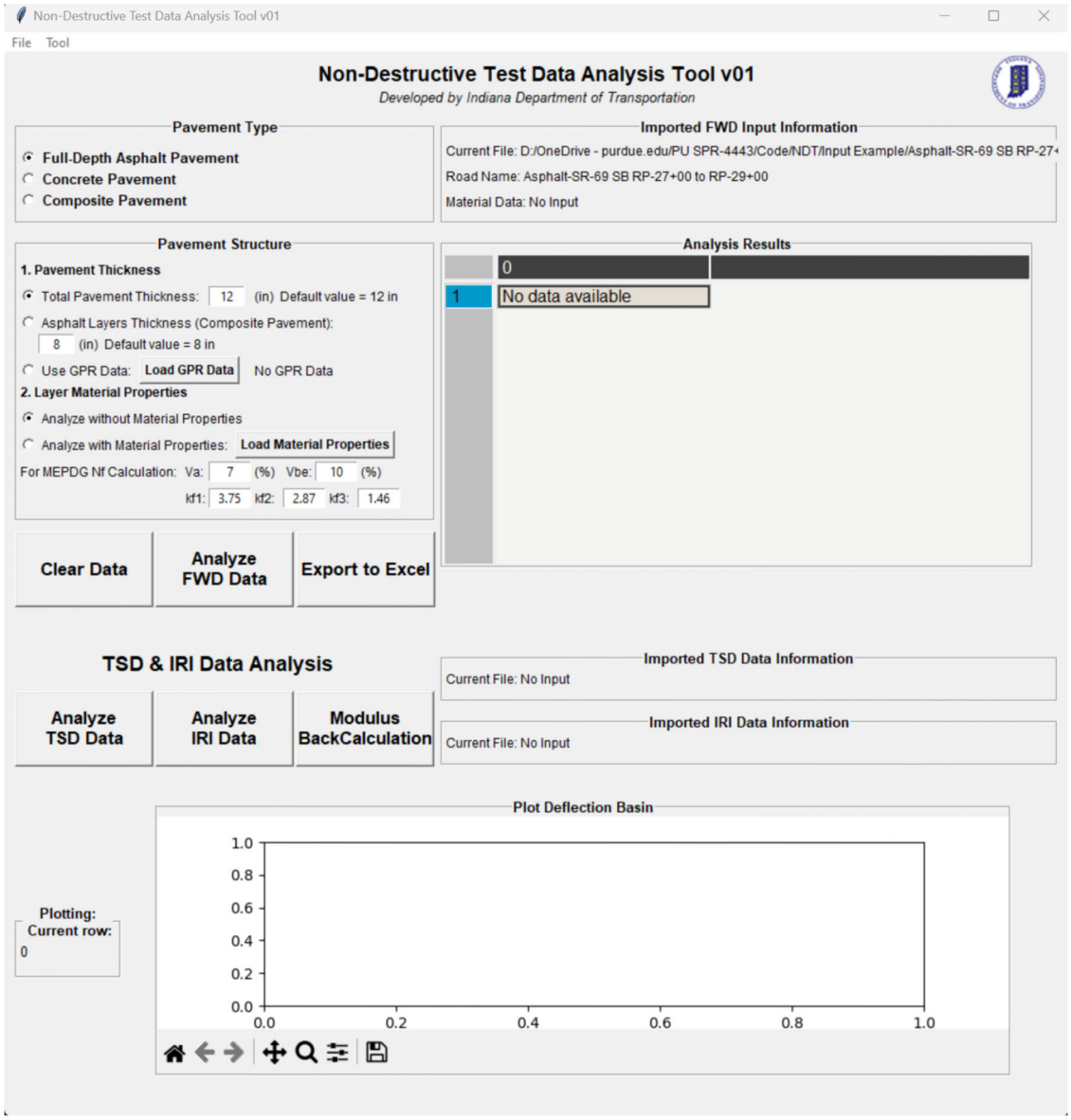

(a)

Figure 8.4 Continued.

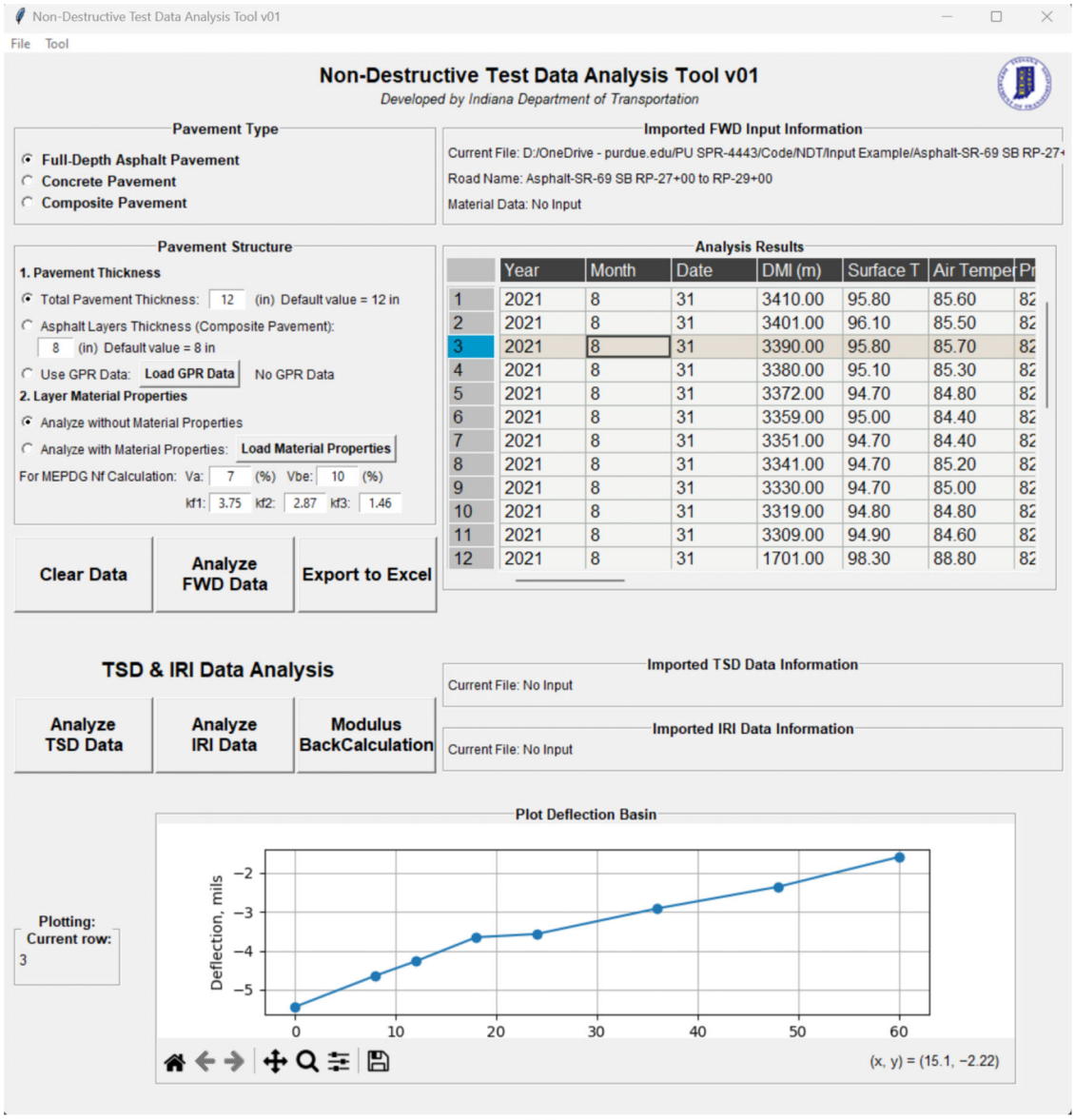

(b)

Figure 8.4 Non-destructive test data analysis software: (a) default view before analysis, and (b) after FWD data analysis.

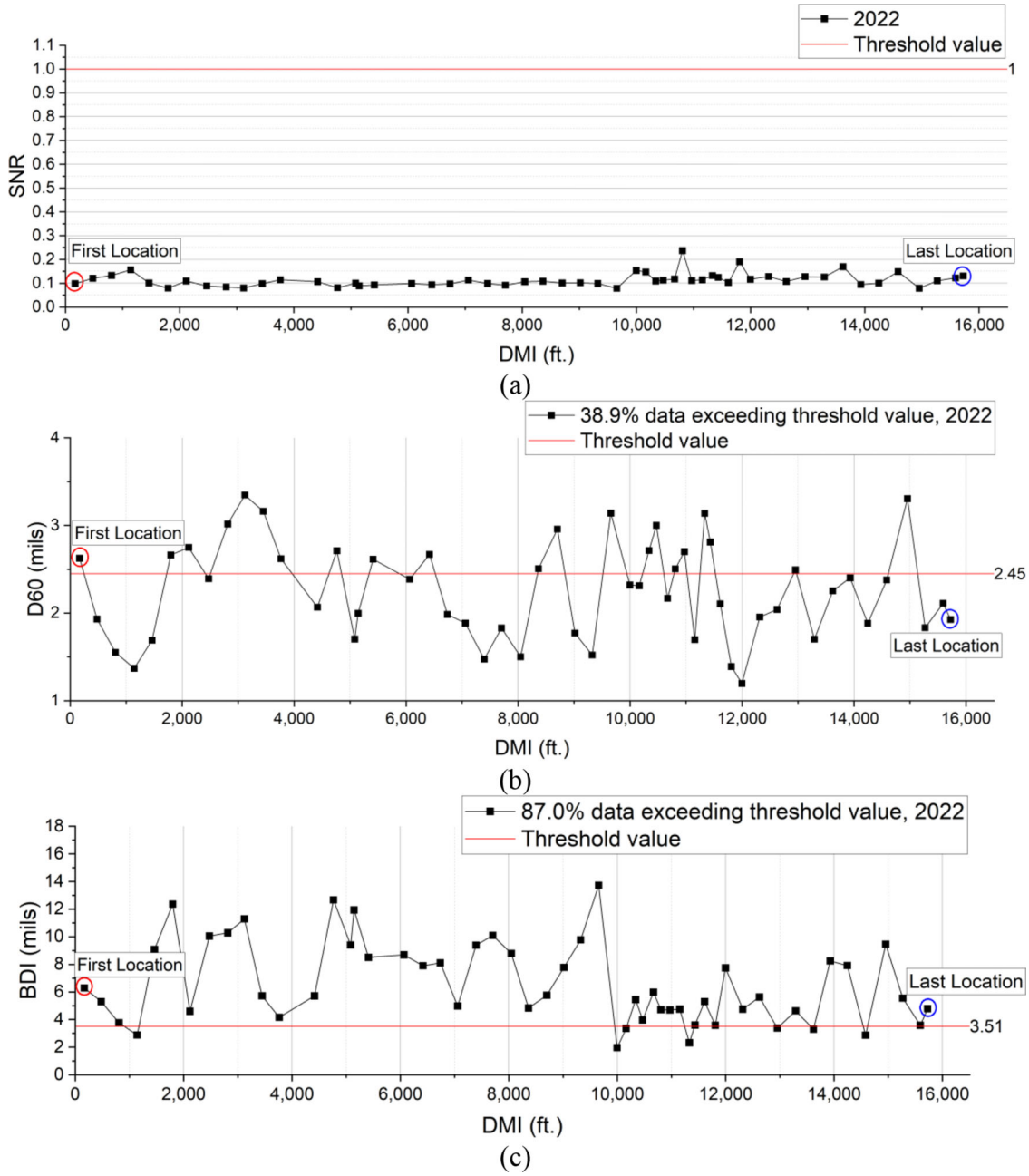

Figure 8.5 Continued.

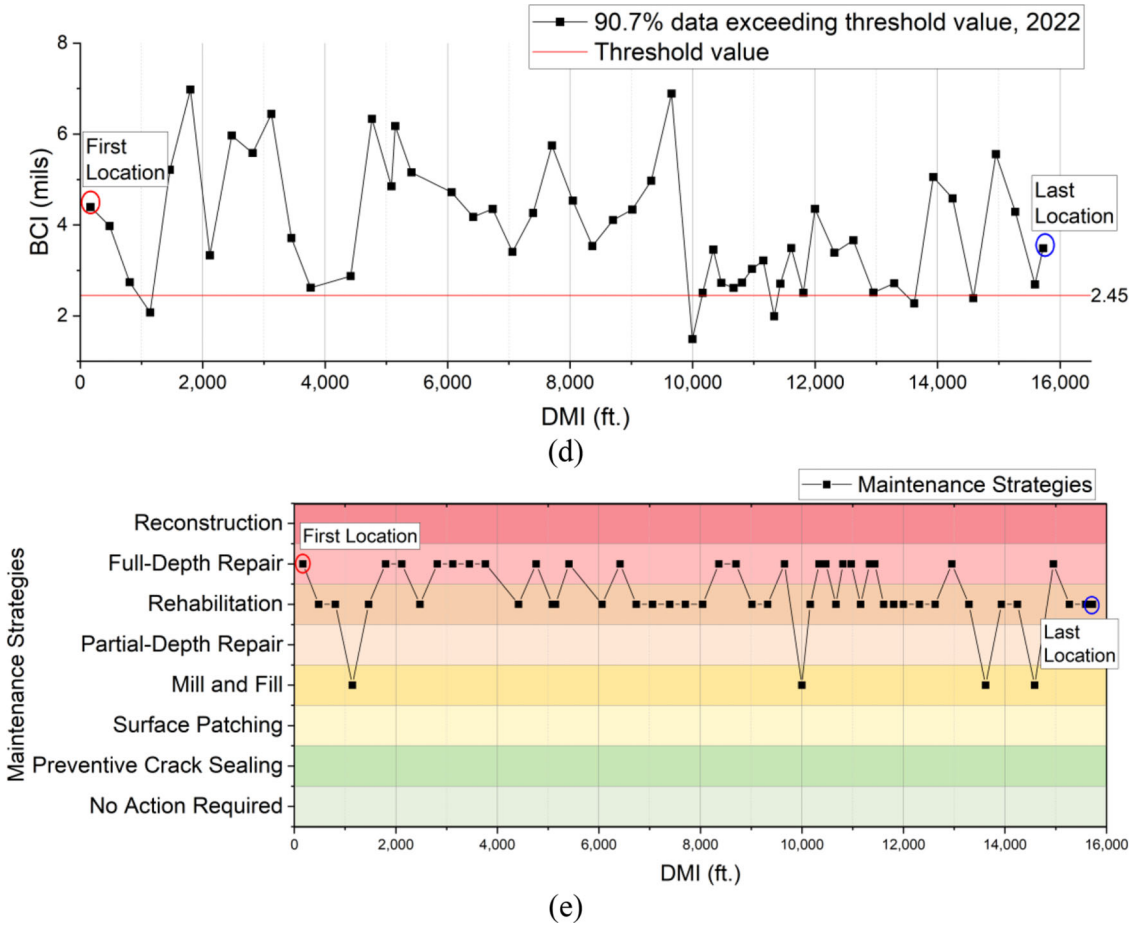

Figure 8.5 Example field data: (a) SNR, (b) D60, (c) BDI, (d) BCI, and (e) suggested maintenance strategies.

9. SUMMARY OF FINDINGS AND FUTURE WORKS

9.1 Findings

In this study, RSL prediction models are developed for INDOT pavements in terms of major pavement distresses using FWD and IRI data. The decision frameworks are developed to determine an appropriate and optimized maintenance strategy for in-service pavements, based on both structural and functional conditions. The structural condition indicators and prediction models are developed to evaluate the structural conditions of in-service full-depth asphalt flexible, rigid, and composite pavements. All indicators used for the decision framework can be easily obtained by processing raw FWD data. The IRI prediction models are developed for INDOT pavements using an enhanced approach for analyzing historical IRI databases. The main findings of the study are the following.

Full-depth asphalt flexible pavement

- SN_{eff} is an essential indicator to estimate the structural condition of full-depth asphalt flexible pavements. The prediction model developed in the work is able to determine the SN_{eff} nearly identical to the calibrated Rohde model, while using only two input parameters (AUPP and pavement thickness), a more practical approach.
- Critical strain at the bottom of the asphalt layer can be used to estimate subgrade and asphalt base layer properties. Critical strain prediction models have been successfully validated using field-measured strains and can therefore be used for in-service full-depth asphalt flexible pavements, to conduct structural evaluations.
- Deflection basin shape parameters generally exhibit a better correlation with critical responses, compared to the sole deflection value, indicating that deflection basin shape interpretation may be necessary to achieve a better estimate of pavement structural conditions.
- Regardless of the pavement structure, the AUPP and BDI can be used to predict transverse tensile strain at the bottom of the asphalt base layer and vertical compressive strain at the top of the subgrade, respectively. The equations based on the AUPP and BDI provided acceptable accuracy (R^2 = 0.98) in terms of the critical strain prediction for full-depth asphalt flexible pavements.

Rigid pavement

- The stress-strength ratio (SSR) prediction model developed in the research can be used to estimate the structural capacity of in-service rigid pavements using FWD deflection data. The SSR is primarily affected by slab curling conditions within the acceptable range (less

than 0.45), while the curling effect is insignificant for less stiff PCC slabs with higher SSR.
- The effect of curling on FWD deflection basin curves is greater when the PCC slab is stiffer. However, for any stiffness level of the PCC slab, the shapes of the FWD deflection basin curves near the loading center are similar, regardless of the curling conditions.
- The surface curvature index (SCI) exhibits the strongest correlation with SSR and is selected as an input for the SSR prediction model. The accuracy of the SSR prediction model is good, with an R^2 of 0.98 and a low RMSE of 0.026, further confirming the potential error in the SSR prediction is insignificant.

Composite pavement

- The PCC slab joints in composite pavements play a crucial role in the mechanical responses of such pavements during FWD testing. Due to the effects of the PCC slab joint, the normal and shear strains in the longitudinal direction at the bottom of the asphalt layer show second fluctuations.
- The extreme value of shear strain in second fluctuation can be utilized to evaluate reflective cracking. For a given loading distance, the shear strain increases as the reflective crack depth increases. When the reflective crack depth reaches 75% of the asphalt layer thickness, the shear strain increases sharply.
- The BDI is adjusted as the $BDI_{composite}$, designed to identify the PCC slab joint location in composite pavements. The $BDI_{composite}$ shows a strong correlation with the extreme value of the normal strain in second fluctuation, with a Pearson correlation coefficient of 97.8%.
- The SCI is highly correlated (Pearson's $r = 98.4\%$) with the extreme value of shear strain, making it a reasonable indicator for assessing reflective cracking development based on FWD testing.
- Reflective cracking can be recognized and estimated by the $BDI_{composite}$ and SCI based on FWD testing. When both $BDI_{composite}$ and SCI show large values in routine surveys, reflective cracks are likely propagating.

9.2 Future Work

While this study developed RSL prediction models for the three INDOT pavement types and classifications, additional research is recommended to further validate the models using additional field data, especially data that cover an entire pavement in-service life. Furthermore, additional research is recommended for specific prediction models in the framework of maintenance strategy determination.

The study found the accuracy of critical strain prediction models is sufficient to allow model implementation, but additional research is recommended to further validate the models with additional field sections under various structural and environmental conditions, to cover an extended range of strain levels and pavement conditions. Specifically, additional strain values measured from various pavement sections are needed to further validate the critical strain prediction models, because this study included limited field measured strains. Furthermore, it is recommended to include field data and FE analysis results for pavements with a shallow bedrock, since pavement structural behavior and critical responses may be changed when bedrock is located at a shallow depth.

The new model was verified using INDOT full-depth asphalt flexible pavements and it can be applied to such pavements in other states and countries when the total pavement thicknesses and layer moduli are within the range evaluated in this study. However, additional research is recommended to extend the new SN_{eff} prediction model to other full-depth asphalt flexible pavement structures (i.e., additional layer thicknesses and layer moduli combinations) and other pavement types, including conventional flexible, rigid, and composite pavements, following the approach presented herein.

While this study developed the SSR prediction model using a synthetic database, covering a broad range of rigid pavement structures, further research is recommended to enhance the accuracy of SSR prediction by including additional pavement structures. These additional pavement structures may consider various aggregate base layer thicknesses and different stiffness levels for the base and subgrade.

This study mainly focuses on mid-slab FWD testing for evaluating the structural capacity of PCC slabs, while PCC slab joint FWD testing is also important to understand the LTE of in-service JPCP, which affects the structural capacity of rigid pavements. Since this study successfully developed an FE model to simulate joint conditions, it is recommended to investigate joint behavior under FWD loading using the FE model presented in this study. Consequently, a parametric study on joint behavior using the FE model may provide more insights regarding the assessment of the LTE of in-service pavements.

In further research, more simulations will be conducted to refine the relationship between SCI and reflective cracking depth to support informed maintenance decisions. Additionally, more field data (e.g., ground penetrating radar (GPR) and core samples) will be collected to verify the relationship between the $BDI_{composite}$ and the loading distance.

After verifying with additional field data, it is recommended that the SCI and $BDI_{composite}$ be incorporated into the maintenance decision matrix for composite pavements. This will facilitate accurate maintenance decisions. Additionally, selecting a maintenance strategy for reflective cracking using the proposed FE approach and analysis warrants further research. The FE analysis can be used to simulate the mechanical response of the composite pavements under various maintenance strategies to allow for predictions regarding the effectiveness of the maintenance.

REFERENCES

AASHTO. (1993). *AASHTO guide for design of pavement structures*. American Association of State Highway and Transportation Officials.

AASHTO. (2020). *Mechanistic-empirical pavement design guide* (3rd ed.). American Association of State Highway and Transportation Officials.

Abd El-Raof, H. S., Abd El-Hakim, R. T., El-Badawy, S. M., & Afify, H. A. (2020). Structural number prediction for flexible pavements using the long-term pavement performance data. *International Journal of Pavement Engineering*, *21*(7), 841–855. https://doi.org/10.1080/10298436.2018.1511786

Abdelaziz, N., Abd El-Hakim, R. T., El-Badawy, S. M., & Afify, H. A. (2020). International Roughness Index prediction model for flexible pavements. *International Journal of Pavement Engineering*, *21*(1), 88–99. https://doi.org/10.1080/10298436.2018.1441414

ACI. (2022). *ACI CODE-318–19(22): Building code requirements for structural concrete and commentary*. American Concrete Institute.

Al-Abbasi, A., & Shalaby, A. (2021). Evaluation of composite pavement joints using the Falling Weight Deflectometer. *Journal of Transportation Engineering, Part B: Pavements*, *147*(2), 04021007. https://doi.org/10.1061/JPEODX.000262

Albuquerque, F. S., & Núñez, W. P. (2011). Development of roughness prediction models for low-volume road networks in northeast Brazil. *Transportation Research Record*, *2205*(1), 198–205. https://doi.org/10.3141/2205-25

Al-Suleiman, T. I., & Shiyab, A. M. (2003). Prediction of pavement remaining service life using roughness data—Case study in Dubai. *International Journal of Pavement Engineering*, *4*(2), 121–129. https://doi.org/10.1080/10298430310001634834

Ban, H., Im, S., Kim, Y.-R., & Jung, J. S. (2018). Laboratory tests and finite element simulations to model thermally induced reflective cracking of composite pavements. *International Journal of Pavement Engineering*, *19*(3), 220–230. https://doi.org/10.1080/10298436.2017.1279491

Bayrak, M. B., & Ceylan, H. (2008). Neural network-based approach for analysis of rigid pavement systems using deflection data. *Transportation Research Record*, *2068*(1), 61–70. https://doi.org/10.3141/2068-07

Bryce, J., Flintsch, G., Katicha, S., & Diefenderfer, B. (2013). Developing a network-level structural capacity index for asphalt pavements. *Journal of Transportation Engineering*, *139*(2), 123–129. https://doi.org/10.1061/(ASCE)TE.1943-5436.0000494

Chen, D., Hildreth, J., & Mastin, N. (2019). Determination of IRI limits and thresholds for flexible pavements. *Journal of Transportation Engineering, Part B: Pavements*, *145*(2), 04019013. https://doi.org/10.1061/JPEODX.0000113

Crovetti, J. A. (2002). Deflection-based analysis techniques for jointed concrete pavement systems. *Transportation Research Record*, *1809*(1), 3–11. https://doi.org/doi.org/10.3141/1809-01

Dalla Rosa, F., Liu, L., & Gharaibeh, N. G. (2017). IRI prediction model for use in network-level pavement management systems. *Journal of Transportation Engineering, Part B: Pavements*, *143*(1), 04017001. https://doi.org/10.1061/JPEODX.0000003

Das, A., Bhuyan, M. R., Khattak, M. J., & Zhang, Q. (2020). Mitigating reflective cracking in composite pavements through the use of a ductile concrete interlayer. *Construction and Building Materials*, *259*, 120383. https://doi.org/10.1016/j.conbuildmat.2020.120383

Delatte, N. (2018). *Concrete pavement design, construction, and performance*. CRC Press. https://doi.org/10.1201/9781482288483

Deilami, S., & White, G. (2020). Review of reflective cracking in composite pavements. *International Journal of Pavement Research and Technology*, *13*(5), 524–535. https://doi.org/10.1007/s42947-020-0332-5

Gopalakrishnan, K., Kim, S., & Ceylan, H. (2010). Nondestructive evaluation of in-place rehabilitated concrete pavements. *Journal of Civil Engineering and Management*, *16*(4), 552–560. https://doi.org/10.3846/jcem.2010.61

Horak, E., Hefer, A., Emery, S., & Maina, J. (2015). Flexible road pavement structural condition benchmark methodology incorporating structural condition indices derived from Falling Weight Deflectometer deflection bowls. *Journal of Civil Engineering and Construction*, *4*(1), 1–14.

INDOT. (2024). *2024 Indiana Department of Transportation standard specifications*. Indiana Department of Transportation. https://www.in.gov/dot/div/contracts/standards/book/sep23/2024%20Standard%20Specifications.pdf

Isla, F., Luccioni, B., Ruano, G., Torrijos, M. C., Morea, F., Giaccio, G., & Zerbino, R. (2015). Mechanical response of fiber reinforced concrete overlays over asphalt concrete substrate: Experimental results and numerical simulation. *Construction and Building Materials*, *93*, 1022–1033. https://doi.org/10.1016/j.conbuildmat.2015.05.050

Kavussi, A., Abbasghorbani, M., Moghadas Nejad, F., & Bamdad Ziksari, A. (2017). A new method to determine maintenance and repair activities at network-level pavement management using Falling Weight Deflectometer. *Journal of Civil Engineering and Management*, *23*(3), 338–346. https://doi.org/10.3846/13923730.2015.1073173

Khattab, A. M., El-Badawy, Al Hazmi, A. A., & S. M., Elmwafi, M. (2014). Evaluation of Witczak E* predictive models for the implementation of AASHTOWare-Pavement ME Design in the Kingdom of Saudi Arabia. *Construction and Building Materials*, *64*, 360–369. https://doi.org/10.1016/j.conbuildmat.2014.04.066

Khattak, M. J., Nur, M. A., Bhuyan, M. R.-U.-K., & Gaspard, K. (2014). International Roughness Index models for HMA overlay treatment of flexible and composite pavements. *International Journal of Pavement Engineering*, *15*(4), 334–344. https://doi.org/10.1080/10298436.2013.842237

Kim, K., & Chun, S. (2015). Evaluation of internally cured concrete pavement using environmental responses and critical stress analysis. *International Journal of Concrete Structures and Materials*, *9*(4), 463–473. https://doi.org/10.1007/s40069-015-0115-6

Kim, K., Chun, S., Park, B., & Han, S. (2021). Precast prestressed concrete pavement (PPCP): Effect of thermal gradient on curling deflection and stress. *Construction and Building Materials*, *274*, 121966. https://doi.org/10.1016/j.conbuildmat.2020.121966

Kim, M. Y., Kim, D. Y., & Murphy, M. R. (2013). Improved method for evaluating the pavement structural number with Falling Weight Deflectometer deflections. *Transportation Research Record*, *2366*(1), 120–126. https://doi.org/10.3141/2366-14

Kim, Y. R., Castorena, C., Wang, Y., Ghanbari, A., & Jeong, J. (2018). *Comparing performance of full-depth asphalt pavements and aggregate base pavements in NC* (Report No. HWY-2015-02). North Carolina Department of Transportation.

Lee, H. S., Vavrik, W., & Abdualla, H. (2020). *Development of IDOT's proposed smoothness specification based on the International Roughness Index* (Report No. FHWA-ICT-20-009). Illinois Center for Transportation. https://doi.org/10.36501/0197-9191/20-015

Li, M., Wang, H., Xu, G., & Xie, P. (2017). Finite element modeling and parametric analysis of viscoelastic and nonlinear pavement responses under dynamic FWD loading.

Construction and Building Materials, *141*, 23–35. https://doi.org/10.1016/j.conbuildmat.2017.02.096

Mezhoud, S., Clastres, P., Houari, H., & Belachia, M. (2018). Field investigations on injection method for sealing longitudinal reflective cracks. *Journal of Performance of Constructed Facilities*, *32*(4), 04018041. https://doi.org/10.1061/(ASCE)CF.1943-5509.0001186

Muslim, H. B., Haider, S. W., & Chatti, K. (2022). Influence of seasonal and diurnal FWD measurements on deflection-based parameters for rigid pavements. *International Journal of Pavement Engineering*, *23*(13), 4542–4553. https://doi.org/10.1080/10298436.2021.1958217

Noureldin, S., Zhu, K., Harris, D. A., & Li, S. (2005). *Non-destructive estimation of pavement thickness, structural number and subgrade resilience along INDOT highways* (Joint Transportation Research Program Publication No. FHWA/IN/JTRP-2004/35). West Lafayette, Indiana: Purdue University. https://doi.org/10.5703/1288284313281

Park, B., Cho, S., Rahbar-Rastegar, R., Nantung, T. E., & Haddock, J. E. (2022). Prediction of critical responses in full-depth asphalt pavements using the Falling Weight Deflectometer deflection basin parameters. *Construction and Building Materials*, *318*, 126019. https://doi.org/10.1016/j.conbuildmat.2021.126019

Peraka, N. S. P., & Biligiri, K. P. (2020). Pavement asset management systems and technologies: A review. *Automation in Construction*, *119*, 103336. https://doi.org/10.1016/j.autcon.2020.103336

Pierce, L. M., Bruinsma, J. E., Smith, K. D., Wade, M. J., Chatti, K., & Vandenbossche, J. (2017). *Using falling weight deflectometer data with mechanistic-empirical design and analysis, volume III: Guidelines for deflection testing, analysis, and interpretation*. (United States Department of Transportation Publication No. FHWA-HRT-16-011). Federal Highway Administration. https://www.fhwa.dot.gov/publications/research/infrastructure/pavements/16011/

Plati, C., Georgiou, P., & Papavasiliou, V. (2016). Simulating pavement structural condition using artificial neural networks. *Structure and Infrastructure Engineering*, *12*(9), 1127–1136. https://doi.org/10.1080/15732479.2015.1086384

Ramirez, L., & Morian, D. (2020). Structural characterization of fractured Portland cement concrete pavements in Pennsylvania from Falling Weight Deflectometer data. *Transportation Research Record: Journal of the Transportation Research Board*, *2674*(10), 781–793. https://doi.org/10.1177/0361198120937017

Rohde, G. T. (1994). Determining pavement structural number from FWD testing. *Transportation Research Record*, *1448*(1), 61–68. http://onlinepubs.trb.org/Onlinepubs/trr/1994/1448/1448-008.pdf

Ruiz, H. A. M., Grabe, P. J., & Maina, J. W. (2019). A mechanistic-empirical method for the characterisation of railway track formation. *Transportation Geotechnics*, *18*, 10–24. https://doi.org/10.1016/j.trgeo.2018.10.003

Saleh, M., & Van Der Walt, J. (2019). Evaluation of the structural capacity of rigid pavements at the network level. *Canadian Journal of Civil Engineering*, *46*(5), 439–447. https://doi.org/10.1139/cjce-2018-0363

Sen, S., & Khazanovich, L. (2023). Reconsidering the strength of concrete pavements. *International Journal of Pavement Engineering*, *24*(2), 2020270. https://doi.org/10.1080/10298436.2021.2020270

Shi, X., Mukhopadhyay, A., Zollinger, D., & Huang, K. (2021). Performance evaluation of jointed plain concrete pavement made with portland cement concrete containing reclaimed asphalt pavement. *Road Materials and Pavement Design*, *22*(1), 59–81. https://doi.org/10.1080/14680629.2019.1616604

Singh, A. P., Sharma, A., Mishra, R., Wagle, M., & Sarkar, A. K. (2018). Pavement condition assessment using soft computing techniques. *International Journal of Pavement Research and Technology*, *11*(6), 564–581. https://doi.org/10.1016/j.ijprt.2017.12.006

Sok, T., Hong, S. J., Kim, Y. K., & Lee, S. W. (2020). Evaluation of load transfer characteristics in roller-compacted concrete pavement. *International Journal of Pavement Engineering*, *21*(6), 796–804. https://doi.org/10.1080/10298436.2018.1511782

Suleiman, M. T., Gopalakrishnan, K., & Kevern, J. T. (2011). Structural response of pervious concrete pavement systems using Falling Weight Deflectometer testing and analysis. *Journal of Transportation Engineering*, *137*(12), 907–917. https://doi.org/10.1061/(ASCE)TE.1943-5436.0000295

Suraneni, P., Monical, J., Unal, E., Farnam, Y., Villani, C., Barrett, T. J., & Weiss, W. J. (2016). *Performance of concrete pavement in the presence of deicing salts and deicing salt cocktails* (Joint Transportation Research Program Publication No. FHWA/IN/JTRP-2016/25). West Lafayette, IN: Purdue University. https://doi.org/10.5703/1288284316350

Thompson, M. R., & Hoffman, M. S. (1983). Concepts for developing an NDT-based design procedure for determining asphalt concrete overlay thickness. *Transportation Research Record*, (930), 12–18.

Thompson, M. R., & Garg, N. (1998). *Mechanistic-empirical evaluation of the Mn/ROAD low volume road test sections* (Project IHR-535). Illinois Cooperative Highway and Transportation Research Program.

Wang, C., Xu, S., & Yang, J. (2021). Adaboost algorithm in artificial intelligence for optimizing the IRI prediction accuracy of asphalt concrete pavement. *Sensors*, *21*(17), 5682. https://doi.org/10.3390/s21175682

Wang, H., Li, M., Szary, P., & Hu, X. (2019). Structural assessment of asphalt pavement condition using back-calculated modulus and field data. *Construction and Building Materials*, *211*, 943–951. https://doi.org/10.1016/j.conbuildmat.2019.03.250

Xu, B., Ranjithan, S. R., & Kim, Y. R. (2002). New relationships between Falling Weight Deflectometer deflections and asphalt pavement layer condition indicators. *Transportation Research Record: Journal of the Transportation Research Board*, *1806*(1), 48–56. https://doi.org/10.3141/1806-06

Xu, Y., Fan, W., Cheng, P., & Shan, L. (2021). Mechanical characterisation of interface shear strain of multi-layer composite pavement. *International Journal of Pavement Engineering*, *22*(9), 1116–1122. https://doi.org/10.1080/10298436.2019.1662905

Zaghloul, S., Marukic, I. M., Ahmed, Z., Vitillo, N., Sauber, R., & Jumikis, A. (2004). Development of network-level structural adequacy index model for New Jersey Department of Transportation pavement management system. *Proceedings of the Transportation Research Board 83rd Annual Meeting*. Transportation Research Board.

Zhang, M., Zhang, J., Gong, H., Jia, X., Xiao, R., Huang, H., & Huang, B. (2022). Numerical investigation of pavement responses under TSD and FWD loading. *Construction and Building Materials*, *318*, 126014. https://doi.org/10.1016/j.conbuildmat.2021.126014

Zhu, Z., & Al-Qadi, I. L. (2024). Development of a full-scale approach to predict overlay reflective crack. *International Journal of Pavement Engineering*, *25*(1), 2310095. https://doi.org/10.1080/10298436.2024.2310095

APPENDICES

Appendix A. Abbreviation Table

Appendix B. Laboratory and Field Tests

Appendix C. Finite Element Models

Appendix D. Frameworks of Maintenance Strategy Determination

APPENDIX A. ABBREVIATION TABLE

Table A.1 Abbreviation table

Abbreviation	Full Name
AASHTO	American Association of State Highway and Transportation Officials
AMPT	Asphalt Mixture Performance Tester
ANN	Artificial Neural Network
APT	Accelerated Pavement Testing
AUPP	Area Under Pavement Profile
BCI	Base Curvature Index
BDI	Base Damage Index
$BDI_{composite}$	Composite Pavement Base Damage Index
CBR	California Bearing Ratio
COST	European Cooperation in Science and Technology
DBPs	Deflection Basin Parameters
DOTs	Departments of Transportation
ESALs	Equivalent Single Axle Loads
FE	Finite Element
FWD	Falling Weight Deflectometer
GPR	Ground Penetrating Radar
INDOT	Indiana Department of Transportation
IRI	International Roughness Index
JPCP	Jointed Plain Concrete Pavement
LTE	Load Transfer Efficiency
LTPP	Long-Term Pavement Performance
M&R	Pavement Maintenance and Rehabilitation
MEPDG	Mechanistic-Empirical Pavement Design Guide
NDT	Non-Destructive Testing
PCC	Plain Cement Concrete
PMS	Pavement Management Systems
R^2	Coefficient of Determination
RCD	Reflective Cracking Damage
RM	Resilient Modulus
RMSE	Root Mean Square Error
RSL	Remaining Service Life
RSL_{IRI}	Functional Condition-Based RSL
SC (SC1, SC2)	Structural Coefficients
SCI	Surface Curvature Index
SN	Structural Number
SN_{eff}	Effective Structural Number

SNR	Structural Number Ratio
SN_{req}	Required Structural Number
SSR	Stress-Strength Ratio
TSD	Traffic Speed Deflectometer
VDOT	Virginia Department of Transportation

APPENDIX B. LABORATORY AND FIELD TESTS

B.1 Falling Weight Deflectometer (FWD) Test

Description of FWD Test

The FWD is a non-destructive testing device widely used to assess the structural condition of pavement and is designed to mimic a single heavy moving truck wheel load by applying an impulse load. One FWD loading set consists of three load level drops, including 7,000 lbf (31 kN), 9,000 lbf (40 kN), and 11,000 lbf (49 kN). The resulting pavement deflection is measured by nine geophones placed in a straight line at various distances from the center of the FWD loading plate. Each drop of the FWD weights generates a deflection basin curve. Figure B.1 shows a photo of the FWD equipment and the locations of the nine geophones, along with an example of an FWD deflection basin curve. It should be noted that the deflection measured from the geophone placed at "x (mm or in.)" distance from the loading center is typically denoted as Dx.

(a)

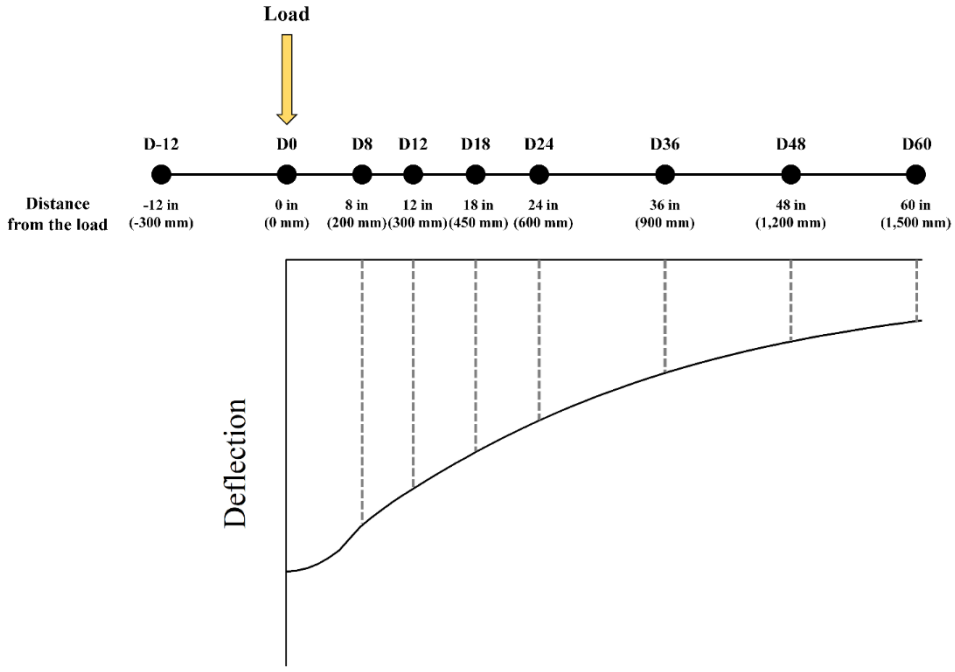

(b)

Figure B.1 FWD test: (a) FWD test equipment, (b) FWD geophone locations.

FWD Deflection Basin Parameters

The deflection basin parameters (DBPs) calculated from FWD test data are widely used to assess pavement structural conditions (Kavussi et al., 2017). Table B.1 summarizes the commonly used DBPs developed by previous researchers to interpret the FWD-induced pavement deflection basin for evaluating pavement structural condition (Horak et al., 2015; Kavussi et al., 2017). Figure B.2 is an example of the AAUP calculation.

Table B.1 FWD deflection basin parameters

Deflection Basin Parameter, Unit		Equation
D_0	Central deflection, mils	–
D_{60}	Deflection 60 inches away from the load center, mils	–
AUPP	Area under pavement profile, mils	$\frac{5 \times D_0 - 2 \times D_{12} - 2 \times D_{24} - D_{36}}{2}$
SCI	Surface curvature index, mils	$D_0 - D_{12}$
BDI	Base damage index, mils	$D_{12} - D_{24}$
BCI	Base curvature index, mils	$D_{24} - D_{36}$

Note: D_0, D_{12}, D_{24}, and D_{36} indicate the deflection (mils) at 0 in., 12 in., 24 in., and 36 in. away from the center of load.

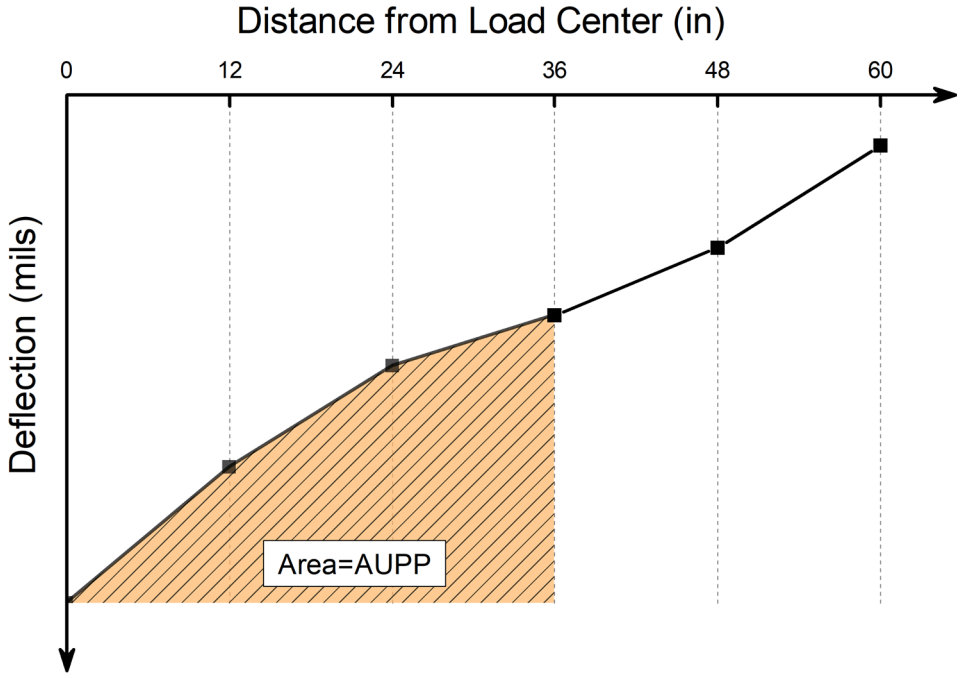

Figure B.2 Determination of area under pavement profile (AUPP).

B.2 Dynamic Modulus Test

The dynamic modulus test was conducted to obtain the viscoelastic material properties of asphalt layers, which were used as input parameters for FE analysis. As shown in Figure B.3, the typical INDOT full-depth asphalt flexible pavement consists of three asphalt layers: surface, intermediate, and base layers. In order to simulate more realistic field conditions, material properties were obtained from each asphalt layer. It was necessary to use small cylindrical specimens for the dynamic modulus tests, following the AASHTO TP 132-19 method. Figure B.3 shows that two small cores were extracted from each asphalt layer in a perpendicular direction and then trimmed using a diamond wet saw to produce the final small specimens of 1.5-in. diameter by 4.3 inches height. It

should be noted that the use of small specimens can provide equivalent dynamic modulus values to that measured from large specimens without significant statistical differences (Bowers et al., 2015; Lee et al., 2017).

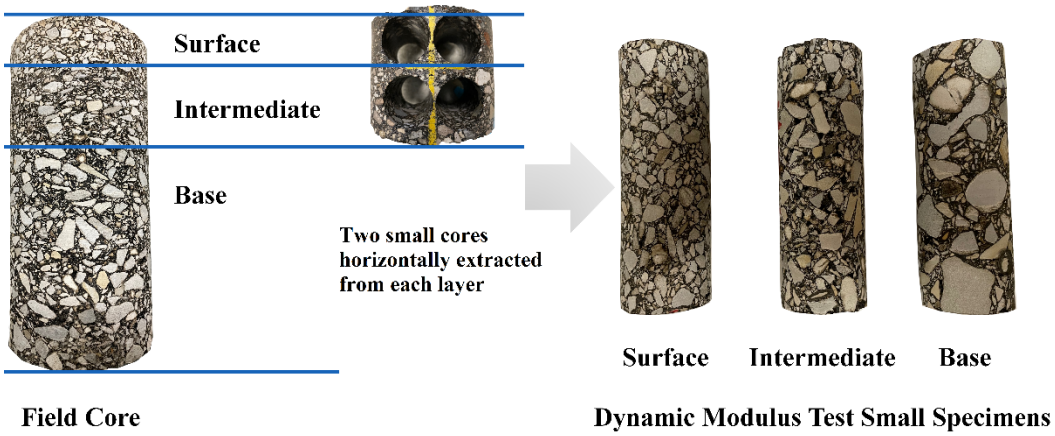

Figure B.3 Preparation of dynamic modulus test small specimens from field cores.

For each asphalt layer, three replicates were tested using the Asphalt Mixture Performance Tester (AMPT) at three temperatures (39.2°F, 68°F, and 104°F). A repeated axial cyclic load was applied at three loading frequencies (0.1 Hz, 1 Hz, and 10 Hz) for each temperature. Figure B.4(a) shows the AMPT test apparatus, including loading plates and three linear variable displacement transformers placed at the side of small specimen at 120° intervals. During the test, time, temperature, load, actuator displacement, and specimen deformation were measured by the AMPT. More details of the testing procedure and analysis can be found in (Park et al., 2022). As an example, Figure B.4(b) shows the AMPT-measured dynamic modulus for all asphalt layers (surface, intermediate, and base) of pavement Section A. For each layer, three replicates exhibited similar dynamic modulus values, indicating the three replicates were sufficient to represent the material properties of each layer for use in FE analyses.

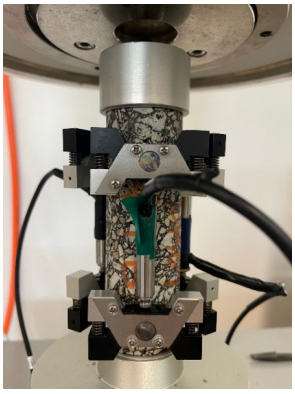

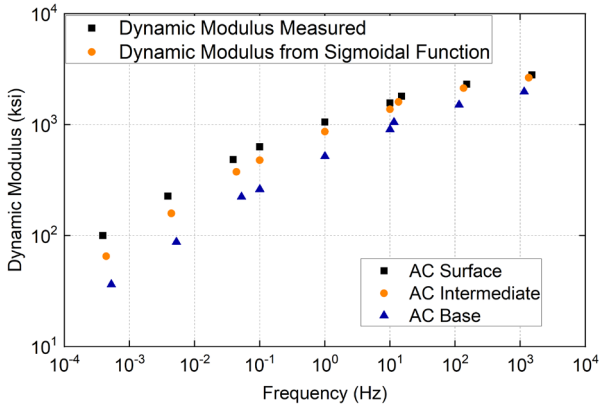

(a) (b)

Figure B.4 Dynamic modulus test: (a) AMPT test setup, (b) example dynamic modulus test results for pavement Section A.

APPENDIX C. FINITE ELEMENT MODELS

C.1 Full-Depth Asphalt Pavement

Pavement Structure and Layer Properties

A FE model was developed based on the representative INDOT full-depth asphalt flexible pavement structure. According to the INDOT specification, full-depth asphalt flexible pavement consists of three asphalt layers, i.e., surface, intermediate and base layers, placed directly on a prepared subgrade (INDOT, 2024). The representative pavement structure for this project was selected from an accelerated pavement testing (APT) test section used in a concurrent INDOT study. Table C.1 summarizes layer thicknesses and elastic material properties for the representative pavement cross section. During APT test section construction, each of the three asphalt mixtures were sampled and dynamic modulus testing conducted to determine viscoelastic and elastic material properties for the asphalt layers. The concept of equivalent elastic approach was employed to determine elastic moduli for asphalt layers using the loading frequency and dynamic modulus master curve (Park et al., 2021). The equivalent elastic moduli were defined as the dynamic modulus corresponding to a frequency of 30 Hz, at a 68°F reference temperature, as recommended for a typical FWD loading frequency (Ayyala et al., 2018).

Table C.1 Layer thicknesses and elastic properties for representative pavement structure

Layer Type	Thickness, inch	Elastic Modulus, ksi	Poisson's Ratio
Asphalt surface	1.5	1,886	0.35
Asphalt intermediate	2.5	1,740	0.35
Asphalt base	6	1,160	0.40
Subgrade	1,000	51	0.45

In addition, viscoelastic material properties for asphalt layers were obtained from the dynamic modulus tests, to consider the viscoelastic behavior of the layers during the FE model development. The relaxation modulus expressed by a Prony series was used as an input for viscoelastic properties in the FE model as shown in Equation C.1.

$$E(t) = E_0\left(1 - \sum_{i=1}^{N} e_i(1 - exp\,(-t/\tau_i))\right) \quad \text{(Eq. C.1)}$$

where, E_0 is instantaneous modulus, e_i is dimensionless relaxation moduli, and τ_i is relaxation times.

Table C.2 presents the viscoelastic properties for each asphalt layer, including instantaneous modulus (E_0), dimensionless relaxation modulus (e_i), and relaxation times (τ_i). Details on the determination of viscoelastic and equivalent elastic properties using dynamic modulus test results can be found elsewhere (Ayyala et al., 2018). For subgrade, the typical elastic modulus of INDOT pavements was used for both viscoelastic and equivalent elastic analyses. It should be noted that layer properties presented in Tables C.1 and C.2 were used as a reference to develop the FE model.

Table C.2 Viscoelastic material properties for representative pavement structure

Asphalt Surface		**Asphalt Intermediate**		**Asphalt Base**	
E_0	2,930 ksi	E_0	2,857 ksi	E_0	2,260 ksi
τ_i	e_i	τ_i	e_i	τ_i	e_i
1.00E-05	0.00658	1.00E-05	0.00020	1.00E-05	4.3E-07
1.00E-04	0.16795	1.00E-04	0.19214	1.00E-04	0.22900
1.00E-03	0.13606	1.00E-03	0.16213	1.00E-03	0.21698
1.00E-02	0.18942	1.00E-02	0.20676	1.00E-02	0.21355
1.00E-01	0.19642	1.00E-01	0.19600	1.00E-01	0.17179
1.00E+00	0.15068	1.00E+00	0.13271	1.00E+00	0.09820
1.00E+01	0.09068	1.00E+01	0.06738	1.00E+01	0.04243
1.00E+02	0.03234	1.00E+02	0.02346	1.00E+02	0.02163
1.00E+03	0.02316	1.00E+03	0.01109	1.00E+03	0.00640
1.00E+04	0.00014	1.00E+04	0.00035	1.00E+04	1.4E-05

Finite Element Model Description

Figure C.1 shows the FE model for the representative full-depth asphalt pavement system. The axisymmetric model was selected, which is more beneficial for simulating the circular load and requires less computational time and effort than a 3-dimensional model, without significant accuracy loss (Li et al., 2017). The model size and mesh density were determined based on sensitivity analysis. A finer mesh was applied to the area near the loading center, where the responses were acquired. Furthermore, a subgrade thickness of 1,000 inches was required to ensure no boundary effects at the bottom, as shown in Figure C.1. Meanwhile, a roller boundary condition was used for the center line (symmetric line) of the FE model, and a fixed boundary condition was applied to the bottom of subgrade. It should be noted that interfaces between all layers were considered as a fully bonded condition.

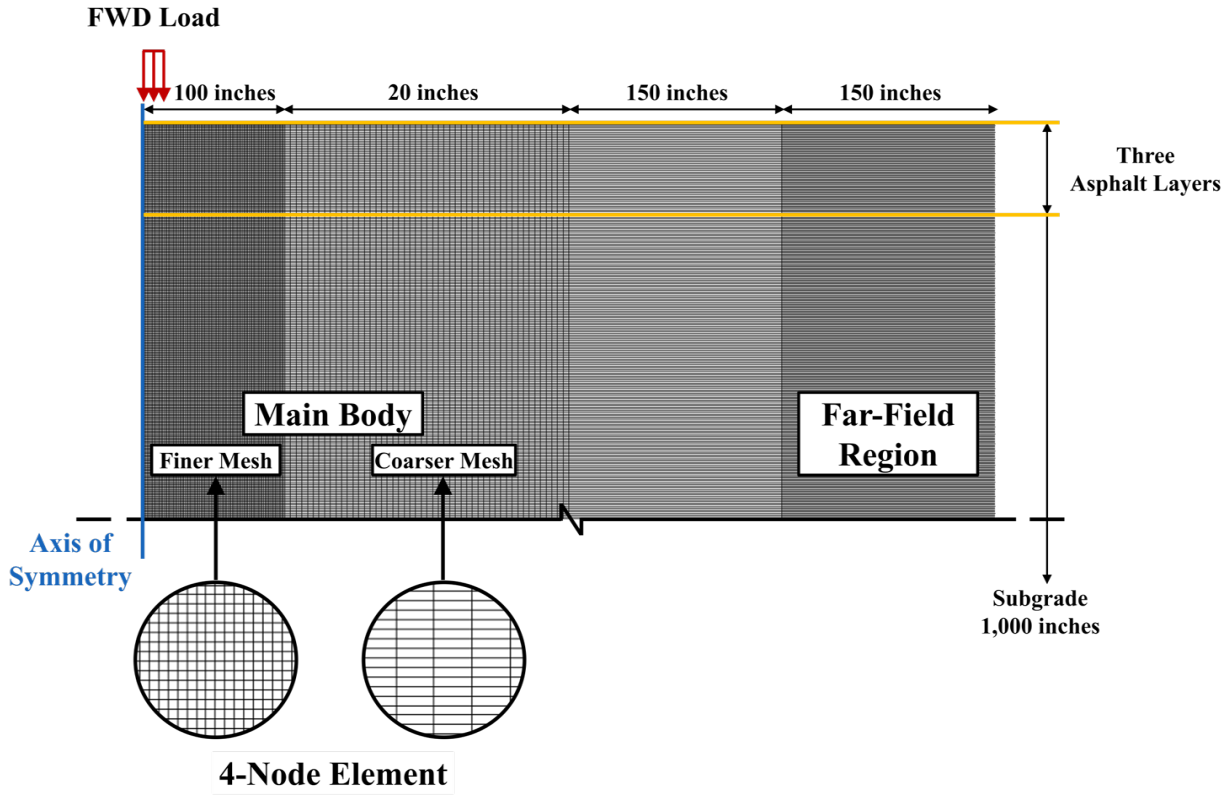

Figure C.1 Finite element model mesh description.

Loading Configuration

The 9,000 lbf static circular load (6-in. diameter, 80 psi pressure) was applied for an elastic FE model to represent the FWD loading. For viscoelastic analysis, the stationary half-sine load was applied at a 30 Hz loading frequency, the same frequency used for determining equivalent elastic material properties of asphalt layers. Figure C.2 shows the stationary half-sine loading curve, and the peak load pressure (80 psi) was consistent with the static load used for an elastic analysis. All results of the FE viscoelastic model were obtained at the peak load. In this way, the viscoelastic FE analysis results are comparable with other approaches under the same condition, while time-dependent behavior of viscoelastic material is considered.

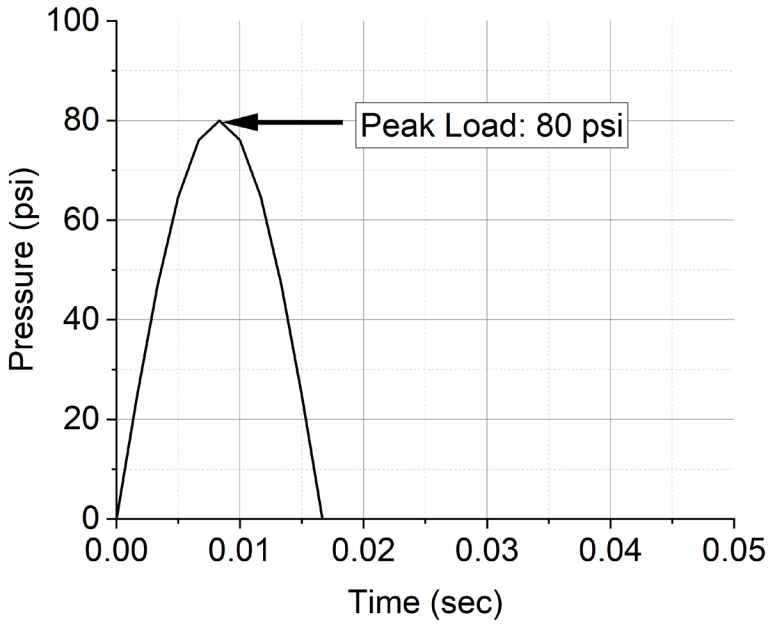

Figure C.2 Viscoelastic analysis loading curve.

Critical Locations and Finite Element Model Validation

The pavement responses predicted by the following three approaches were compared to verify the FE model: (1) viscoelastic FE analysis, (2) elastic FE analysis, and (3) layered elastic analysis (WESLEA). The transverse and vertical strain distributions through the pavement depth under the center of loading were employed to identify the locations of critical horizontal and vertical strains, as shown in Figure C.3. It should be noted that the positive sign indicates tension, and the negative value indicates compression for all results presented in this study. The maximum transverse tensile strain occurred at the bottom of the asphalt base layer, while the maximum vertical compressive strain was induced at the top of subgrade. These two locations were selected as critical locations for further evaluation and FE model verification.

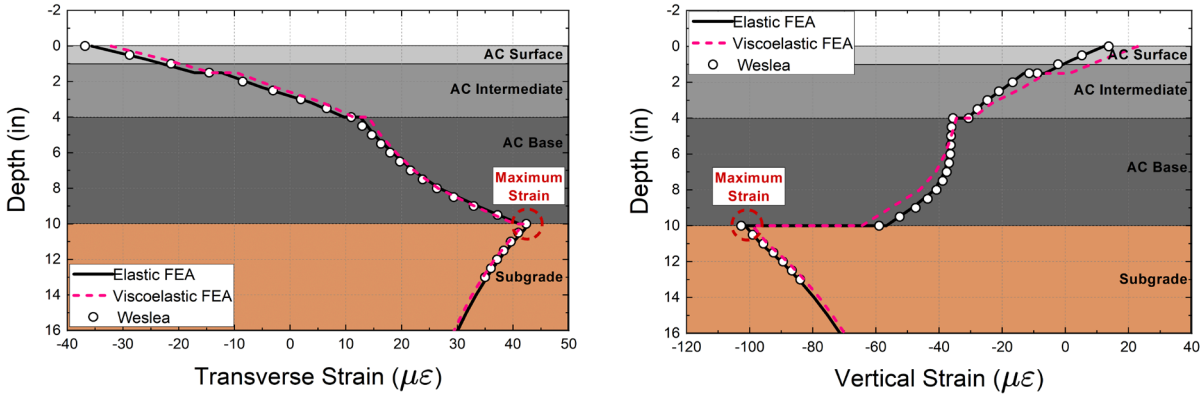

(a) (b)

Figure C.3 Critical strain location for: (a) bottom-up cracking, and (b) rutting.

Figure C.4 shows the deflection distributions at the surface and strains at the critical locations predicted from the viscoelastic and equivalent elastic FE models are similar, with the locations derived from layered elastic analysis results (analytical solution from WESLEA). These results clearly demonstrate the accuracy of the FE model in terms of the prediction of deflections and critical strains in full-depth asphalt flexible pavements. Furthermore, the results from elastic FE analysis exhibit a similar trend to the viscoelastic FE analysis results. This indicates that elastic analysis can be used in lieu of viscoelastic approach for the specific loading and environmental conditions. Therefore, the elastic FE model is considered sufficient to conduct a parametric study for the establishment of relationships between FWD parameters and critical strains.

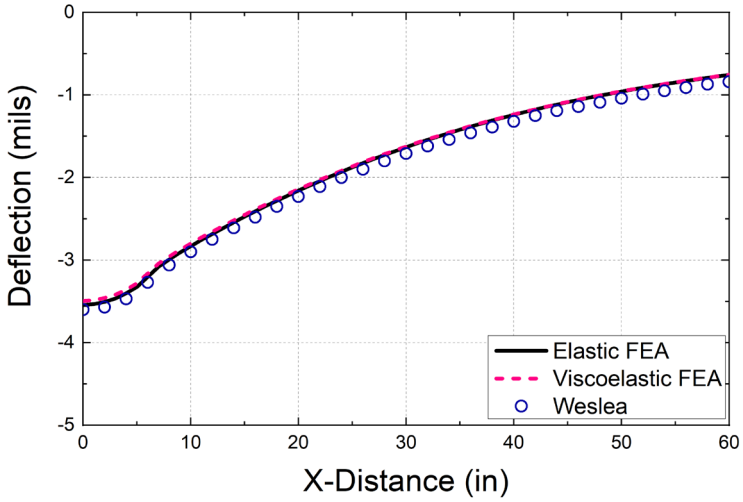

(a)

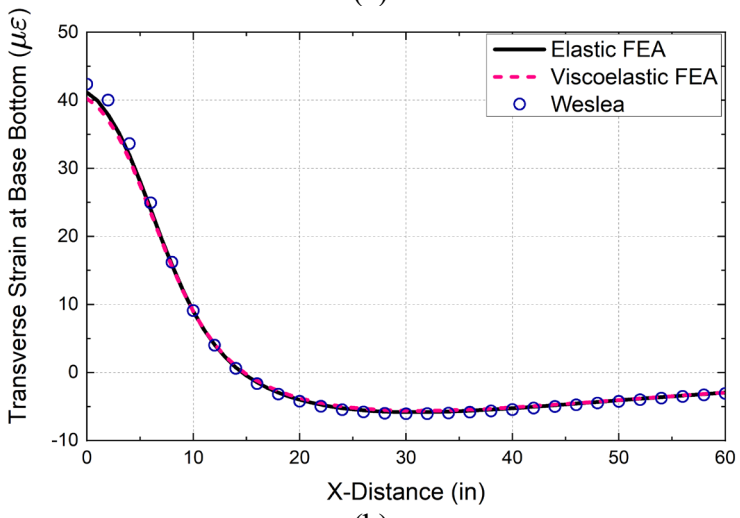

(b)

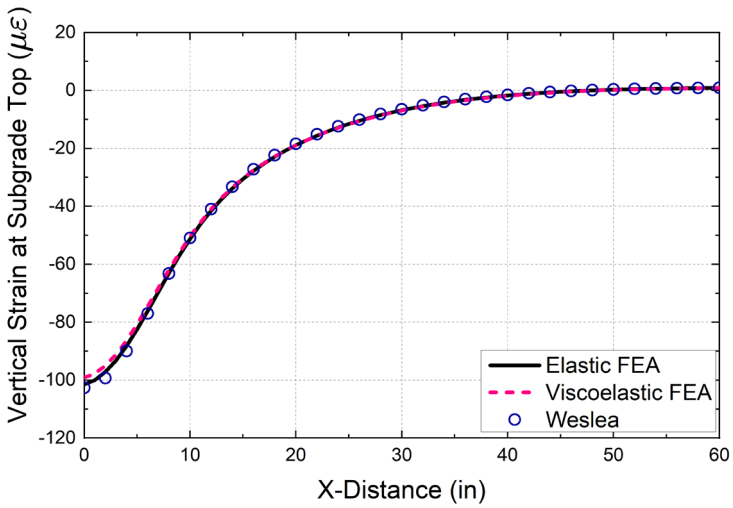

(c)

Figure C.4 Comparison of FE and layered elastic analysis results: (a) deflection basin curve, (b) transverse strain at the bottom of asphalt base layer, and (c) vertical strain at the top of the sub-grade.

For the two instrumented pavements, the FWD tests were conducted at the strain gauge locations. The FE model successfully provided almost identical deflection basin curves to those measured for both field sections, as shown in Figure C.5(a). Furthermore, Figure C.5(b) shows the strain calculated from the FE model exhibits good agreement with field measured strains in both field sections. The difference between the field-measured strains and the FE-calculated strains was 2.44 με and 1.74 με for Sections A and B, respectively. As expected, Section B exhibited smaller deflections and strains than Section A, due to the treated subgrade in Section B. Therefore, the FE model can be used to validate the remaining field sections without the use of strain gauges.

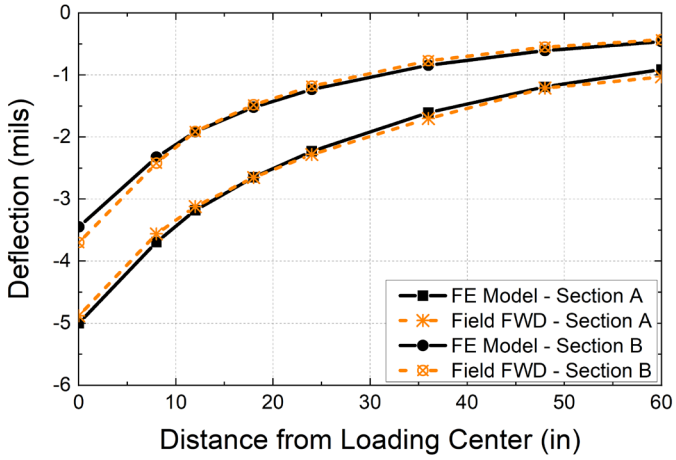

(a)

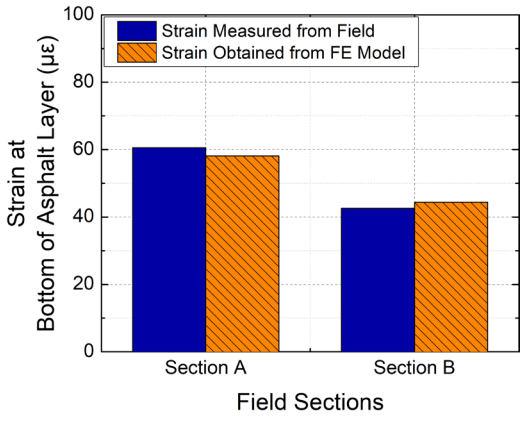

(b)

Figure C.5 FE model validation: (a) comparison of deflection basin curves, (b) comparison of strains at the bottom of asphalt layer.

Collection of Finite Element Model-Based FWD Data

The range of structural parameters representing INDOT full-depth asphalt flexible pavements was selected based on the INDOT standard specification (INDOT, 2024), as presented in Table C.3. Eight moduli were selected for the elastic modulus of each layer to represent the new pavement cases. The three asphalt base thicknesses were included to cover asphalt base thickness. Only one thickness was used for the asphalt surface (1.5 inches) and intermediate (2.5 inches) layers, due to their less significant effects.

Table C.3. The range of structural variables for the new pavement cases

Structural Variable	**New Pavement Cases**
Asphalt base thickness, inches	6, 9, 12
Asphalt surface modulus, ksi	800; 900; 1,000; 1,100; 1,200; 1,300; 1,400; 1,500
Asphalt intermediate modulus, ksi	800; 900; 1,000; 1,100; 1,200; 1,300; 1,400; 1,500
Asphalt base modulus, ksi	500; 600; 700; 800; 900; 1,000; 1,100; 1,200
Subgrade modulus, ksi	30; 40; 50; 60; 70; 80; 90; 100

In addition, two types of damaged pavement were included to cover a more extensive range of pavement responses: (1) 60% damaged asphalt surface case, and (2) damaged asphalt base and subgrade case. Table C.4 summarizes the structural variables for the pavements with 60% damaged asphalt surface. Eight combinations of asphalt surface modulus and asphalt intermediate modulus were selected, and three asphalt base thicknesses, eight asphalt base and subgrade moduli were used for each combination. Table C.5 presents the structural variable range for the damaged asphalt base and subgrade cases that include four additional lower asphalt base moduli and five reduced subgrade moduli. Consequently, a total of 3,927 structural combinations were simulated to identify a relationship between FWD parameters and critical pavement responses.

Table C.4 Structural variables range for 60% damaged asphalt surface cases

Structural Variable	**Sixty Percent Damaged Asphalt Surface Cases**
Asphalt base thickness, inches	6, 9, 12
Asphalt surface modulus, ksi	480; 540; 600; 660; 720; 780; 840; 900
Asphalt intermediate modulus, ksi	800; 900; 1,000; 1,100; 1,200; 1,300; 1,400; 1,500
Asphalt base modulus, ksi	500; 600; 700; 800; 900; 1,000; 1,100; 1,200
Subgrade modulus, ksi	30; 40; 50; 60; 70; 80; 90; 100

Table C.5 Structural variables range for damaged asphalt base and subgrade cases

Structural Variable	Damaged Asphalt Base and Subgrade Cases
Asphalt base thickness, inches	6, 9, 12
Asphalt surface modulus, ksi	800; 900; 1,000; 1,100; 1,200; 1,300; 1,400; 1,500
Asphalt intermediate modulus, ksi	800; 900; 1,000; 1,100; 1,200; 1,300; 1,400; 1,500
Asphalt base modulus, ksi	100; 200; 300; 400
Subgrade modulus, ksi	5; 10; 15; 20; 25

C.2 Rigid Pavement

Finite Element Model Description

Figure C.6 shows an example of the developed linear elastic FE model for the INDOT JPCP structure. A 3D FE model was used to simulate a JPCP structure, which consists of multiple concrete slabs with joints. As shown in Figure C.6(a), three concrete slabs were modeled and placed on top of the aggregate base layer. The middle concrete slab is used as the main slab for collecting data, while the other two slabs are used to account for the effect of adjacent slabs and joints.

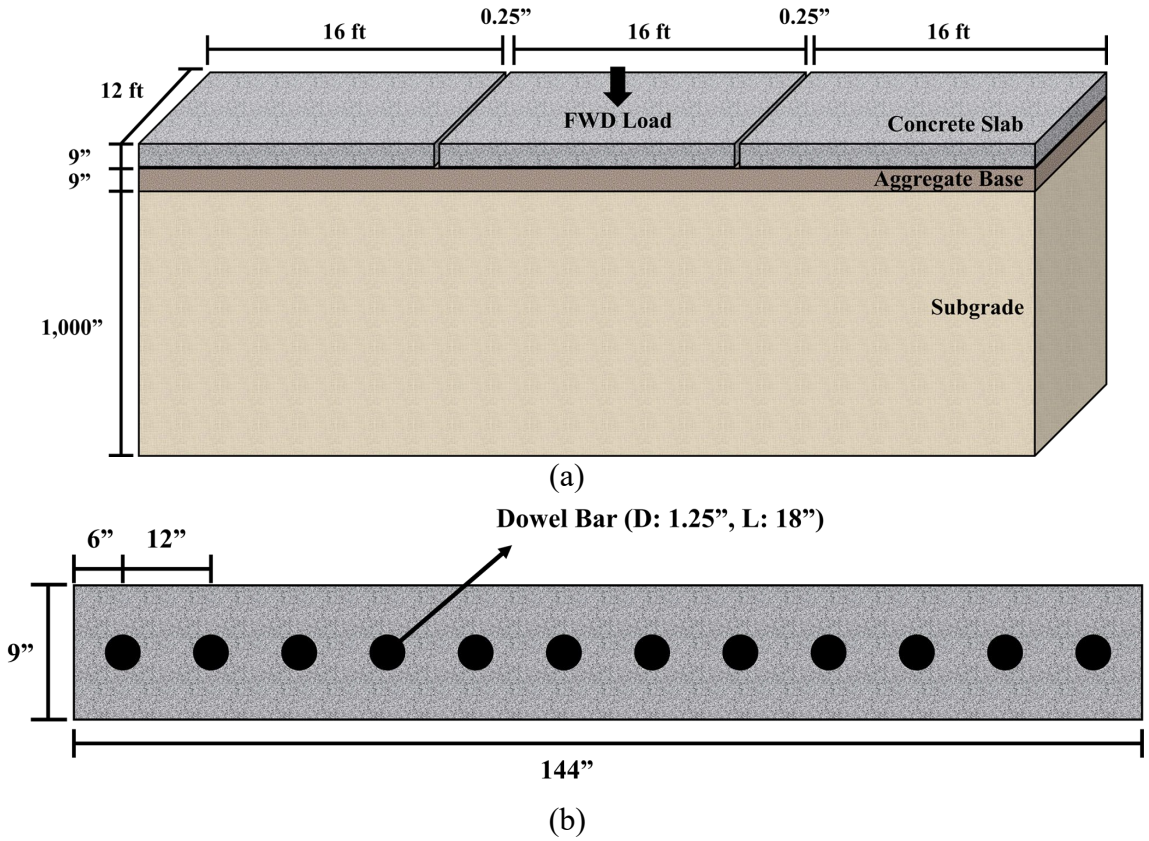

Figure C.6 JPCP FE model: (a) schematic of the entire structure, (b) schematic of the joint with dowel bars.

Joint conditions was modeled based on the INDOT specification (INDOT Standard Specifications, 2020). The spacing between concrete slabs was 0.25 inches, and concrete slabs were connected by 12 dowel bars, as shown in Figure C.6(b). The dowel bars were designed with a diameter of 1.25 inches, a length of 18 inches, and a center-to-center spacing of 12 inches. The material properties of the dowel bars were defined with an elastic modulus of 29,000 ksi and a Poisson's ratio 0.3. In addition, the subgrade was modeled with a thickness of 1,000 inches to minimize the effect of the fixed boundary condition at the bottom of the subgrade, simulating bedrock support (Kim et al., 2021). It is important to note that symmetric boundary conditions were applied with roller supports on all four sides of the FE model.

In order to simulate the curling effects, a contact model with a coefficient of friction of 1.5 was applied at the interface between concrete slab and the aggregate base layer for the effect of friction. Furthermore, the interface between the concrete slab and dowel bars was modeled as a frictional surface with a coefficient of friction of 0.6, while the dowel bar was confined by the weight of the concrete slab.

A square load of 12 inches by 12 inches was used to simulate the circular FWD loading with a 12-in. diameter, because it is more practical to apply a pressure load to various locations in a 3D FE model. The magnitude of pressure load was determined as 62.4 psi to match the total FWD load of 9,000 lbf. In addition, the temperature differential between the top and bottom of the concrete slab was defined to simulate the curling conditions.

Finite Element Model Validation

The developed FE model was validated with the field FWD deflection basin curve. For FE model validation, field cores were collected from the field section immediately after the FWD test to measure material properties and layer thickness. A compressive strength test was conducted to measure the compressive strength of concrete slab, following ASTM C39, as shown in Figure C.7. The measured compressive strength was then converted to the modulus of elasticity using the Equation 5.3 (ACI, 2022).

(a) (b)

Figure C.7 Material property measurements: (a) field core, (b) after the compressive strength test.

The measured compressive strength was 10.3 ksi, and the calculated elastic modulus was 5,540 ksi, which was used as material properties in the FE model. For the aggregate base layer and subgrade, elastic moduli were back calculated from the field FWD deflection basin curve. The values were 42 ksi and 41 ksi, respectively. Furthermore, the temperature differential was assumed as 2°C based on the measured concrete slab surface temperature during the FWD testing.

Figure C.8 shows that the deflection basin curve obtained from the developed FE model was almost identical to the field FWD deflection basin curve, indicating that the developed FE model is capable of accurately simulating FWD tests. Therefore, the developed FE model was used to establish synthetic database to develop the SSR prediction model.

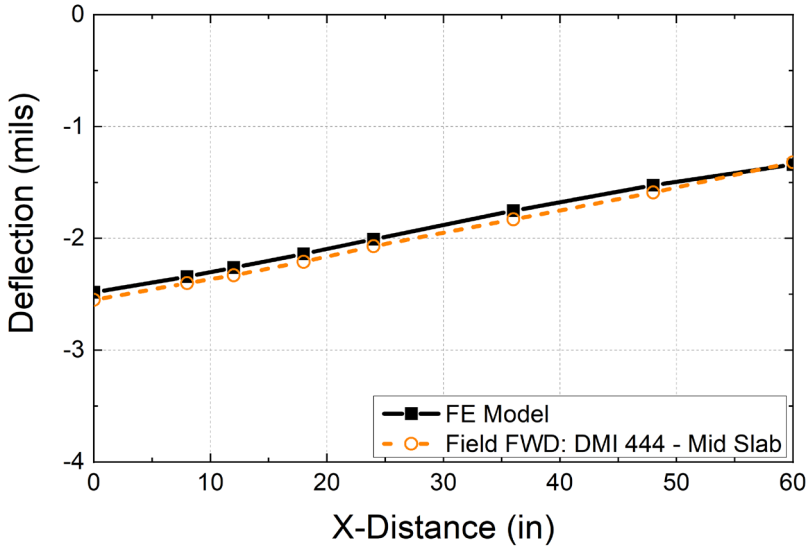

Figure C.8 Comparison between the finite element model deflection basin curve and field measured FWD deflection basin curve.

C.3 Composite Pavement

Geometry and Material

Model No. 8 is used as a representative example to introduce model development in the following sections. As shown in Figure C.9, the FE model consists of four layers: an asphalt surface, a PCC intermediate course, an aggregate base, and a soil subgrade. The PCC intermediate course contains three PCC slabs connected with 12 dowels uniformly distributed in the transverse direction. The dowels have a length of 18 inches and a diameter of 1.25 inches, with a joint width of 0.25 inches. The depth from the top of the soil subgrade to the bedrock is assumed to be 500 inches in the FE model to minimize the boundary effect.

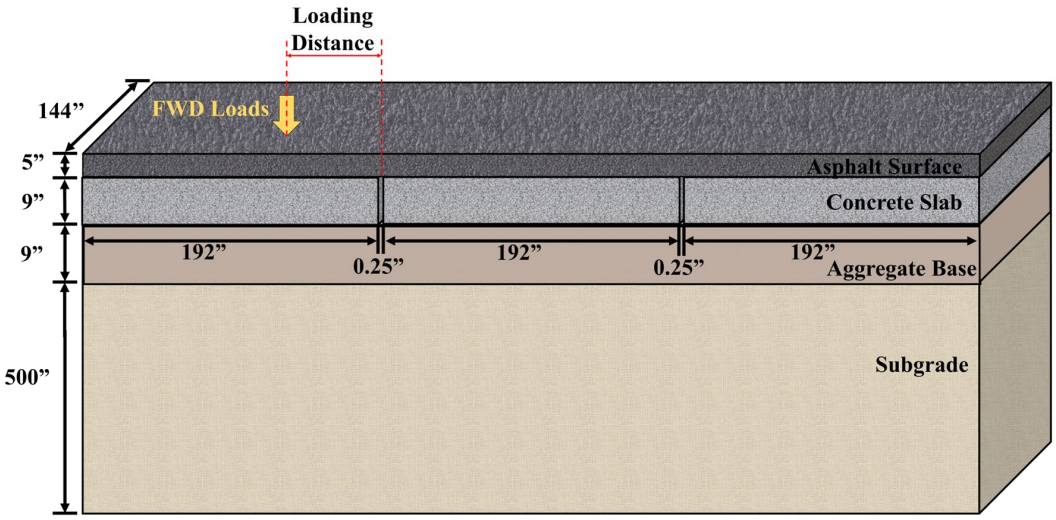

Figure C.9 The configuration of the FE model.

In the model, the PCC slabs, aggregate base, and unbound subgrade were considered as linear elastic materials (Table C.6). The asphalt mixture was treated as a viscoelastic material. The Prony series was used to characterize the material properties of the asphalt mixture, with parameters determined by regressing the measured dynamic modulus, as shown in Table C.7.

Table C.6 Material properties

No.	Layer	Density (lb/ft^3)	Elastic Modulus (ksi)
1	Asphalt concrete	145	2,930[1]
2	PCC slab	145	2,250
3	Aggregate base	86	17
4	Unbound subgrade	73	17

[1] Indicates the instantaneous modulus for the viscoelastic material in this table.

Table C.7 Prony series

i	G (i)	K (i)	Tau (i)
1	0.006583	0	1.00E-05
2	0.167946	0	0.0001
3	0.136063	0	0.001
4	0.18942	0	0.01
5	0.196419	0	0.1
6	0.150683	0	1
7	0.090681	0	10
8	0.032335	0	100
9	0.023156	0	1000
10	0.00014	0	10000

Loading and Boundary Conditions

The FWD load exhibits a half-sine waveform based on the field test data. The impulse loading was simplified into five loading steps to reduce computation time, as illustrated in Figure C.10. The loading pressure was uniformly distributed over a 12 inches square area. The magnitude of the impulse loading was 80 psi in model No. 8.

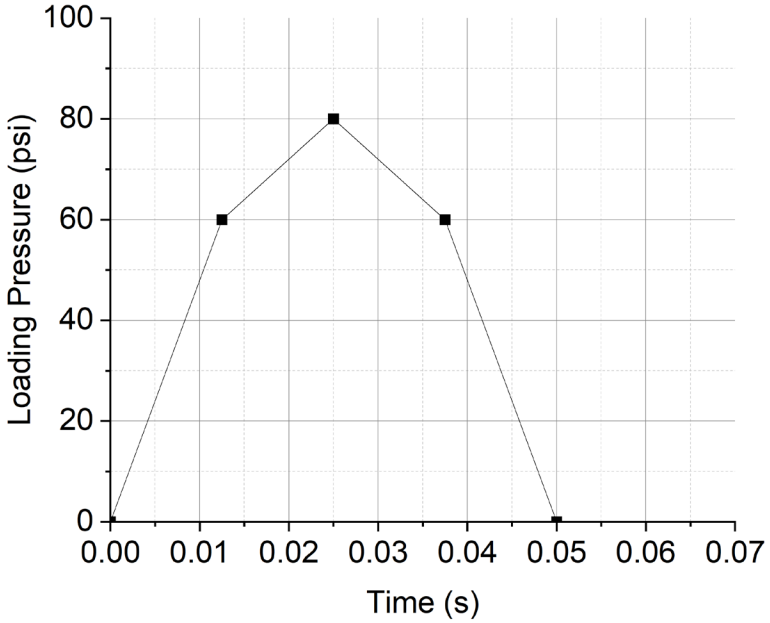

Figure C.10 Simplified impulse loading.

The bottom of the model was fixed to simulate bedrock support, while the sides were restricted to horizontal movements to represent surrounding constraints. The interfaces between the layers were set to hard contact in the normal direction, and the penalty friction formulation was used to model tangential behavior with a friction coefficient of 0.6. A 0.2-inch-wide notch was created at the bottom of the asphalt layer over the PCC joint to simulate reflective cracking.

Model Verification

After the composite FE model development, the parameters were verified using FWD data collected from the US 40 project. A total of 32 sets of FWD data were collected in the project, with 328 feet testing interval. The measured deflections are presented in the box chart in Figure C.11. The deflections at D_0 were corrected using the temperature correction equations specified in the AASHTO guidelines. The simulated deflections from the FE model are indicated with red dots in Figure C.11. The simulated deflections are close to the mean of the measured deflections, with a mean relative error of 6.21%. The FE model provides a reasonable simulation for the composite pavement, indicating the mechanical responses of the composite pavement in the FWD tests can be effectively analyzed using FE simulation results.

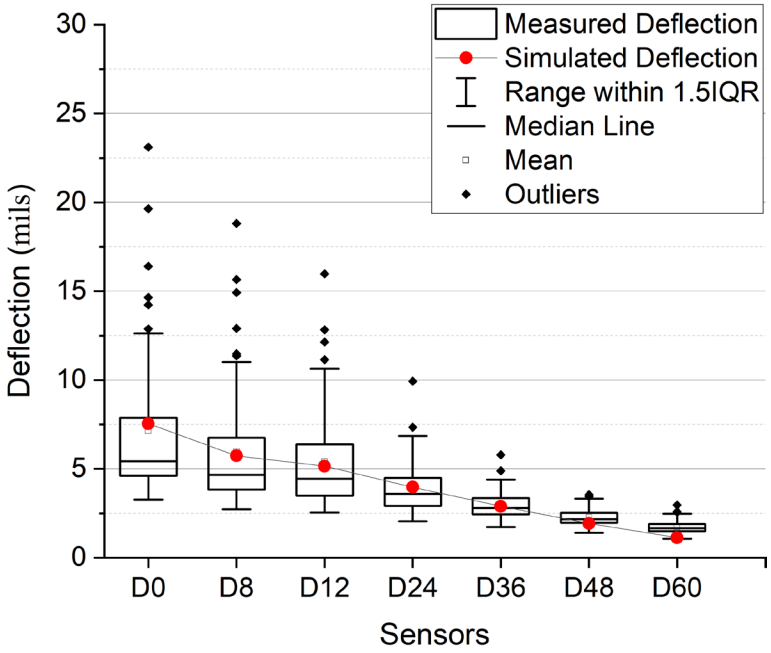

Figure C.11 Verification of the FE model using field data (US 40).

APPENDIX D. FRAMEWORKS OF MAINTENANCE STRATEGY DETERMINATION

D.1 Framework of Maintenance Strategy Determination for Full-depth Asphalt Flexible Pavements

Figure D.1 shows a decision framework to determine the maintenance strategy for asphalt pavements, requiring FWD and IRI measurements to consider both structural and functional conditions. A stepwise approach was applied to the proposed decision framework to determine the most appropriate maintenance strategy.

The SNR is defined as the ratio of the effective structural number (SN_{eff}) to the required structural number (SN_{req}), as expressed in Equation D.1. The SN_{eff} represents the overall structural conditions of in-service asphalt pavements, while the SN_{req} indicates the minimum structural number required for asphalt pavements to ensure desirable structural performance under traffic and environmental loads. Since the SN_{eff} of asphalt pavements with adequate structural capacity is expected to be greater than the SN_{req}, the theoretical minimum requirement for SNR is one.

$$SNR = \frac{SN_{eff}}{SN_{req}} \quad \text{(Eq. D.1)}$$

In the first step, two primary categories can be defined using the SNR: (1) pavements with sufficient structural capacity, and (2) pavements with insufficient structural capacity. The SN_{req} can be determined based on Equation D.2 (AASHTO, 1993).

$$\log ESAL = Z_R \times S_0 + 9.36 \times \log(SN_{req} + 1) - 0.2 + \frac{\log\left(\frac{\Delta PSI}{4.2 - 1.5}\right)}{0.4 + \frac{1094}{(SN_{req} + 1)^{5.19}}} + 2.32 \times \log M_R - 8.07 \quad \text{(Eq. D.2)}$$

$$M_R = \frac{0.24 \times P}{d_r \times r}$$

where ESAL is the equivalent single axle load, ΔPSI is a reduction in serviceability, S_0 is a standard deviation, Z_R is a standard normal deviate, M_R is a subgrade resilient modulus (ksi), P is the FWD load (lbs.), r is a distance from the center of load (in.), and d_r is a deflection at a distance r from the center of the load (in.).

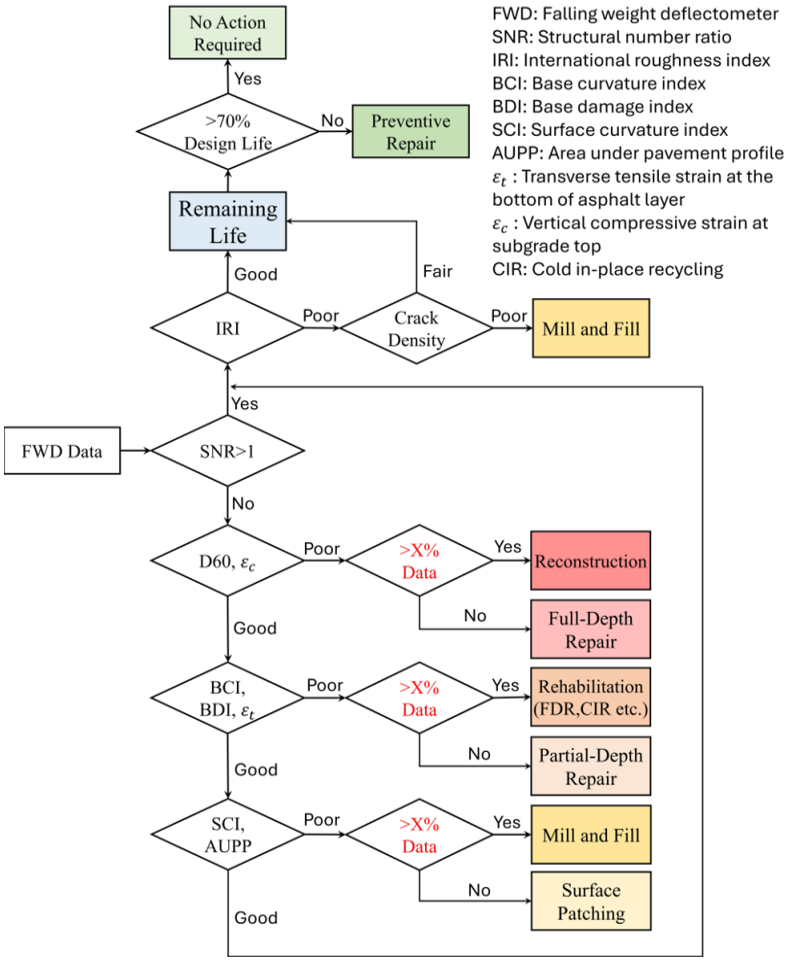

Figure D.1 Maintenance strategy framework for full-depth asphalt flexible pavements.

*Full-depth Asphalt Flexible Pavements with Sufficient Structural Capacity (**$SNR \geq 1$**)*

When the testing location exhibits sufficient structural capacity ($SNR \geq 1$), the functional conditions will be evaluated using the IRI measurements. If the measured IRI is smaller than the IRI thresholds (indicating a good condition), a functional condition-based RSL (RSL_{IRI}) is calculated using Equation 7.4. Preventive crack sealing is recommended for pavement with an RSL_{IRI} less than 70% of design life, while no further action is required when the RSL_{IRI} is more than 70% of design life. If the measured IRI exceeds the IRI thresholds (indicating a poor condition), investigating the crack density data is recommended. When crack density data indicates a fair condition, the RSL_{IRI} can be calculated to recommend either "a preventive crack sealing" or "no action required." If the crack density data indicates a poor condition, "mill and fill" is recommended. It should be noted that the step for investigating crack density can be skipped if no crack density data is available.

Full-depth Asphalt Flexible Pavements with Insufficient Structural Capacity ($\boldsymbol{SNR < 1}$)

When the testing location exhibits poor structural condition ($SNR < 1$), only structural conditions are considered in determining treatments. Then, the proposed framework suggests assessing from the subgrade (bottom layer) to the surface (top layer). Since maintenance activities to repair subgrade require the reconstruction of upper layers, it is more effective to evaluate the lower layer prior to assessing the upper layers.

First, as shown in Figure D.1, the subgrade structural capacity is assessed using either D_{60} or vertical compressive strain at the top of subgrade (ε_c). When the subgrade is indicated to be in poor condition, either "full-depth repair" or "reconstruction" is recommended, depending on the severity of the damages.

This study proposes to define the severity of damages based on the number of data points exceeding the threshold values within the tested section. In many cases, the pavement condition is not consistent even within the tested section. Thus, it is reasonable to consider the global condition of the target pavement section when determining the maintenance strategy for a specific location. As shown in Figure D.1, the decision point "> X% data," highlighted in red, was used to determine the damage severity and to recommend the final maintenance strategy. The specific percentage value can be determined based on the available budget and the specifications.

When the subgrade is in good condition, the base or subbase layers are evaluated using BCI and BDI. For full-depth asphalt flexible pavements, the transverse tensile strain at the bottom of the asphalt base layer (ε_t) can be used in this decision stage, while ε_t at the bottom of asphalt surface layer can be used in the next decision stage (evaluation of top layers). If the structural conditions of the base or subbase layers are identified as poor condition, either "rehabilitation" or "partial-depth repair" is recommended based on the damage severity.

The surface layer (top layers) can be evaluated using the SCI and AUPP in the last decision stage. Depending on the damage severity, either "mill and fill" or "surface patching" is recommended for the target pavement section. When the surface layer is determined to be in good condition, the functional condition of the target pavement section is assessed following the procedure described in the previous section.

D.2 A Framework of Maintenance Strategy Determination for Rigid Pavements

Figure D.2 shows a decision framework to determine the maintenance strategy for rigid pavements, requiring SSR and IRI measurements to consider both structural and functional conditions. This decision framework is designed to provide a maintenance strategy for individual testing location within the target section. Four levels of maintenance strategies were considered depending on the pavement conditions: "no action required," "preventive repair," "partial-depth repair," and "full-depth repair." In the first step, two primary categories can be defined using the SSR: (1) pavements with sufficient structural capacity, and (2) pavements with insufficient structural capacity.

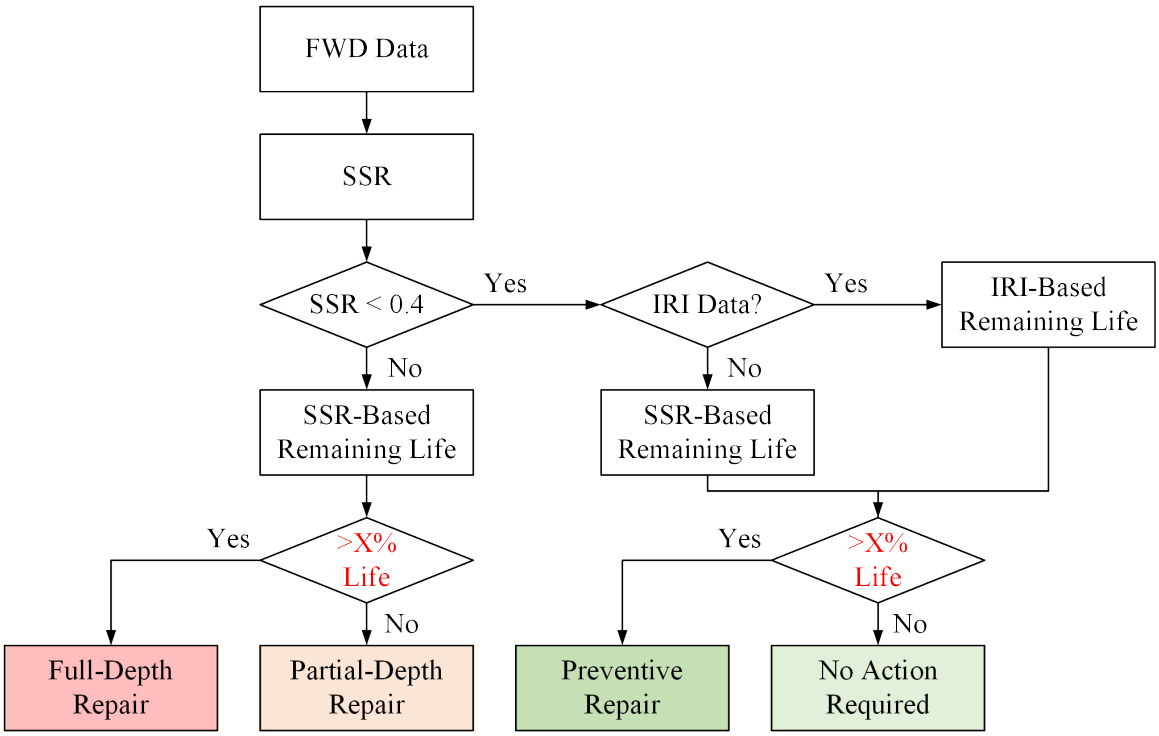

Figure D.2 Maintenance strategy framework for rigid pavements.

*Rigid Pavements with Sufficient Structural Capacity (**$SSR \geq 0.4$**)*

When the test data exhibits sufficient structural capacity ($SSR \geq 0.4$), the functional conditions will be evaluated using the IRI measurements. If the measured IRI is smaller than the IRI thresholds (indicating good condition), a functional condition-based RSL (RSL_{IRI}) is calculated using Equation 7.4. Preventive repair is recommended for pavement with an RSL_{IRI} less than 70% of design life, while no further action is required when the RSL_{IRI} is more than 70% of design life.

*Rigid Pavements with Insufficient Structural Capacity (**$SSR < 0.4$**)*

When the testing location exhibits poor structural condition ($SNR < 0.4$), it is not necessary to assess functional conditions, only structural conditions are considered in this case. A structural condition-based RSL is calculated using Equation 5.6. As discussed for the full-depth pavements, in many cases, the pavement condition is not consistent even within the tested section. Thus, it is reasonable to consider the global condition of the target rigid pavement section when determining the maintenance strategy for a specific location. As shown in Figure D.2, the decision point, ">X% data," highlighted in red, was used to determine the damage severity and to recommend the final maintenance strategy. The specific percentage value can be determined based on the available budget and the specifications. For example, if the agency defines the severe damage limit as 70% and more than 70% of data exceed the thresholds, then "reconstruction" is recommended for the target pavement section. Furthermore, it is important to note that the agency can determine an

appropriate testing interval to collect sufficient data, although collecting more data is desirable for making more accurate maintenance strategy decisions.

D.3 A Framework of Maintenance Strategy Determination for Composite Pavements

Figure D.3 shows a decision framework to determine the maintenance strategy for composite pavements, requiring RCD and IRI measurements to consider both structural and functional conditions. This decision framework is designed to provide a maintenance strategy for individual testing location within the target section, because pavement conditions may be inconsistent even within the same pavement section. Four levels of maintenance strategies were considered depending on the pavement conditions: "no action required," "preventive repair," "partial-depth repair," and "full-depth repair." A stepwise approach was applied to the proposed decision framework to determine the most appropriate maintenance strategy. In the first step, two primary categories can be defined using the RCD: (1) pavements with sufficient structural capacity, and (2) pavements with insufficient structural capacity.

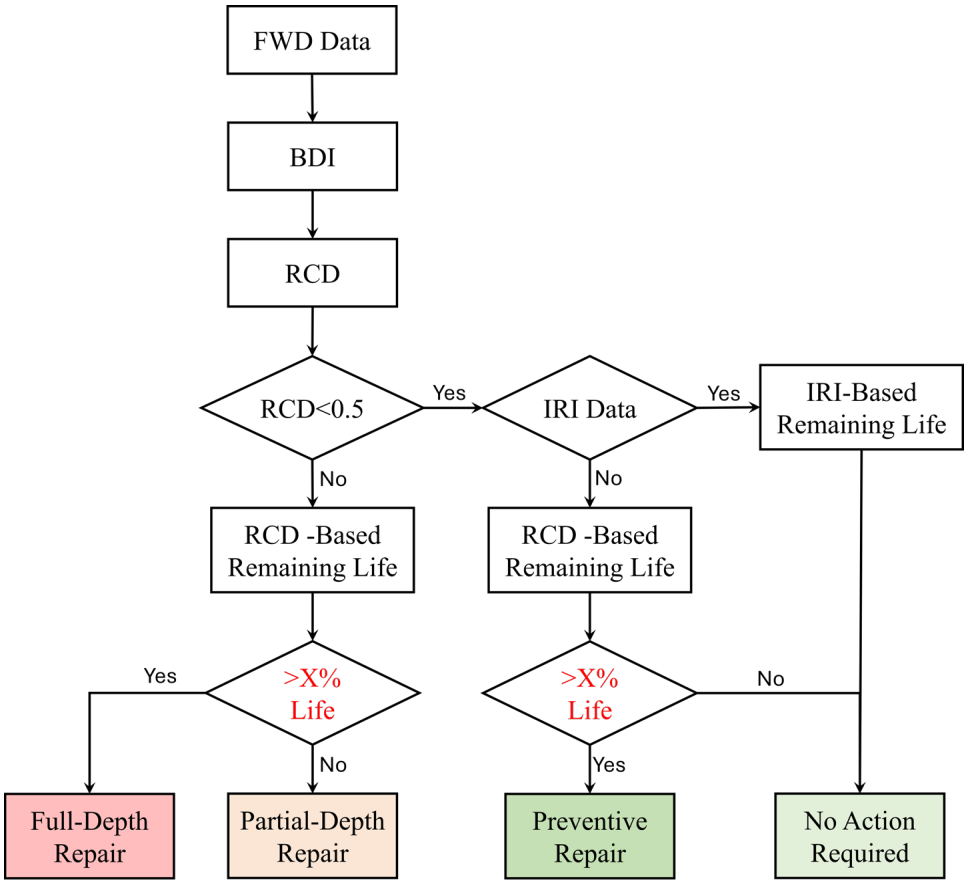

Figure D.3 Maintenance strategy framework for composite pavements.

*Composite Pavements with Sufficient Structural Capacity (**$RCD < 0.5$**)*

When the test data exhibits sufficient structural capacity ($RCD < 0.5$), the functional conditions will be evaluated using the IRI measurements. If the measured IRI is smaller than the IRI thresholds (indicating good condition), a functional condition-based RSL (RSL_{IRI}) is calculated using Equation 7.4. Preventive repair is recommended for pavement with an RSL_{IRI} less than 70% of design life, while no further action is required when the RSL_{IRI} is more than 70% of design life.

*Composite Pavements with Insufficient Structural Capacity (**$RCD \geq 0.5$**)*

When the test data exhibits poor structural condition ($RCD \geq 0.5$), it is not necessary to assess functional conditions, only structural conditions need to be considered. A structural condition-based RSL is calculated using Equation 6.7. The decision point, ">X% data," highlighted in red, was used to determine the damage severity and to recommend the final maintenance strategy. The specific percentage value can be determined based on the available budget and the specifications. For example, if the agency defines the severe damage limit as 70% and more than 70% of data exceed the thresholds, then "reconstruction" is recommended for the target pavement section. Furthermore, it is important to note that the agency can determine an appropriate testing interval to collect sufficient data, although collecting more data is desirable for making more accurate maintenance strategy decisions.

D.4 User-Friendly Software Development

The decision framework was developed to determine a specific maintenance strategy for the individual testing location, while numerous non-destructive testing data points are typically collected from one target pavement section. User-friendly software was developed to analyze all non-destructive test data and practically implement the decision framework, regardless of the number of test locations or the length of target pavement section. Figure D.4(a) shows the developed software interface, which can process raw data to calculate all structural and functional indicators presented in this study. For example, the software can import raw FWD data file with a ".f25" extension for analysis, including load calibration, temperature correction, and calculation of DBPs, critical strains, SN_{eff}, and structural condition-based RSL, as shown in Figure D.4(b). Furthermore, deflection basin curve can be displayed during the FWD data analysis. Similarly, historical IRI data can be processed to report average IRI, along with the left and right wheel path IRI values. Consequently, the developed software can be used to analyze raw FWD and IRI data, and the analyzed data can be exported in Excel format for the decision framework. It should be noted that the software provides a distance measuring instrument (DMI) for each test location, allowing for the practical matching of FWD and IRI data.

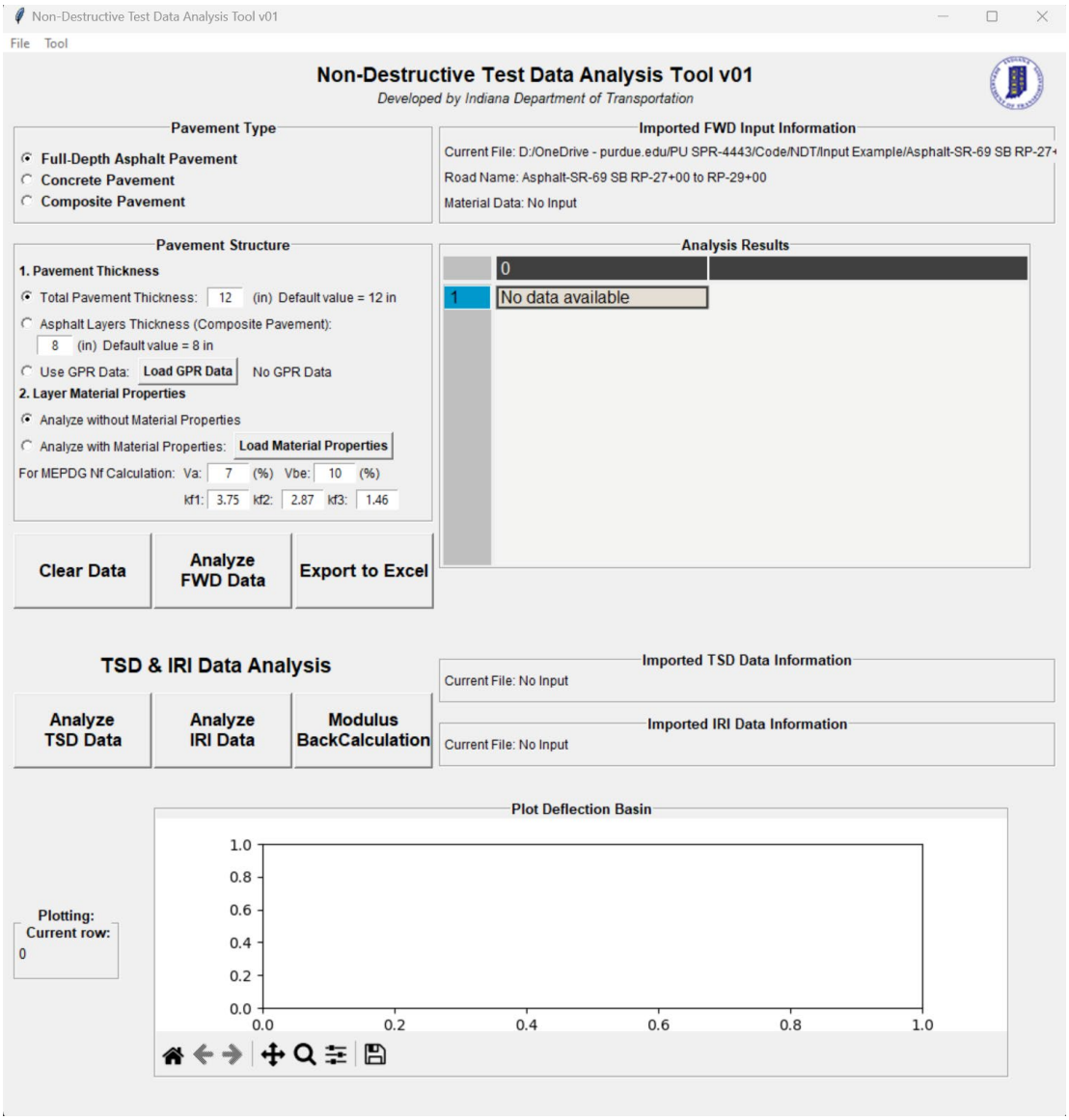
Non-Destructive Test Data Analysis Tool v01
File Tool
Non-Destructive Test Data Analysis Tool v01
Developed by Indiana Department of Transportation
Pavement Type
Full-Depth Asphalt Pavement
Concrete Pavement
Composite Pavement
Imported FWD Input Information
Current File: D:/OneDrive - purdue.edu/PU SPR-4443/Code/NDT/Input Example/Asphalt-SR-69 SB RP-27
Road Name: Asphalt-SR-69 SB RP-27+00 to RP-29+00
Material Data: No Input
Pavement Structure
1. Pavement Thickness
Total Pavement Thickness: 12 (in) Default value = 12 in
Asphalt Layers Thickness (Composite Pavement):
8 (in) Default value = 8 in
Use GPR Data: Load GPR Data No GPR Data
2. Layer Material Properties
Analyze without Material Properties
Analyze with Material Properties: Load Material Properties
For MEPDG Nf Calculation: Va: 7 (%) Vbe: 10 (%)
kf1: 3.75 kf2: 2.87 kf3: 1.46
Analysis Results
0
1 No data available
Clear Data
Analyze FWD Data
Export to Excel
TSD & IRI Data Analysis
Imported TSD Data Information
Current File: No Input
Analyze TSD Data
Analyze IRI Data
Modulus BackCalculation
Imported IRI Data Information
Current File: No Input
Plot Deflection Basin
Plotting:
Current row:
0
1.0
0.8
0.6
0.4
0.2
0.0
0.0
0.2
0.4
0.6
0.8
1.0

(a)

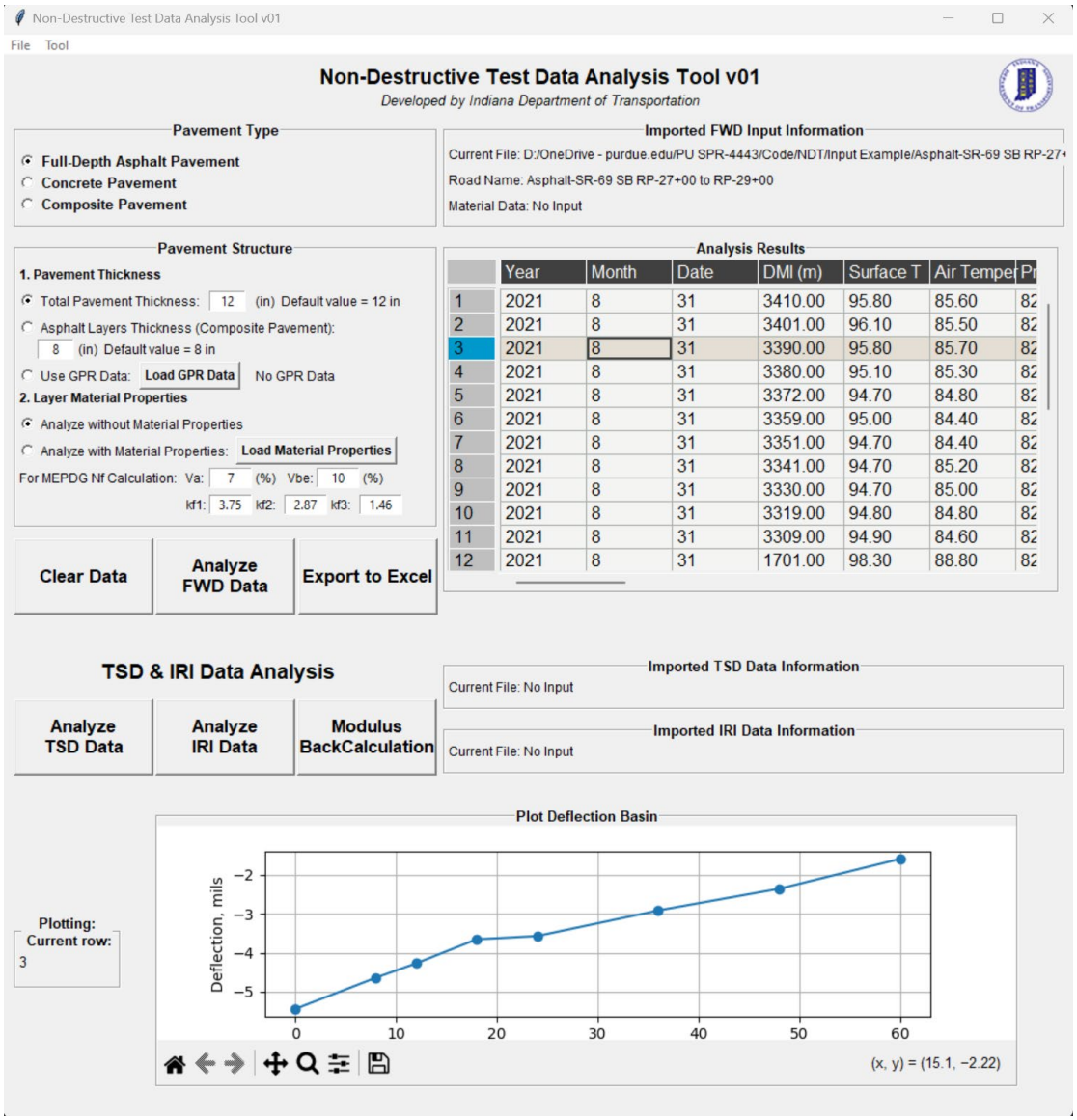

(b)

Figure D.4 Non-destructive data analysis software: (a) default view before analysis, (b) after FWD data analysis.

Integration of the software into the proposed decision framework will allow a more practical implementation of the decision framework within the PMS to determine the maintenance strategy for each testing location. Furthermore, the software can provide a structural condition-based RSL estimated by critical strains, which can be used to prioritize the need for maintenance, if necessary. In addition, the software has a feature to analyze other non-destructive test data, the GPR and TSD data, which can be potentially incorporated into the decision framework in the future study. It should be noted that software development is currently in the second phase, which aims to implement the decision framework proposed in this study. Consequently, the final version of software will provide maintenance strategies for all testing locations, after processing and analyzing raw non-destructive test data.

APPENDIX E. TRAFFIC SPEED DEFLECTOMETER

E.1 Introduction

Background

The traffic speed deflectometer (TSD) was developed to continuously measure pavement surface deflections, which are considered the most reliable measurements for estimating the structural strength of in-service pavements, at regular traffic speeds (Ferne et al., 2009; Nasimifar et al., 2017). The TSD may be beneficial for the network-level PMS to evaluate the structural conditions of in-service pavements, because the TSD allows for testing wider areas of pavement sections without road closure or traffic control, compared to the conventional stationary deflectometers (Ferne et al., 2009; Katicha et al., 2022). In addition, the TSD device can collect additional pavement performance or distress indicators related to roughness, cracking, potholes, and rutting. Even though the accuracy and repeatability of TSD measurements have been verified, standards for data collection and guidelines for the implementation of TSD data into the PMS are limited due to the relatively short history of the TSD (Katicha et al., 2022; Levenberg et al., 2018; Shrestha et al., 2022).

To incorporate the TSD measurements into the PMS, the TSD should be capable of distinguishing between weak and strong pavements in terms of their structural capacities (Katicha et al., 2022). Several researchers have investigated the correlations between TSD measurements and asphalt pavement performance indicators such as cracking and rutting to evaluate the capability of TSD in assessing flexible pavement structural performance (Huang et al., 2022; Katicha et al., 2020). However, no clear correlations between TSD deflections and performance indicators were identified from the previous studies. Huang et al. (2022) compared the TSD maximum deflections with the area of fatigue cracking, rut depth, and international roughness index (IRI) data collected from the field sections in Tennessee using the TSD. They found that the TSD maximum deflection exhibited no correlation with the performance indicators, and lower levels of IRI and fatigue cracking were identified from some field sections with high TSD maximum deflections (Huang et al., 2022). In addition, Katicha et al. (2020) conducted a correlation analysis between the TSD surface curvature index (SCI), the DBP widely used to characterize the conditions of upper asphalt layer, and the cracking and rutting data obtained from the Virginia Department of Transportation (VDOT) PMS database. They reported weak correlations between the TSD SCI and both cracking and rutting.

While several studies have attempted to establish a direct relationship between TSD measurements and pavement performance data, many researchers have conducted comparative studies between TSD and falling weight deflectometer (FWD) measurements (Huang et al., 2022; Katicha et al., 2014; Morovatdar et al., 2023; Shrestha et al., 2018). Since the FWD has been successfully applied to PMS for many years, the reliability of TSD measurements can be verified with a strong agreement between TSD and FWD measurements (Levenberg et al., 2018). Even though previous studies have concluded that TSD measurements exhibit similar trends to the FWD measurements in distinguishing structural variations, it has been reported that TSD measurements are statistically

different than FWD measurements, mainly due to the different loading mechanisms (Katicha et al., 2017; Katicha et al., 2014).

Previous studies have also indicated inconsistent results regarding the comparison between TSD and FWD measurements due to the challenges of collecting and comparing TSD and FWD data under the same structural and environmental conditions (Morovatdar et al., 2023; Shrestha et al., 2018). For example, Morovatdar et al. (2023) found that FWD deflections were 12% to 36% greater than the corresponding TSD deflections due to the variations in testing temperatures and moisture levels, despite both FWD and TSD deflections being adjusted to a reference temperature. Shrestha et al. (2018) found that in some cases, TSD and FWD maximum deflections had identical values, while for most cases, the TSD maximum deflections differed from the FWD data. It should be noted that data used for the Shrestha et al. (2018) study were collected in different years (FWD: 2007, 2010, 2012, 2013, 2015, and TSD: 2015), and for the 2015 data, the TSD maximum deflections were generally greater than the FWD maximum deflections.

Limited studies have collected FWD and TSD data during similar seasons and applied advanced FWD-based structural indicators, such as DBPs and SN_{eff} to assess the reliability of TSD data. Katicha et al. (2014) used two DBPs, SCI and BDI to compare TSD and FWD data. Even though the SCI and BDI from TSD were comparable to those from FWD, relationships of SCI and BDI between TSD and FWD depended on pavement types and structures. Thus, the SN_{eff}, which accounts for the pavement structure (pavement thicknesses) during the SN_{eff} calculation, has been recommended to interpret TSD data for pavement structural evaluation (Nasimifar et al., 2019; Uddin Ahmed Zihan et al., 2018). Zihan et al. (2018) developed and validated a nonlinear regression model to determine the SN_{eff} from TSD data; their model demonstrated strong correlations with SN_{eff} determined from FWD data. In addition, Nasimifar et al. (2019) calibrated the Rohde model using a database generated by 3D-move software to estimate TSD-based SN_{eff}. The calibrated Rohde model was validated with field data, demonstrating a good agreement with the SN_{eff} from FWD data. However, these proposed models were only validated with local field measurements from a limited number of pavement structures, specifically conventional flexible pavements.

In summary, there are currently no clear guidelines or structural indicators for interpreting TSD measurements to evaluate structural conditions of in-service pavements, due to the short history of TSD and a lack of correlation between TSD measurements and performance indicators. Even though the reliability of TSD has been verified by comparison to FWD data, most studies have mainly focused on conventional flexible pavements and used local field data. Furthermore, correlations between TSD and FWD measurements are still questionable due to challenges associated with collecting FWD and TSD data under the same structural and environmental conditions. In addition, since a full-depth asphalt flexible pavement is one of most common INDOT pavement types due to its structural benefits, a study is needed to evaluate the feasibility of using TSD to assess the structural conditions of these pavements. Therefore, this study focused on identifying appropriate structural indicators for TSD data to accurately assess the structural conditions of in-service full-depth asphalt flexible pavements. Comparative studies were conducted using TSD and FWD data, both of which were carefully collected under the identical structural and environmental conditions.

Objectives and scope

The primary objective of this task is to determine whether the FWD-based structural indicators can be used for the TSD data and to evaluate the agreement between TSD and FWD measurements. To achieve this objective, both TSD and FWD tests were conducted on the same field sections during the same month to collect TSD and FWD deflections by minimizing the influence of environmental and traffic loading factors. Three INDOT full-depth asphalt flexible pavement sections were selected, the total test section length of 40 miles. In addition, the pavement thickness information was collected using the 3D ground-penetrating radar (GPR) to consider more accurate thickness values for each data point. The TSD and FWD data were compared using six FWD-based structural indicators, including the maximum deflection, four DBPs, and the SN_{eff} to identify the most reliable structural indicator for interpreting TSD data.

E.2 Description of Traffic Speed Deflectometer (TSD)

Figure E.1 shows the TSD truck and conceptually illustrates the deflection measurement technology. The rear axle of the TSD truck applies approximately 22,480 lbf of moving load (11,240 lbf wheel load) and uses Doppler lasers positioned on a servo-hydraulic beam to measure the vertical velocity of deflections under the TSD loading. A total of 11 lasers are mounted at various distances from the load, including seven lasers located in front of the load (at 5, 8, 12, 18, 24, 36, and 60 inches), three lasers placed behind the load (at -8, -12, and -18 inches), and one reference laser at 120 inches from the load (Schmidt et al., 2022). It should be noted that the reference laser is positioned outside the load influence zone, which is the area of the deflection bowl, to eliminate any unwanted measurements from the primary lasers (Katicha et al., 2017; Katicha et al., 2014). In addition, the height of the lasers from the pavement surface is maintained at a constant level using the servo-hydraulic beam; the trailer temperature is maintained at 68°F by a climate control system to avoid a thermal distortion of the servo-hydraulic beam. As shown in Figure E.1., the TSD measures the vertical velocity of deflection and the horizontal vehicle velocity, and the deflection slope can be derived by dividing the vertical deflection velocity by the horizontal vehicle velocity, as expressed in Equation E.1.

$$S = \frac{v_v}{v_h} \qquad \text{(Eq. E.1)}$$

where, S is the deflection slope, v_v is the vertical velocity of deflections (mph), and v_h is the horizontal velocity of vehicle (mph).

The pavement surface deflection can be calculated from the measured deflection slope, which is a derivative of deflection. The algorithm to obtain the pavement surface deflections from the measured deflection slope uses a combination of Gaussian (symmetric) and stable distribution (asymmetric) functions to determine the deflection slope curve by optimizing fitting parameters based on the measured TSD deflection slopes (Nasimifar et al., 2018; Pedersen, 2013). The pavement surface deflections are obtained by calculating the area under the optimized curve of deflection slopes. As shown in Figure E.1., the TSD reports 12 pavement surface deflections, and the surface deflection at a specific distance "x (inch)" from the TSD loading is denoted as Dx.

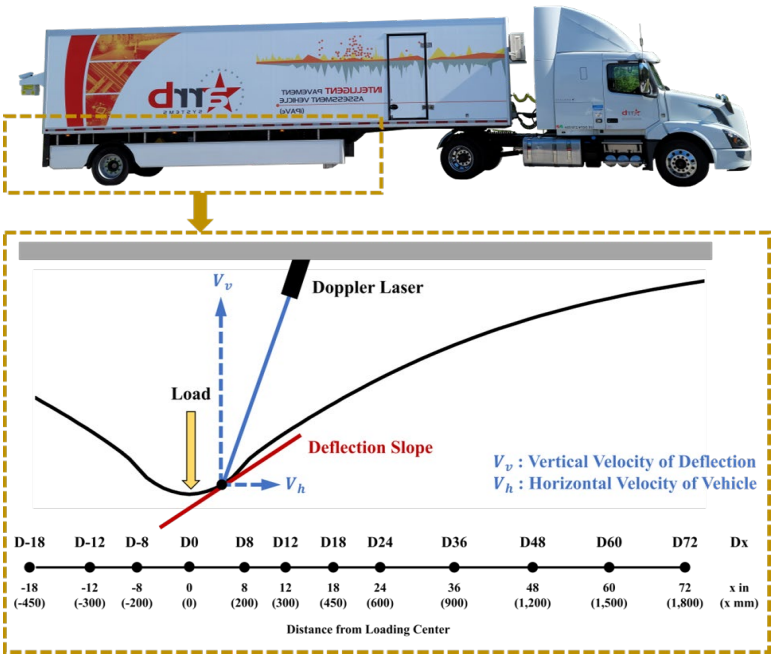

Figure E.1 TSD measurements description.

Since this task focused on evaluating the applicability of FWD-based structural indicators to the TSD data and the agreement between TSD and FWD data, it is important to understand the difference between TSD and FWD mechanisms. As summarized in Table E.1, the TSD applies a realistic moving truck load using a dual tire, while the FWD simulates the standard truck loading by applying a stationary impact load using a single circular loading plate, And the TSD load magnitude (11,000 lbf) is greater than the FWD load magnitude (9,000 lbf). It should be noted the load magnitude of both TSD and FWD can be adjusted, although the load magnitudes presented in Table E.1 are widely used for pavement structural evaluation. In addition, the TSD measures vertical velocities of deflection to obtain pavement surface deflections, whereas the FWD measures pavement surface deflections using geophones. This implies the TSD applies a more realistic traffic loading condition, but the FWD may provide more accurate pavement deflection measurements.

Table E.1 Comparison of TSD and FWD mechanisms

	TSD	**FWD**
Load type	Moving load (Dual tire load)	Stationary impact load (Single circular loading plate)
Load magnitude	11,000 lbf	9,000 lbf
Measurements	Deflection velocities	Deflections

E.3 Falling Weight Deflectometer (FWD) Structural Indicators

Many structural indicators have been developed to interpret the FWD deflection data for assessing the structural conditions of in-service pavements. Six structural indicators, originally developed

for FWD data interpretation, were selected to determine whether the FWD-based structural indicators can be used for TSD data analysis. The selected structural indicators consist of five FWD deflection parameters and the SN_{eff}, which are widely used for PMS.

FWD deflection Basin Parameters

The five FWD deflection parameters (D_0, AUPP, SCI, BDI, BCI) selected for this study are presented in Table B.1. Generally, during FWD testing, nine surface deflections are measured at various distances from the FWD loading plate center. The central deflection (D_0) measured from the center of the FWD loading plate is the maximum deflection, commonly used to assess the overall structural condition of in-service pavements. The AUPP is defined as the normalized area under a deflection basin curve from 0 to 36 inches, while the SCI is calculated as the deflection difference between D_{12} and D_0. Both AUPP and SCI are used to assess the structural conditions of upper layers (Hoffman, 1980; Plati et al., 2016; Vyas et al., 2021; Xu et al., 2002). The BDI is the difference between deflections measured at D_{12} and D_{24}, whereas the BCI is defined as the difference in deflections between D_{24} and D_{36}. Both BDI and BCI are used to estimate the structural conditions of lower pavement layers, such as subbase and subgrade (Pierce et al., 2017; Rabbi & Mishra, 2021).

Effective Structural Number (SNeff)

The SN_{eff} represents the structural capacity of existing flexible pavements and has been widely employed in the INDOT PMS to estimate the structural conditions of in-service flexible pavements. The AASHTO 1993 pavement design guide, which originally developed the structural number concept, introduced the SN_{eff} calculation method based on the non-destructive testing results (AASHTO, 1993). However, the AASHTO 1993 method requires a trial-and-error procedure that may not be practical and tends to overestimate the SN_{eff} for full-depth asphalt flexible pavements, due to its significant dependence on the total pavement thickness, regardless of the pavement conditions. Recently, researchers developed a new model to estimate the SN_{eff} of full-depth asphalt flexible pavements to overcome the drawbacks of the AASHTO 1993 method in terms of accuracy and calculation procedure (Park et al., 2024). The new model is expressed in Equation E.2 and has only two inputs, the AUPP and total pavement thickness above subgrade, making it simpler than the AASHTO 1993 method. Furthermore, the new model was calibrated and validated with field data and is able to provide more reasonable SN_{eff} for full-depth asphalt flexible pavements than was the AASHTO 1993 method. Therefore, this study adopted this new model to calculate the SN_{eff} to compare FWD and TSD data.

$$SN_{eff} = 3.097 \times H_p^{0.2746} \times AUPP^{-0.3247} \quad \text{(Eq. E.2)}$$

where, H_p is the pavement thickness above subgrade (in.), and AUPP is the area under pavement profile (mils).

E.4 Collection of Field Data

Both TSD and FWD tests were performed on the same field sections during the same month to compare the TSD and FWD data under identical structural and environmental conditions. Three INDOT full-depth asphalt flexible pavement sections were used, as summarized in Table E.2. Even though the TSD and FWD tests were conducted on the same field sections, the TSD provided more data points than the FWD test, due to different testing mechanism and resolution. As shown in Figure E.2, the deflections measured using the TSD were collected approximately every 52 feet, while the FWD tests were performed at approximately 300-feet intervals, following the INDOT FWD test protocol. Thus, the TSD data was selected based on the FWD test locations, as shown in Figure E.2, and the TSD data then compared to the corresponding FWD data. In addition, a 3D GPR test was simultaneously conducted during TSD testing. The pavement thickness above subgrade, obtained from the 3D GPR results, was used to more accurately calculate SN_{eff} and temperature correction factors.

Table E.2 Description of selected field sections

ID	Road Classification	Pavement Type	Collection Year	Length
Section A	Interstate highway	Full-depth asphalt	2021	7 miles
Section B	Interstate highway	Full-depth asphalt	2022	12 miles
Section C	Interstate highway	Full-depth asphalt	2022	21 miles

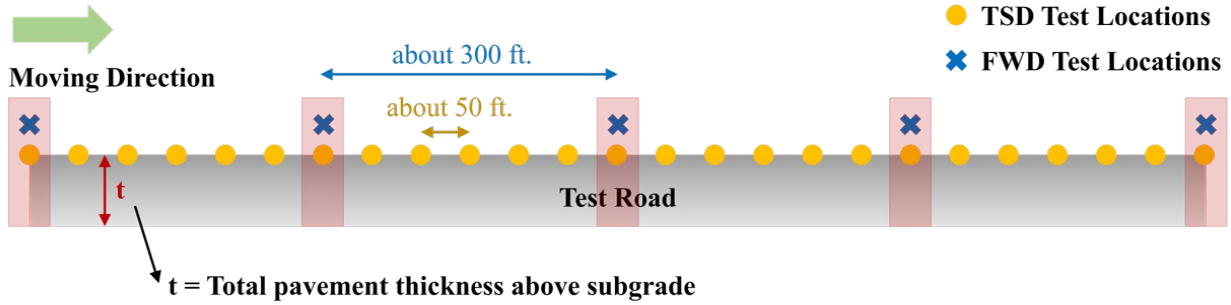

Figure E.2 FWD and TSD data collection.

Since the TSD and FWD use different loading magnitudes (11,000 and 9,000 lbf, respectively), the TSD deflection data was normalized to the FWD loading level using the Equation E.3, to ensure comparability. It is important to note that Equation E.3 is typically used for load calibration of the FWD deflection data.

$$d_{normalized} = d_{measured} \times \frac{Load_{Target}}{Load_{Applied}} \quad \text{(Eq. E.3)}$$

where, $d_{normalized}$ is a normalized deflection (mils), $d_{measured}$ is a measured deflection (mils), $Load_{Applied}$ is the applied load during testing (TSD load level, lbf), and $Load_{Target}$ is a target load (FWD load level, lbf).

The D_0 deflections measured from FWD and TSD were corrected to the reference temperature of 68°F using the AASHTO 1993 temperature adjustment factors, to eliminate the temperature effects. Following the AASHTO 1993 design guide, the temperature adjustment factors were determined for each test location based on the pavement thickness and pavement surface temperatures during testing, which were measured using the 3D GPR and deflectometers (FWD and TSD), respectively. The temperature corrected D_0 deflection was then used to calculate the DBPs. It should be noted that in some cases, the TSD D_0 deflection values were overcorrected, leading to several corrected TSD D_0 deflection values that were smaller than deflections measured at 8 inches from the loading center (D_8). As these overcorrected TSD D_0 deflection values can result in irrational DBP values, they were excluded from the analyses. Consequently, 223 datasets of FWD and TSD deflections were used for a comparative study.

Figure E.3 shows an example of collected field data. Three non-destructive testing results were obtained from each test location: FWD and TSD corrected D_0 deflections, and pavement thickness. As shown in Figure E.3, the pavement thickness was not consistent within the same field section. Since pavement thickness is one of the most important factors affecting the structural behavior of full-depth asphalt flexible pavements, it should be considered during the interpretation of deflection data (Park et al., 2022, 2024).

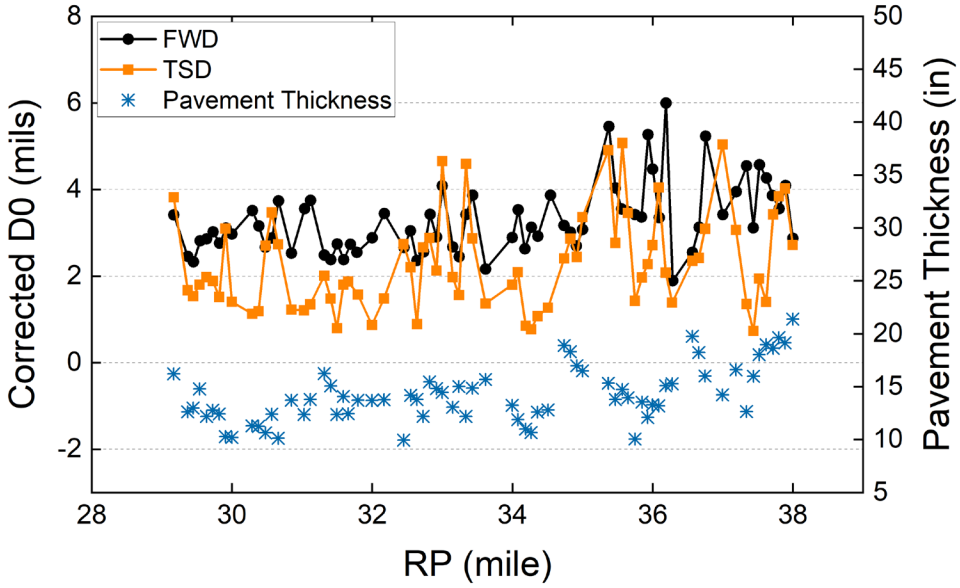

Figure E.3 Data examples from Section C.

E.5 Comparison of FWD and TSD Data

Figure E.4(a) through (e) show that FWD DBPs generally exhibited larger values than the TSD DBPs, but the correlations between TSD and FWD DBPs are unclear. Due to the use of different loading mechanisms, TSD deflection levels can be different from those from the FWD. This implies that a direct comparison between TSD and FWD deflection values may not be appropriate, and thresholds for DBPs previously developed based on FWD data may not be applicable to TSD data. Furthermore, as shown in Figure E.5, the TSD deflection basin curve exhibited a flatter slope

and smaller deflection values as compared to the FWD curve obtained from the same testing location. A flatter and smaller TSD deflection basin curve may reduce the sensitivities of DBPs to variations in pavement structural conditions. For example, Figure E.4(d) and (e) show that TSD data provided identical values of BDI and BCI for multiple test locations, whereas the corresponding BDI and BCI based on FWD data exhibited a sufficient range to make a relative comparison of the structural conditions of the test locations. Thus, the use of DBPs for TSD data may be limited in accurately distinguishing differences in structural conditions captured by FWD DBPs, and caution is advised when using DBPs developed from TSD data.

Figure E.4(f) shows that SN_{eff} calculated from TSD data was generally larger than the SN_{eff} from FWD data, because smaller values of TSD deflections resulted in a larger SN_{eff} values as compared to the FWD data. Even though there was no clear correlation between TSD and FWD SN_{eff}, the SN_{eff} data were more converged to the line of equality as compared to other DBPs. In addition, the sensitivity of TSD SN_{eff} was closer to that of FWD SN_{eff}. The use of additional structural information (i.e., total pavement thickness) during SN_{eff} calculation may allow for a more accurate estimation of pavement structural conditions compared to using only DBPs. However, further analysis is needed, because the direct comparisons shown in Figure E.4 may be insufficient to determine the most reliable structural indicator for interpreting TSD data accurately.

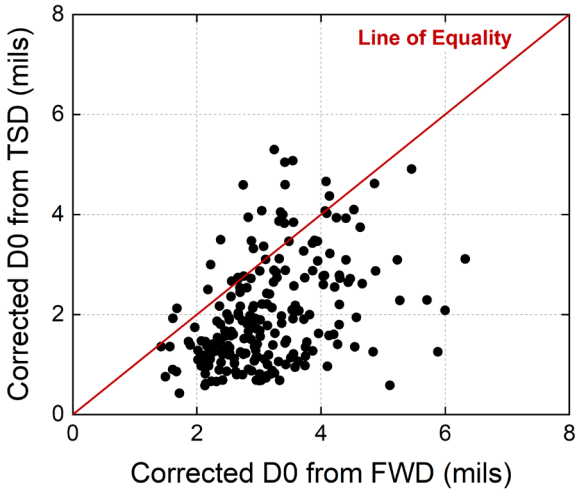

(a)

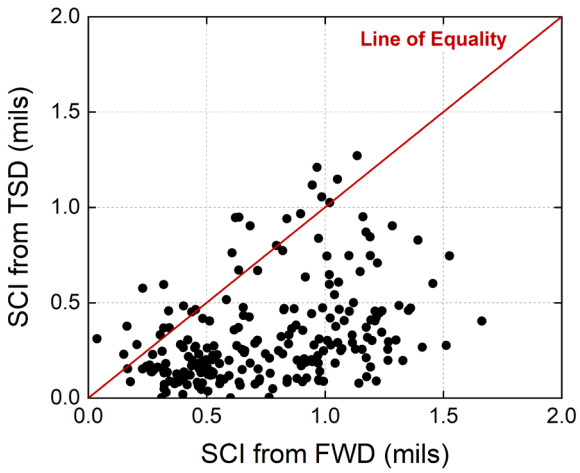

(b)

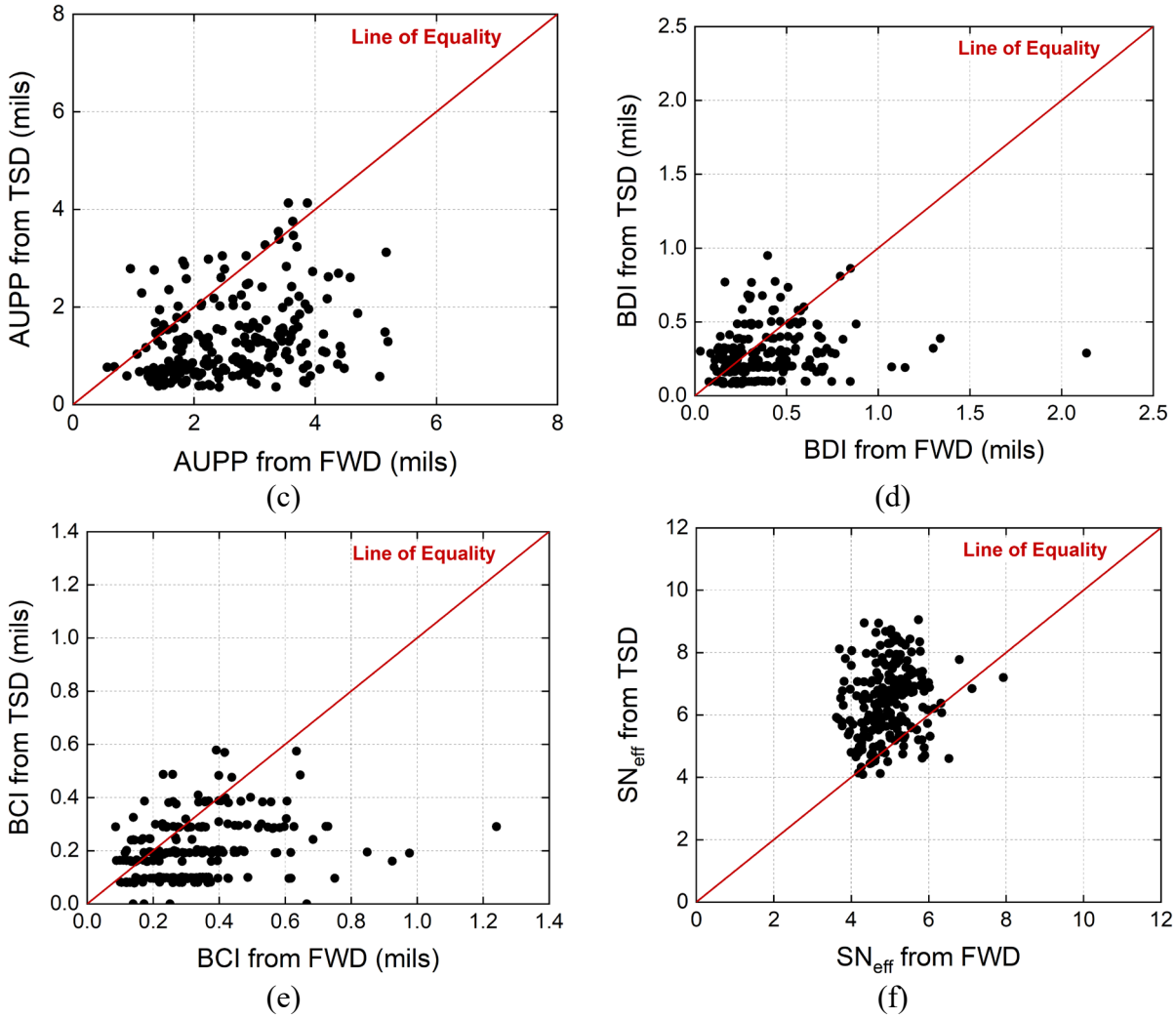

Figure E.4 Comparison of TSD and FWD deflection basin parameters: (a) D_0, (b) SCI, (c) AUPP, (d) BDI, (e) BCI, and (f) S_{Neff}.

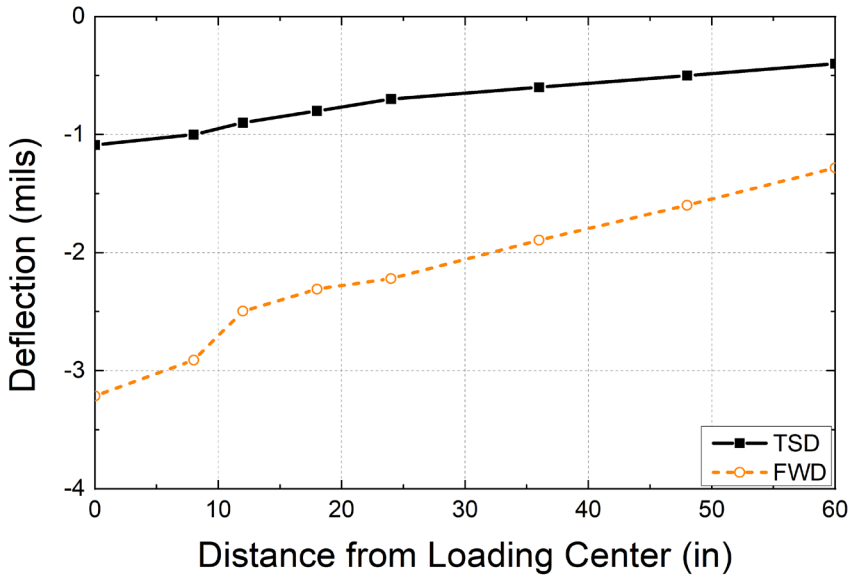

Figure E.5 TSD and FWD deflection basin curves comparison.

E.6 Determination of Structural Parameter for TSD Data Analysis

Since a direct comparison between TSD and FWD data was insufficient to identify appropriate structural indicators for TSD data, the agreement between TSD and FWD data was evaluated using the Bland-Altman approach, also called the limits of agreement method. Bland and Altman (Bland, 1986) suggested this method to evaluate the agreement between a new measurement device and a well-established old device, because correlation coefficients may be misleading in assessing the agreement between two devices. The Bland-Altman method allows the visualization of the level of agreement between two devices by plotting the difference between the two measurements as a function of the mean of the two measurements, along with the limits of agreement calculated by Equation E.4.

$$Mean\ Difference = \bar{d} = \frac{1}{n}\sum_{i=1}^{n}(x_i - y_i) \qquad \text{(Eq. E.4)}$$

$$Limits\ of\ Agreement = \bar{d} \pm 1.96 \times s$$

where, x_i is a measurement of the well-established old device (FWD parameter in this study), y_i is a measurement from the new device (TSD parameter in this study), n is the sample size, and s is the standard deviation of the differences. The limits of agreement, calculated by Equation E.4, have been widely used to quantify the statistical agreement between two devices, and a narrow range and small values of the limits of agreement indicate a good agreement between two measurements.

The corrected D_0 deflection and SN_{eff} were selected to evaluate the agreement between TSD and FWD data because both parameters represent the overall structural conditions of full-depth asphalt

flexible pavements. Figure E.6(a) and (b) show the Bland-Altman plots for the corrected D_0 deflections and SN_{eff}. It should be noted that the differences between FWD and TSD parameters (subtract TSD data from the FWD data) were plotted against the FWD values in lieu of the mean of FWD and TSD parameters to determine whether the magnitude of FWD parameters affect the differences between FWD and TSD parameters. As shown in Figure E.6(a), the mean difference for the corrected D_0 deflection was 1.15 mils, and the limits of agreement ranged from -0.94 to 3.24 mils, resulting in a total range of 4.10 mils. A larger upper limit of agreement (3.24 mils) and a positive mean difference value (1.15 mils) indicate the corrected FWD D_0 deflection is generally larger than the TSD corrected D_0 deflection, which is consistent with the previous observation in Figure E.4. Conversely, the SN_{eff} exhibited an opposite trend to the corrected D_0 deflection, with a negative mean difference (-1.47) and a total range of 4.69 for the limits of agreement (upper limit: 0.87 and lower limit: -3.82), as shown in Figure E.6(b). However, due to the different scales and sensitivities of corrected D_0 deflections and SN_{eff}, the Bland-Altman method was not able to compare the corrected D_0 deflections and SN_{eff} using the limits of agreement between TSD and FWD. Furthermore, no relationships were observed between the differences in FWD and TSD data and the magnitude of FWD data for both corrected D_0 deflections and SN_{eff}.

To compare the limits of agreement of corrected D_0 and SN_{eff} on the same scale, both FWD and TSD corrected D_0 and SN_{eff} were normalized by their respective maximum values. Since the TSD data scale and sensitivity to pavement structural conditions are different with the FWD data due to a different loading mechanism, a promising TSD parameter should provide the consistent rankings of structural conditions with the FWD parameter, rather than matching the magnitudes. The normalized data represents sensitivities of each parameter to the pavement structural conditions and allows for rescaling the data from 0 to 1. It is important to note that a normalization based on the maximum value was used to reflect the relative gap between FWD and TSD data points by maintaining the relative difference in their respective ranges (Al-Qadi et al., 2004; Yu et al., 2009). As shown in Figure E.6(c) and (d), the normalization allows the comparison of the limits of agreement for the corrected D_0 and SN_{eff} on the same scale, while maintaining the individual range of each parameter. The normalized SN_{eff} exhibited a smaller mean difference (-0.08) and a narrower range for the limits of agreement (0.53), compared to the normalized corrected D_0 (mean difference: 0.12 and a range of limits of agreement: 0.75). This indicates that SN_{eff} may provide a better agreement between FWD and TSD data than the corrected D_0, in terms of assessing the structural conditions of full-depth asphalt pavements.

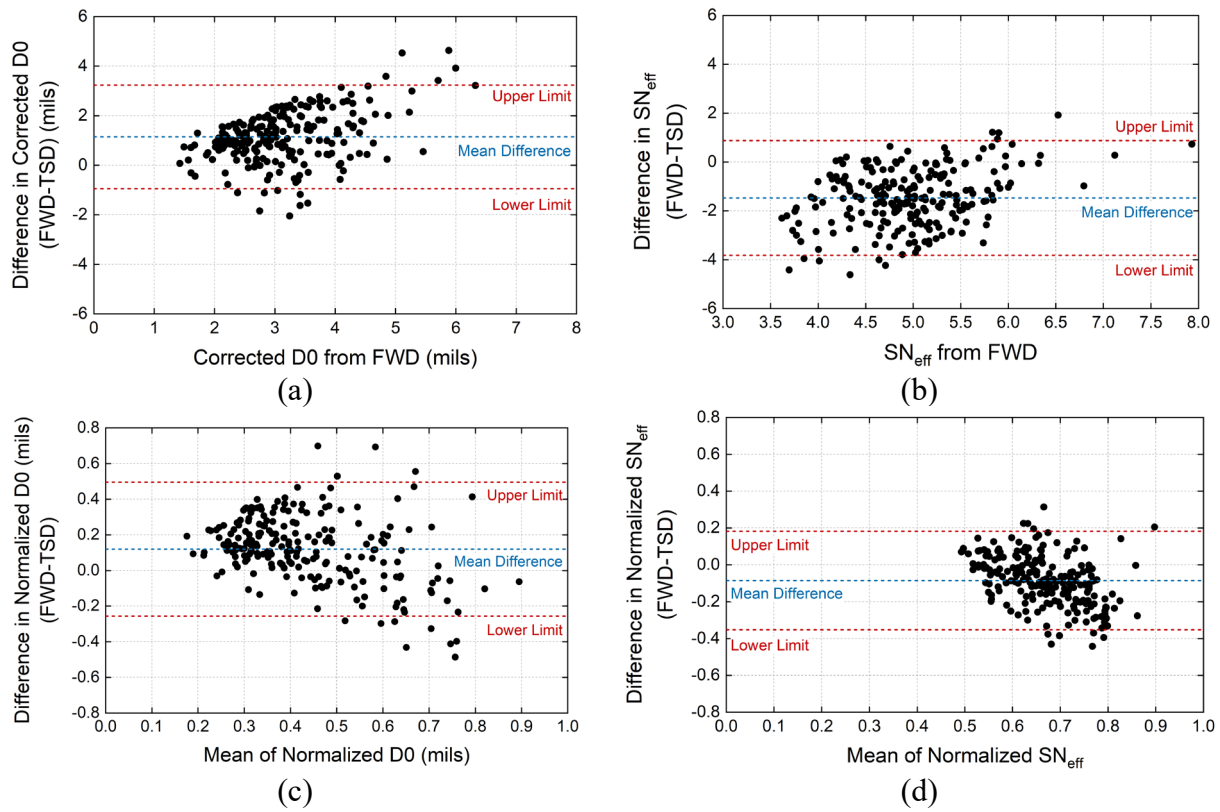

Figure E.6 Limits of agreement between TSD and FWD data: (a) corrected D_0 deflection, (b) SN_{eff}, (c) normalized corrected D_0 deflection, and (d) normalized SN_{eff}.

The use of pavement thickness during SN_{eff} calculation may improve agreement between TSD and FWD data. This was confirmed by comparing two segments with distinct structural conditions and pavement thicknesses within field section A, as shown in Figure E.7 (Segment A: reference post (RP) 17.4 to 19.3 miles and Segment B: RP 21.1 to 25 miles). Figure E.7: (a) shows that Segment B exhibited better structural condition with a smaller average FWD corrected D_0 deflection value (2.37 mils) than did Segment A (3.41 mils), while almost identical average values of TSD corrected D_0 deflections were observed from Segments A and B (Segment A: 1.08 mils and Segment B: 1.11 mils). This indicates the thicker asphalt layer in Segment B may contribute to the smaller values of FWD corrected D_0 deflections than the Segment A, but the TSD corrected D_0 may not be sensitive enough to capture the structural difference between the two segments. However, as shown in Figure E.7(b), the TSD SN_{eff} exhibited the same trend, with the FWD SN_{eff} of Segment B generally larger than the SN_{eff} of Segment A. Specifically, Figure E.7(c) shows that for both TSD and FWD, the SN_{eff} clearly distinguished the structural difference between Segments A and B, while the TSD corrected D_0 deflections provided similar results for both segments. For the FWD data, the average SN_{eff} of Segment B was 17.4% greater than that of Segment A, whereas the average TSD-based SN_{eff} of Segment B was 9.9% greater than that of Segment A. These field data demonstrate that the use of SN_{eff} for TSD data interpretation may result in better agreement with the FWD data to assess structural conditions of in-service pavements, because the SN_{eff} can reflect the effect of pavement thickness.

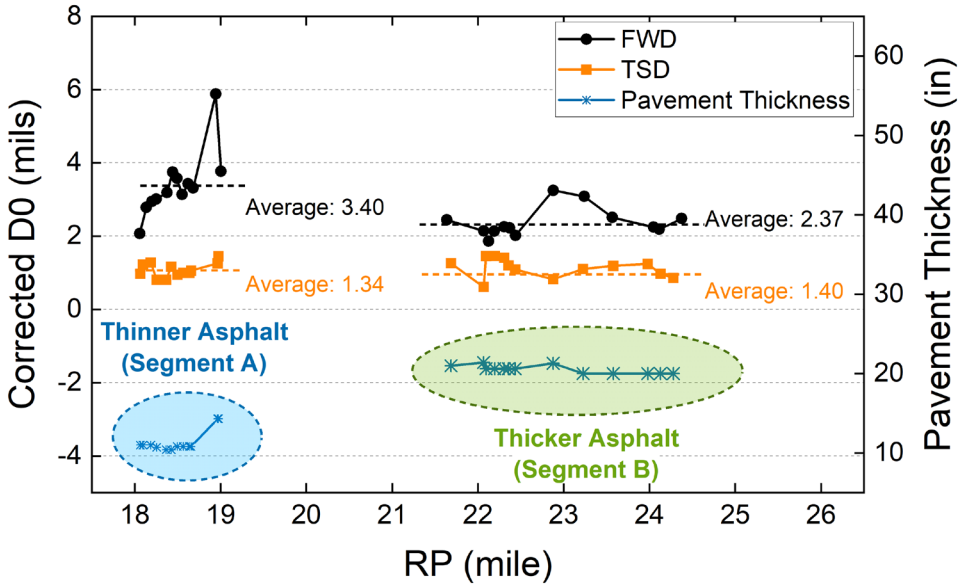
FWD
TSD
Pavement Thickness
Corrected D0 (mils)
Pavement Thickness (in)
RP (mile)
Average: 3.40
Average: 1.34
Average: 2.37
Average: 1.40
Thinner Asphalt
(Segment A)
Thicker Asphalt
(Segment B)

(a)

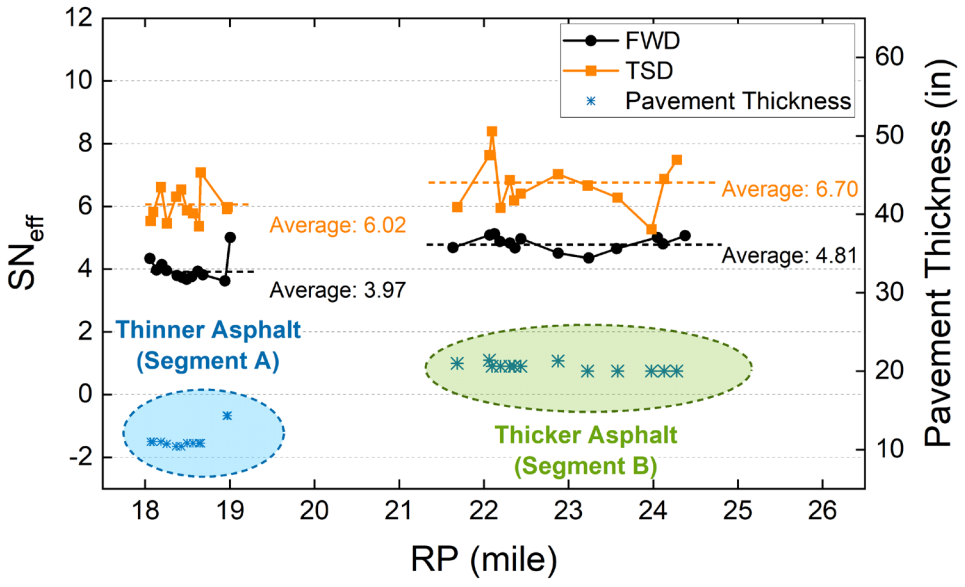
FWD
TSD
Pavement Thickness
SNeff
Pavement Thickness (in)
RP (mile)
Average: 6.02
Average: 3.97
Average: 6.70
Average: 4.81
Thinner Asphalt
(Segment A)
Thicker Asphalt
(Segment B)

(b)

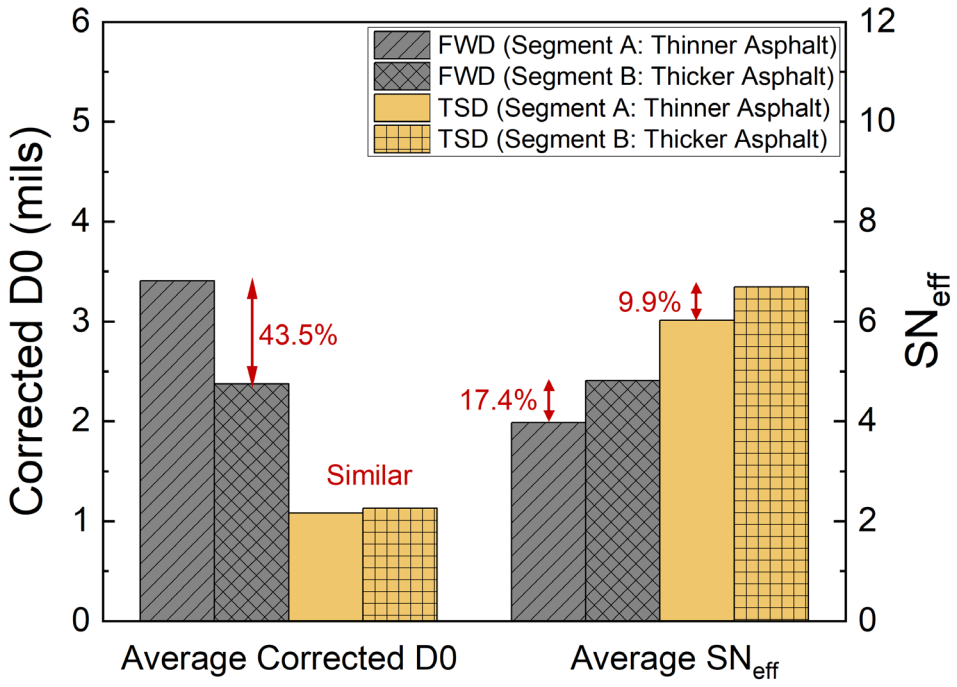

(c)

Figure E.7 Field section comparison of TSD and FWD data: (a) corrected D_0 deflection, (b) SN_{eff}, and (c) percent difference between average corrected D_0 deflection and SN_{eff}.

E.7 Summary and Conclusions

In this task, the reliability of TSD measurements was evaluated by comparing TSD data with FWD data, and an appropriate structural indicator was identified for interpreting TSD data to accurately assess structural conditions of in-service full-depth asphalt flexible pavements. The findings are as follows.

- The deflection parameters measured from the FWD are generally larger than those measured from the TSD, but correlations between TSD and FWD measurements are unclear.
- A flatter and smaller TSD deflection basin curve may reduce sensitivities of deflection parameters to variation in pavement structural conditions. This indicates that caution is needed when using deflection parameters for TSD data analysis.
- The SN_{eff} exhibits a smaller mean difference and a narrower range for the limits of agreement between TSD and FWD data, as compared to the maximum deflection.
- The SN_{eff} from TSD data clearly distinguishes the structural difference between two field segments, captured by the FWD maximum deflections. However, the TSD maximum deflection exhibits similar values for both field segments. Since the SN_{eff} can reflect the effect of pavement thickness, the SN_{eff} may provide an improved agreement between TSD and FWD data to prioritize the structural conditions of full-depth asphalt flexible pavements.

Based on these findings, it is concluded that the SN_{eff} calculated from the TSD measurements may be used to estimate the structural conditions of in-service full-depth asphalt flexible pavements. The SN_{eff} from TSD may provide a similar trend to that from FWD in relation to the ranking of structural conditions, while the TSD can provide wider spatial coverage than the FWD testing.

Therefore, the use of SN_{eff} for TSD data analysis may allow for the integration of TSD measurements into the network-level PMS to assess in-service full-depth asphalt flexible pavements based on their structural conditions.

E.8 Future Research

Further research is recommended to accurately estimate the required SN_{req} from TSD measurements. The combination of SN_{eff} and SN_{req} will allow the calculation of the structural number ratio (SNR), which can determine the theoretical stability of pavement structural conditions. Since the SN_{eff} obtained from the TSD exhibited different scales and magnitudes than the SN_{eff} from FWD data, further calibration of SN_{eff} may be necessary to accurately calculate the SNR.

Additionally, future studies are needed to further verify the effectiveness of SN_{eff} for TSD data analysis by including additional field sections to cover an extended range of structural conditions. This task only considered data from interstate highways, which represent relatively better (stronger) pavements than other road classifications. Furthermore, comparative studies should be conducted with TSD and FWD data, using the same approach as outlined in this study, for other pavement types, such as conventional flexible, rigid, and composite pavements.

REFERENCES

AASHTO. (1993). *AASHTO guide for design of pavement structures*. American Association of State Highway and Transportation Officials.

Al-Qadi, I. L., Loulizi, A., Elseifi, M., & Lahouar, S. (2004). The Virginia Smart Road: The impact of pavement instrumentation on understanding pavement performance. *Journal of the Association of Asphalt Paving Technologists*, *73*(3), 427–465.

Ayyala, D., Lee, H., & Von Quintus, H. L. (2018). *Characterizing existing asphalt concrete layer damage for mechanistic pavement rehabilitation design* (Publication No. FHWA-HRT-17-059). Applied Research Associates, Inc.

Bland, J. (1986). Statistical methods for assessing agreement between two methods of clinical measurement. *Lancet*, *1*(8476), 307–10.

Bowers, B. F., Diefenderfer, B. K., & Diefenderfer, S. D. (2015). Evaluation of dynamic modulus in asphalt paving mixtures utilizing small-scale specimen geometries. *Journal of the Association of Asphalt Paving Technologists*, *84*, 497–526.

Ferne, B. W., Langdale, P., Round, N., & Fairclough, R. (2009). Development of a calibration procedure for the U.K. highways agency traffic-speed deflectometer. *Transportation Research Record*, *2093*(1), 111–117.

Hoffman, M. S. (1980). *Mechanistic interpretation of nondestructive pavement testing deflections* [Doctoral dissertation, University of Illinois at Urbana-Champaign]. http://hdl.handle.net/2142/66882

Horak, E., Hefer, A., Emery, S., & Maina, J. (2015). Flexible road pavement structural condition benchmark methodology incorporating structural condition indices derived from Falling Weight Deflectometer deflection bowls. *Journal of Civil Engineering and Construction*, *4*(1), 1–14.

Huang, B., Zhang, M., Gong, H., & Polaczyk, P. (2022). *Evaluation of traffic speed deflectometer for collecting network level pavement structural data in Tennessee* (Report No. RES 2020-08). Tennessee Department of Transportation.

INDOT. (2024). *2024 standard specifications*. Indiana Department of Transportation. https://www.in.gov/dot/div/contracts/standards/book/sep23/2024Changes.pdf

Katicha, S., Flintsch, G., & Diefenderfer, B. (2022). Ten years of traffic speed deflectometer research in the United States: A review. *Transportation Research Record*, *2676*(12), 152–165.

Katicha, S., Flintsch, G., Shrestha, S., & Thyagarajan, S. (2017). *Demonstration of network-level structural evaluation with traffic speed deflectometer: Final Report* (Contract No. DTFH61-11-D-00009-T-13008. Virginia Tech Transportation Institute.

Katicha, S. W., Flintsch, G. W., Ferne, B., & Bryce, J. (2014). Limits of agreement method for comparing TSD and FWD measurements. *International Journal of Pavement Engineering*, *15*(6), 532–541.

Katicha, S. W., Shrestha, S., Flintsch, G. W., & Diefenderfer, B. K. (2020). *Network level pavement structural testing with the traffic speed deflectometer* (Final Report VTRC 21-R4). Virginia Transportation Research Council.

Kavussi, A., Abbasghorbani, M., Moghadas Nejad, F., & Bamdad Ziksari, A. (2017). A new method to determine maintenance and repair activities at network-level pavement management using Falling Weight Deflectometer. *Journal of Civil Engineering and Management*, *23*(3), 338–346. https://doi.org/10.3846/13923730.2015.1073173

Lee, K., Pape, S., Castorena, C., & Kim, Y. R. (2017). Evaluation of small specimen geometries for asphalt mixture performance testing and pavement performance prediction. *Transportation Research Record*, *2631*(1), 74–82.

Levenberg, E., Pettinari, M., Baltzer, S., & Christensen, B. M. L. (2018). Comparing traffic speed deflectometer and falling weight deflectometer data. *Transportation Research Record*, *2672*(40), 22–31.

Li, M., Wang, H., Xu, G., & Xie, P. (2017). Finite element modeling and parametric analysis of viscoelastic and nonlinear pavement responses under dynamic FWD loading. *Construction and Building Materials*, *141*, 23–35.

Morovatdar, A., Mandal, T., Arabzadeh, A., & Kemp, P. (2023). Mechanistic assessment of flexible pavements in Wisconsin using traffic speed deflectometer. *Transportation Research Record*, *2677*(8), 331–346.

Nasimifar, M., Thyagarajan, S., Chaudhari, S., & Sivaneswaran, N. (2019). Pavement structural capacity from traffic speed deflectometer for network level pavement management system application. *Transportation Research Record*, *2673*(2), 456–465. https://doi.org/10.1177/0361198118825122

Nasimifar, M., Thyagarajan, S., & Sivaneswaran, N. (2017). Backcalculation of flexible pavement layer moduli from traffic speed deflectometer data. *Transportation Research Record*, *2641*(1), 66–74.

Nasimifar, S. M., Thyagarajan, S., & Sivaneswaran, N. (2018). Computation of pavement vertical surface deflections from traffic speed deflectometer data: Evaluation of current methods. *Journal of Transportation Engineering, Part B: Pavements*, *144*(1), 04018001.

Park, B., Cho, S., Rahbar-Rastegar, R., Nantung, T. E., & Haddock, J. E. (2022). Prediction of critical responses in full-depth asphalt pavements using the Falling Weight Deflectometer deflection basin parameters. *Construction and Building Materials*, *318*, 126019. https://doi.org/10.1016/j.conbuildmat.2021.126019

Park, B., Cho, S., Rahbar-Rastegar, R., Nantung, T. E., & Haddock, J. E. (2024). Use of falling weight deflectometer data to determine the effective structural number of full-depth asphalt pavements for structural condition assessment. *Road Materials and Pavement Design*, *25*(2), 276–290. https://doi.org/10.1080/14680629.2023.2200843

Park, B., Zou, J., Hernando, D., Roque, R., & Waisome, J. A. M. (2021). Investigating the use of equivalent elastic approach to identify the potential location of bending-induced interface debonding under a moving load. *Materials and Structures*, *54*, 18. https://doi.org/10.1617/s11527-020-01612-7

Pedersen, L. (2013). *Viscoelastic modelling of road deflections for use with the traffic speed deflectometer* [Doctoral dissertation, Technical University of Denmark].

Pierce, L. M., Bruinsma, J. E., Smith, K. D., Wade, M. J., Chatti, K., & Vandenbossche, J.. (2017). *Using falling weight deflectometer data with mechanistic-empirical design and analysis, Volume III: Guidelines for deflection testing, analysis, and interpretation* (Publication No. FHWA-HRT-16-011). Applied Pavement Technology Inc.

Plati, C., Georgiou, P., & Papavasiliou, V. (2016). Simulating pavement structural condition using artificial neural networks. *Structure and Infrastructure Engineering*, *12*(9), 1127–1136. https://doi.org/10.1080/15732479.2015.1086384

Rabbi, M. F., & Mishra, D. (2021). Using FWD deflection basin parameters for network-level assessment of flexible pavements. *International Journal of Pavement Engineering*, *22*(2), 147–161. https://doi.org/10.1080/10298436.2019.1580366

Schmidt, B., Tetley, S., & Daleiden, J. (2022). Intelligent pavement assessment vehicle for structural and functional evaluation of road pavements. *Eleventh International Conference on the Bearing Capacity of Roads, Railways and Airfields, Volume 2* (pp. 242–250).

Shrestha, S., Katicha, S. W., Flintsch, G. W., & Diefenderfer, B. K. (2022). Implementing traffic speed deflection measurements for network level pavement management in Virginia. *Journal of Transportation Engineering, Part B: Pavements*, *148*(2), 04022021. https://doi.org/10.1061/JPEODX.0000371

Shrestha, S., Katicha, S. W., Flintsch, G. W., & Thyagarajan, S. (2018). Application of traffic speed deflectometer for network-level pavement management. *Transportation Research Record*, *2672*(40), 348–359.

Uddin Ahmed Zihan, Z., Elseifi, M. A., Gaspard, K., & Zhang, Z. (2018). Development of a structural capacity prediction model based on traffic speed deflectometer measurements. *Transportation Research Record*, *2672*(40), 315–325.

Vyas, V., Singh, A. P., & Srivastava, A. (2021). Prediction of asphalt pavement condition using FWD deflection basin parameters and artificial neural networks. *Road Materials and Pavement Design*, *22*(12), 2748–2766.

Xu, B., Ranjithan, S. R., & Kim, Y. R. (2002). New relationships between Falling Weight Deflectometer deflections and asphalt pavement layer condition indicators. *Transportation Research Record: Journal of the Transportation Research Board*, *1806*(1), 48–56. https://doi.org/10.3141/1806-06

Yu, L., Pan, Y., & Wu, Y. (2009). Research on data normalization methods in multi-attribute evaluation. *2009 International Conference on Computational Intelligence and Software Engineering* (pp. 1–5).

About the Joint Transportation Research Program (JTRP)

On March 11, 1937, the Indiana Legislature passed an act which authorized the Indiana State Highway Commission to cooperate with and assist Purdue University in developing the best methods of improving and maintaining the highways of the state and the respective counties thereof. That collaborative effort was called the Joint Highway Research Project (JHRP). In 1997 the collaborative venture was renamed as the Joint Transportation Research Program (JTRP) to reflect the state and national efforts to integrate the management and operation of various transportation modes.

The first studies of JHRP were concerned with Test Road No. 1—evaluation of the weathering characteristics of stabilized materials. After World War II, the JHRP program grew substantially and was regularly producing technical reports. Over 1,600 technical reports are now available, published as part of the JHRP and subsequently JTRP collaborative venture between Purdue University and what is now the Indiana Department of Transportation.

Free online access to all reports is provided through a unique collaboration between JTRP and Purdue Libraries. These are available at http://docs.lib.purdue.edu/jtrp.

Further information about JTRP and its current research program is available at http://www.purdue.edu/jtrp.

About This Report

An open access version of this publication is available online. See the URL in the citation below.

Cho, S., Park, B., Zhang, C., & Haddock, J. E. (2025). *Remaining service life prediction of Indiana pavements using mechanistic methods* (Joint Transportation Research Program Publication No. FHWA/IN/JTRP-2025/10). West Lafayette, IN: Purdue University. https://doi.org/10.5703/1288284317854